AD NUMBER
AD842055
LIMITATION CHANGES

TO:

Approved for public release; distribution is unlimited.

FROM:

Distribution: Further dissemination only as directed by Air Force Space and Missile Systems Organization, SMSD, Los Angeles AFB, CA 90045, MAY 1968, or higher DoD authority.

AUTHORITY

samso, usaf ltr, 28 feb 1972

SAMSO TR-68-362 VOL III

SEMIANNUAL PROGRESS REPORT

ADVANCED PENETRATION PROBLEMS

EXOTHERMIC ADDITIVES FOR WAKE MODIFICATION

J. L. Richardson and R. J. Getz
Space and Re-Entry Systems
Division of Philco-Ford Corporation

15 May 1968

SEMIANNUAL PROGRESS REPORT

ADVANCED PENETRATION PROBLEMS

EXOTHERMIC ADDITIVES FOR WAKE MODIFICATION

J. L. Richardson and R. J. Getz
Space and Re-Entry Systems
Division of Philco-Ford Corporation

15 May 1968

FOREWORD

(U) This Semiannual Progress Report by Philco-Ford, Space and Re-entry
Systems Division, Newport Beach, California, on the Advanced Penetration
Problems Task of Exothermic Additives for Wake Modification was prepared
for the Advanced Research Projects Agency, Department of Defense, ARPA
Order No. 888. The research was monitored by the Space and Missile
Systems Organization, USAF, under Contract FO4701-68-C-0032.

(U) The authors are Dr. J. L. Richardson and R. J. Getz of Philco-Ford,
Space and Re-entry Systems Division. The data herein covers the
reporting period of 16 October 1967 through 15 April 1968.

(U) This technical report has been reviewed and is approved.

W. D. McComb
Advanced Penetration Problems
Project Officer

ABSTRACT

The progress achieved in the first four and one-half months of the program was reviewed. The principal effort of this period has consisted of the design of experiments for demonstrating the effect of exothermic energy release on turbulent flow structure, the development of sensitive instrumentation for the accurate measurement of both time-average and fluctuating scalar quantities (temperature and concentration), the development of techniques for reducing the raw data derived from the sensors and their associated electronics to forms suitable for correlation and analysis, and the completion of several experiments in both nonreacting and nonequilibrium reacting gases. Calculations of the effectiveness parameter for the NO_2 reacting system have shown that the recombining NO_2 system (to form N_2O_4) will exhibit a sufficiently large effectiveness parameter under laboratory conditions so that the turbulence in a wake flow should be significantly modified. Appropriate experiments for demonstrating this effect were designed. An improved fiber optic probe was developed for use in the heated reacting gases (T to $800^{\circ}K$, P to 10 atm). Several experiments were completed with both high temperature air and reacting NO_2. Both total rms and spectral data were obtained. In the case of heated fully developed turbulent tube flow, the temperature and concentration intensities were found to be an order of magnitude higher in the nonequilibrium reacting gas than in nonreacting air.

iii

BLANK PAGE

CONTENTS

v

ILLUSTRATIONS

ILLUSTRATIONS (Continued)

NOMENCLATURE

a = proportionality constant relating the light intensity incident on the end of the photomultiplier tube to the resulting voltage output of the tube (intensity/volts)

a_ξ = frozen speed of sound (ft/sec)

b_i = product of extinction coefficient and transmitted light path length $\equiv \epsilon_i(\lambda, T)\ell$ (gm moles/liter)$^{-1}$

B = proportionality factor relating the effectiveness parameter to the characteristic energy and time ratios and the turbulence Mach number (1)

BW = bandwidth of wave analyzer (cycles/second or Hertz)

C = conversion factor relating voltage output of thermo-couple to sensed temperature (volts/$^\circ$F)

C = coefficient of discharge of orifice plate

C = total molar concentration of the gas system (moles/cm^3)

c_i = molar concentration of species i (gm moles/liter)

C_p = isobaric specific heat (Btu/lb$_m$ $^\circ$R)

d = diameter of orifice in orifice plate (ft)

d_p = probe diameter (inches)

D = test section inside diameter (ft)

$\bar{D}$ = averaged binary diffusion coefficient for NO_2-O_2 and NO_2-NO systems (cm^2/sec)

e = fluctuating voltage (volts)

e_{S+N} = fluctuating voltage with signal and noise information (volts)

e_N = fluctuating voltage with only noise information (volts)

E = voltage applied to heater at location of test probes (volts)

ix

E	=	instantaneous voltage from the sample beam (volts)
E_o	=	instantaneous voltage from the reference beam (volts)
f	=	Fanning friction factor
f	=	frequency (cycles/second or Hertz)
f_D	=	frequency based on test section diameter and center-line axial flow velocity (Hz)
$f_{\ell_{TS}}$	=	frequency based on test section length (5 ft) and centerline axial flow velocity (Hz)
g	=	local acceleration due to gravity (ft/sec^2)
g_c	=	gravitational constant = 32.17 lb$_m$ ft/lb$_f$ sec^2
G	=	mass flow rate (lb$_m$/sec ft^2)
G	=	gain of amplifier(s)
h	=	vertical displacement of liquid level in manometer (inches H_2O)
h	=	elevation (kft)
H	=	specific enthalpy (Btu/lb$_m$)
$\Delta \tilde{H}_R$	=	molar heat of reaction (cal/mole)
ΔH_R	=	specific heat of reaction (Btu/lb or cal/gm)
I	=	current through heater at location of test probes (amps)
I	=	light intensity transmitted through the gap of absorbing gas (intensity)
I_o	=	incident light intensity (intensity)
k	=	thermal conductivity (Btu/ft·hr·°F)
k_D	=	forward specific reaction rate constant used by Rosser and Wise (26)(cm^3/mole·sec)
k_F	=	forward specific reaction rate constant [(cm^3/gm mole)$^{n-1}$ sec^{-1} where n = order of reaction $\geq$ 1]

k_R = reverse specific reaction rate constant $[(cm^3/gm\ mole)^{n-1}\ sec^{-1}$ where n = order of reaction $\geq 1]$

k_1 = one-dimensional wave number (cm^{-1})

k_{1_D} = one-dimensional wave number based on test section diameter (cm^{-1})

$k_{1_{\ell_{TS}}}$ = one-dimensional wave number based on test section length (5 ft) (cm^{-1})

K = flow coefficient for an orifice plate defined by the equation

$$K \equiv \frac{C}{\sqrt{1 - \beta^4}}$$

K = distance from pressure port to upper level of manometer fluid (in.)

ℓ = characteristic turbulent scale (cm)

ℓ = gap width of optical probe (cm)

ℓ_{TS} = length of center test section = 5 feet

L = length of heater or distance between static pressure ports; distance in axial direction (ft)

m = mass velocity (lb_m/sec)

M = molecular weight (gm/gm mole)

M = mesh (distance between square openings of rods or wires in grid or screen) (cm)

$N_{Da_{II_{NO_2}}}^{(t)}$ = Damkohler number of the second type for NO_2 defined by

$$N_{Da_{II_{NO_2}}}^{(t)} \equiv \frac{k_D \left(\bar{C}_{NO_2}\right)_c}{\bar{D}\ k_{1_D}^2}$$

N_{Le_ξ} = frozen Lewis number defined by $N_{Le_\xi} \equiv \dfrac{C_{P_\xi} \rho D_{12}}{k_\xi}$

N_{Ma} = turbulence Mach number

$$N_{Ma} = \frac{u}{a_\xi}$$

$N_{Pe}^{(t)}$ = Peclet number defined by $N_{Pe}^{(t)} \equiv \theta_u' / \overline{D} k_{1_D}$

N_{Pr} = Prandtl number defined by $N_{Pr} \equiv C_p \mu/k$

N_{Re} = Reynolds number defined by $N_{Re} \equiv DG/\mu$

N_{Sc} = Schmidt number defined by $N_{Sc} \equiv \mu/\rho \overline{D} = N_{Pr_\xi}/N_{Le_\xi}$

P = total system pressure (atm)

ΔP = pressure drop in system or across flow meter (lb_f/ft^2)

P_R = power introduced into (or extracted from) the turbulent flow due to the presence of chemical reaction (cal/sec)

P_T = power passing through the turbulent flow due to the inertial forces themselves (cal/sec)

q = heat flux (positive if direction of transport is from wall to fluid) (Btu/hr)

Q = heat flux density = q/A (Btu/hr·ft^2)

r = radial distance from the centerline of the tube to a point of interest (ft)

r_o = tube radius (feet)

R = gas constant equal to 10.731 ft^3 $lb_f/in.^2$ lb mole °R = 1.987 cal/mole °K = 82.06 cm^3 atm/mole °K

t = time (min)

T = temperature (°F)

U = local longitudinal velocity at some location within the test section (ft/sec)

u = turbulent (or fluctuating) velocity (cm/sec)

U	=	mass average velocity defined by $U \equiv m/\rho_b \pi r_o^2$ (ft/sec)
x	=	distance between two locations of temperature measurement (in.)
x_{NO_2}	=	mole fraction of NO_2
y	=	distance from the pipe wall to a point of measurement (ft)
y_i	=	mass fraction of species i
Y	=	an expansion factor related empirically to the discharge or flow coefficient for a gas to that for a liquid at the same Reynolds number
z	=	longitudinal position in test section (ft)

Greek Symbols:

β	=	ratio of orifice diameter to pipe diameter
ϵ	=	wall roughness (rms inches)
$\epsilon_{NO_2}(\lambda, T)$	=	extinction coefficient for NO_2 at wavelength, λ, and temperature, T [$(mole/liter)^{-1} cm^{-1}$]
η	=	effectiveness parameter (see Equation 2)
λ	=	wavelength of light (angstroms)
μ	=	viscosity (lb_m/ft sec)
ξ	=	degree of advancement of a chemical reaction, for the NO_2 decomposition (Reference 31)

$$\xi = \frac{1 - x_{NO_2}}{1 + \frac{x_{NO_2}}{2}} \quad (gm\ moles)$$

π	=	3.1416
ρ	=	mass density (lb_m/ft^3)
τ	=	shear stress (lb_f/ft^2)

xiii

τ_e = characteristic turbulent eddy life-time (sec)

τ_c = characteristic energy addition or extraction rate due to exothermic or endothermic reaction (sec)

$\theta_t'(f)$ = rms fluctuating temperature at frequency f ($^\circ$F/cps)

$$\theta_t'(f) = \left[\overline{\theta_t^2(f)} \right]^{1/2}$$

$\theta_C'(f)$ = rms fluctuating concentration at frequency f [(moles/liter)/cps]

θ_t' = total rms fluctuating temperature ($^\circ$F)

θ_u' = total rms fluctuating velocity (ft/sec)

θ_C' = total rms fluctuating concentration (moles/liter)

Superscripts:

' = root mean square value of a fluctuating quantity

* = refers to orifice plate measurement, property based on orifice plate measurement; or parameter derived from nonreacting flow experiments

Subscripts:

A = refers to the cross sectional area of the test section wall or to the upper static pressure port

b = refers to properties of the bulk gas

B = refers to the lower static pressure port

c = refers to a value corrected for instrument error or to test section centerline

e = chemical equilibrium state

f = refers to properties evaluated at the film temperature defined by $T_f \equiv (T_w + T_b)/2$

f' = refers to properties evaluated at a film temperature corresponding to $H_f \equiv (H_w + H_b)/2$

xiv

F = designates frictional pressure drop

g = refers to the gas used to pressurize instrument lines

h = refers to the period of time during which the heater at the probe location was on

i = refers to insulation or to the inside pipe dimensions

L = refers to longitudinal measurements along the pipe wall

M = refers to the manometer or manometer fluid

ow = refers to measurements made at the outer pipe wall

op = orifice plate (flange taps, squared edged orifice)

pt = pitot tube (or total head - static pressure)

sp = static pressure (at wall along tube length)

T = refers to the total quantity of total time interval

w = refers to measurements made at the inside wall of the test section

1,2 = denotes different radial positions in the test section insulation; or 1 = upstream position, 2 = downstream position

ξ = refers to a property evaluated at (locally) frozen conditions

∞ = refers to bulk gas conditions before entering the test section

<u>Overlines</u>:

___ = time average

SECTION I

INTRODUCTION

1.1 BACKGROUND

Radar backscattering measurements can be used to infer the size and weight characteristics of re-entry bodies from the structure of their turbulent wakes generated as they re-enter the earth's atmosphere. The structure of these wakes can be characterized by such properties as: electron density fluctuation intensity and scale, growth of turbulent electron wake width downstream distance, altitude for the transition from a laminar to turbulent wake, and the transition location relative to the body . If any of these properties can be significantly altered by the injection of modest amounts of appropriate additives, then a new tool would be available to the re-entry system designer whereby small bodies could be made to look, from a radar backscatter signature standpoint, either larger or smaller than they actually are.

That there could be additives which could cause such changes in turbulent re-entry wakes is suggested by some recent theoretical results (References 1 and 2) which indicate that significant changes in turbulent structure would be expected for compressible flows in which exothermic or endothermic chemical reactions occur fast enough and with large enough chemical reaction heat effects. Such a nonlinear alteration of the turbulence by chemical reactions is the converse of the more usual situation in which the turbulence significantly affects the chemistry (Reference 3). Interactions between the transport process and fluid state with the turbulent structure of the flow have been previously predicted (Reference 4). No direct experimental determination has been made of the effect on turbulent structure of chemical reactions which deposit or absorb sufficient energy in the flow at a fast enough rate. An appropriate flow system and instrumentation has now been developed so that such a determination can now be made under will defined conditions for the range of variables of interst. The following paragraph outlines the scope of the program undertaken to obtain the answers needed to evaluate the feasibility of this concept for significantly enhancing re-entry system penetration capability.

1.2 PROGRAM OBJECTIVES

The overall long-range objectives of this program are to: (1) determine which chemical property-flow parameters are sensitive measures of the effect of chemical reaction on turbulence structure, (2) determine, by experimental means, how various turbulent structure properties of a flow depend on those parameters, (3) determine which materials have the desired physico-chemical characteristics to be appropriate candidates for a re-entry application, (4) determine the change in turbulent structure achieved in a turbulent wake as a function of the injection flow rate and state of the most promising candidate materials, and (5) evaluate by

pertinent flow calculations, the effectiveness of this approach for modifying the turbulence of re-entry wakes.

The first year's effort has now been defined in scope so as to include some work in areas (1), (2), and (3), with completion of work in these areas, as well as in areas (4) and (5) planned for the following year.

The main thrust of the first year's program is to carry out some selected experiments in an appropriately modified flow system with suitable instrumentation and with both the chemistry and flow conditions well defined. The subtask breakdown is as follows:

TASK 7.4

EXOTHERMIC ADDITIVES FOR WAKE MODIFICATION

Subtask	Scope	Approximate Percent of Total Task
7.4.1 Experiment Design	Analysis of existing theoretical studies, modification of chemical models for systems of interest, determination of experimental conditions required in order to measure effects.	10
7.4.2 Test Apparatus Design	Development of design for: modified test section of the flow system, injection and pressure control system, modified instrumentation, and modified turbo-blower seal and temperature control system.	10
7.4.3 Fabrication, Assembly, and Calibration	Preparation of flow system and instrumentation for experimental measurements.	20
7.4.4 Experimental Test	Measurements made with both nonreacting and nonequilibrium reacting gases.	30
7.4.5 Data Reduction and Analysis	Procedures developed for reducing the raw data to forms suitable for analysis, and determination of correlations of derived results.	30

For convenients in reporting on the progress achieved on each of these subtasks, Section II treats Subtask 7.4.1 by itself., while Section III deals with the combination of Subtasks 7.4.2 and 7.4.3, and Section IV covers Subtasks 7.4.4 and 7.4.5.

Since the program (Task 7.4) is a new component of the Advanced Penetration Problems Program, actual work on this task did not start until approximately 1 December 1967. Thus, this first semiannual report deals with the progress achieved during the first four and one-half months of the program. The primary emphasis of this report is to describe the modified flow system and instrumentation and to present the first results obtained without injection (self-mixing case) which show interesting differences in turbulent structure (as indicated by total rms measurements of the scalar properties) between the nonequilibrium reacting case and the nonreacting case.

SECTION II

EXPERIMENT DESIGN

2.1 MAGNITUDE OF EFFECTIVENESS PARAMETER FOR VARIOUS EXOTHERMICALLY REACTING SYSTEMS

It has been shown (Reference 2) that the effectiveness parameter, η, defined as the ratio of the power added to the turbulent field by the exothermic energy release of species reacting in the flow to the total power passing through the turbulence is a direct measure of the influence of chemical reactions on turbulent structure. If this power ratio is greater than 0.1, the scale, intensity, and (turbulent) diffusivity for momentum transport are all significantly affected by the presence of the exothermic reaction in the flow. Both intensity and diffusivity, according to the theoretical model, can be increased by approximately an order of magnitude if η is on the order of one. Two principal problems exist: is η the appropriate measure of the influence of exothermic energy release on turbulent structure, and how do the various measures of turbulent structure vary with η? In order to make an application of this interaction for re-entry system design, it is also necessary to determine which chemical species will exhibit a η value on the order of one.

The power ratio,

$$\eta \equiv P_R/P_T \tag{1}$$

has been predicted to depend on the chemical and flow parameters in the following way (Reference 2),

$$\eta = B \left\{ \frac{\left[\xi \Delta H_R/2 \right]}{u^2} \right\} \left(\frac{\tau_e}{\tau_c} \right) N_{Ma}^4 \tag{2}$$

where the proportionality factor, B, is not far from unity and has a relatively narrow dynamic range. We have used Equation (2) to make estimates of η for a hypothetical re-entry flight case and for a situation characteristic of the flow conditions achievable in the recirculating flow system described in Section III. The results of these calculations are as follows:

CASE 1   RE-ENTRY FLIGHT OF CONE

$h \sim 100$ Kft

$U_{BODY} \sim 20$ Kft/sec

$\ell \sim D_{BODY} = 1$ ft

$T_{WAKE} \sim 2000^\circ K$

$u \sim 0.3 \, (\bar{U}_c - \bar{U}_\infty)$

-5-

<u>For Oxygen Atom Recombination:</u>

$$\tau_c = (k_F C_O C_M)^{-1}$$

$$\eta \sim 0.01$$

<u>For Hydrocarbon Oxidation:</u>

$$(\tau_{c_{OXYGEN}} / \tau_{c_{HYDROCARBON}}) \sim 10^4$$

$$(\Delta H_{R_{HYDROCARBON}} / \Delta H_{R_{OXYGEN}}) \sim 3$$

$$\eta \sim 300$$

<u>CASE 2</u> GRID OR SPHERE WAKE IN RECIRCULATING FLOW SYSTEM

$$u \sim 0.3 \, \overline{U}_\infty$$

$$\overline{U}_\infty = 50 \text{ ft/sec}$$

$$\ell = 1''$$

<u>For Nitric Oxide Oxidation:</u>

$$2 \text{ NO} + O_2 = 2 \text{ NO}_2$$
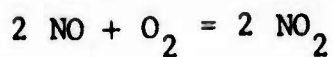
$$u \sim 15 \text{ ft/sec}$$

$$N_{Ma} = u/a_\xi \sim 0.01$$

$$\tau_e \sim \ell/u \sim 0.006 \text{ sec}$$

$$\frac{1}{\tau_c} = -\frac{1}{C_{NO}} \frac{d\,C_{NO}}{dt} = k_{R_1} C_{NO} C_{O_2}$$

$$\tau_{c_{1 \text{ atm, } 800^\circ K}} \sim 6 \text{ sec}; \quad \tau_{c_{10 \text{ atm, } 800^\circ K}} \sim 0.06 \text{ sec}$$

$$(u)^2 \sim 0.005 \text{ cal/gm}$$

$$\left[\xi \Delta H_R / 2 \right] \sim 150 \text{ cal/gm} \quad (\xi \sim 1)$$

$$\eta_{10 \text{ atm}} \sim (0.2) \left(\frac{150}{0.005} \right) \left(\frac{0.006}{0.06} \right) (0.01)^4 \sim 10^{-5}$$

<u>For Nitrogen Dioxide Recombination</u>

$$2 \text{ NO}_2 = N_2 O_4$$
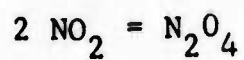
$$\frac{1}{\tau_c} = -\frac{1}{C_{NO_2}} \frac{d\,C_{NO_2}}{dt} = k_{R_2} C_{NO_2}$$

-6-

$$\tau_{c_{10 \text{ atm, } 400^\circ K}} \sim 2.4 \times 10^{-8} \text{ sec}$$

$$\eta = (0.2)(3 \times 10^4) \left(\frac{60 \times 10^{-4}}{2.4 \times 10^{-8}} \right) (10^{-8}) \sim 15$$

These calculations show that in the re-entry case considered the three-body oxygen recombination reaction is too slow to lead to an appreciable effect, but that the much faster and more energetic two-body hydrocarbon oxidation reaction is capable of yielding η values much greater than one. In addition, the two-body recombination of NO_2 is shown to be a suitable material for use in laboratory experiments providing the pressure is kept high and the scale is kept large (on the order of 1 inch).

The exothermic heats of reaction of several systems are compared in the following:

System	$-\Delta H_R$ (cal/gm)
$0 + 0 + M$:	3,700
$HC + O_2$:	11,000
DIBORANE $(B_2H_6) + O_2$:	17,000
HYDRAZINE $(N_2H_4) + O_2$:	4,600
$H_2 + O_2$:	28,500
UDMH $+ O_2$:	7,800
TNT $+ O_2$: [*]	3,600

---

[*] $\Delta H_{EXPLOSION} = 1100$ cal/gm

Selection of a system for practical application will be based primarily on consideration of the value of τ_c for the situation of interest, since the specific exothermic heat of reaction cannot exceed, for most systems, several tens of thousands of calories/gram (η is greatest for the largest $-\Delta H_R$ and the smallest τ_c).

Since the nitrogen dioxide recombination reaction exhibits a high enough η to significantly affect the usual measures of turbulent structure, a series of experiments were designed for the use of this reacting system in the recirculating flow facility described in Section III. In Figure 1 the experiments designed for either flow behind a biplanar grid (injection of NO_2 through small holes in the rods of the grid) or a sphere (injection at the forward and rear stagnation points - injectant brought into sphere

6 SCREENS
30 MESH

FLOW

N_2O_4 (T_C)

$D_1/L_1 \sim 1$

$L_2/D_2 \sim 10$

$D_2/D_3 \sim 24$

NO_2 (T_H)

NO_2 (T_H)

$2NO_2 \rightleftharpoons N_2O_4^+$ (T_C^+)

$d_{OP} \sim 250\mu$

$d_{TC} \sim 60\mu$

$c'(f), \bar{c}_i$

$t'(f), \bar{T}$

OP
S

AMP

$G \sim 10$

$G \sim 10^4$

$\bar{U}$ MM

P

D_3

D_3

D_1

D_2

L_1

x

L_2

FLOW

GRID: $N_{Re_{MESH}} > 10,000$

$M_{GRID} \geq 10\, M_{SCREEN}$

$\dfrac{D_{MESH}}{D_{ROD}} = 16/3$

$x/D_{MESH} < 200$

SPHERE:

$D_2/D_S \geq 6$

$N_{Re_{D_S}} > 10,000$

$2 \leq x/D_S \leq 20$

INJECTION RATE:

$\dot{m}_i < 0.1\, \dot{m}_I$
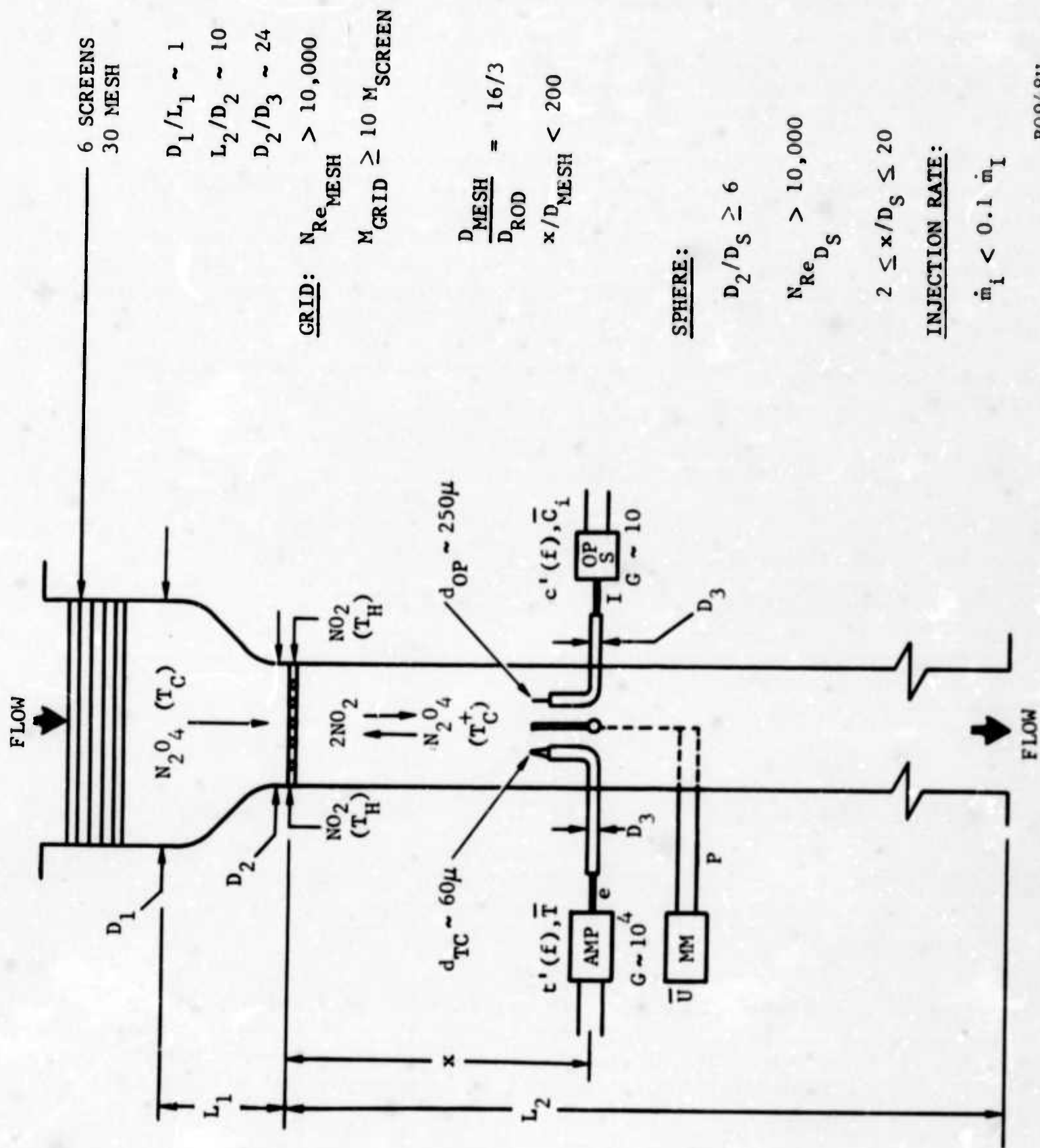
FIGURE 1. EXPERIMENT DESIGN FOR NO₂ RECOMBINATION IN GRID OR SPHERE WAKE - TEST SECTION SCHEMATIC

through its side supporting tubes) located at the entrance to the test section. The instrumentation shown schematically in Figure 1 is described in detail in Section III.

Experiments will be carried out as a function of pressure in order to find the pressure closest to 1 atmosphere at which significant effects can be measured. The initial experiments will be conducted at 10 atmospheres total system pressure in order to ensure the achievement of maximum effect on the turbulent flow structure.

The temperature of the heated NO_2 which will be injected into the much cooler bulk flow of the stoichiometric N_2O_4 - NO_2 mixture is determined by the properties of the N_2O_4 - NO_2 system.* A summary of these properties is given in Figure 2. By referring to the variation of the equilibrium thermal conductivity with temperature at a given pressure and a comparison of the equilibrium value with the frozen (or nonreacting) value, the temperature at which NO_2 should be injected is found to be approximately 450 to $500^{\circ}K$. The temperature of the bulk N_2O_4 - NO_2 system entering the test section should be controlled to as low a temperature as possible without incurring condensation (for $P \leq 10$ atm, $T_{N_2O_4 - NO_2}$ can be $\leq 350^{\circ}K$).

---

* No catalytic reactions are expected for the NO_2 system in contact with the platimum of the thermocouple junctions at temperatures up to $1200^{\circ}F$ based on the data of Brown and Mason (Reference 27). Our experimental measurements generally were confined to temperatures $< 1200^{\circ}F$. No complications in the kinetics of the NO_2 decomposition and the NO oxidation reactions would be expected because the reaction conditions were always selected so that the degree of advancement, ξ, was ~ 0.5 gm moles (or $\sim 50\%$ decomposition). Ashmore and co-workers (References 28 and 29) have shown that NO_3 radical complications occur only for $\leq 10\%$ decomposition of the NO_2. This is also supported by Bodman, et al. (Reference 30) from heat transfer data.
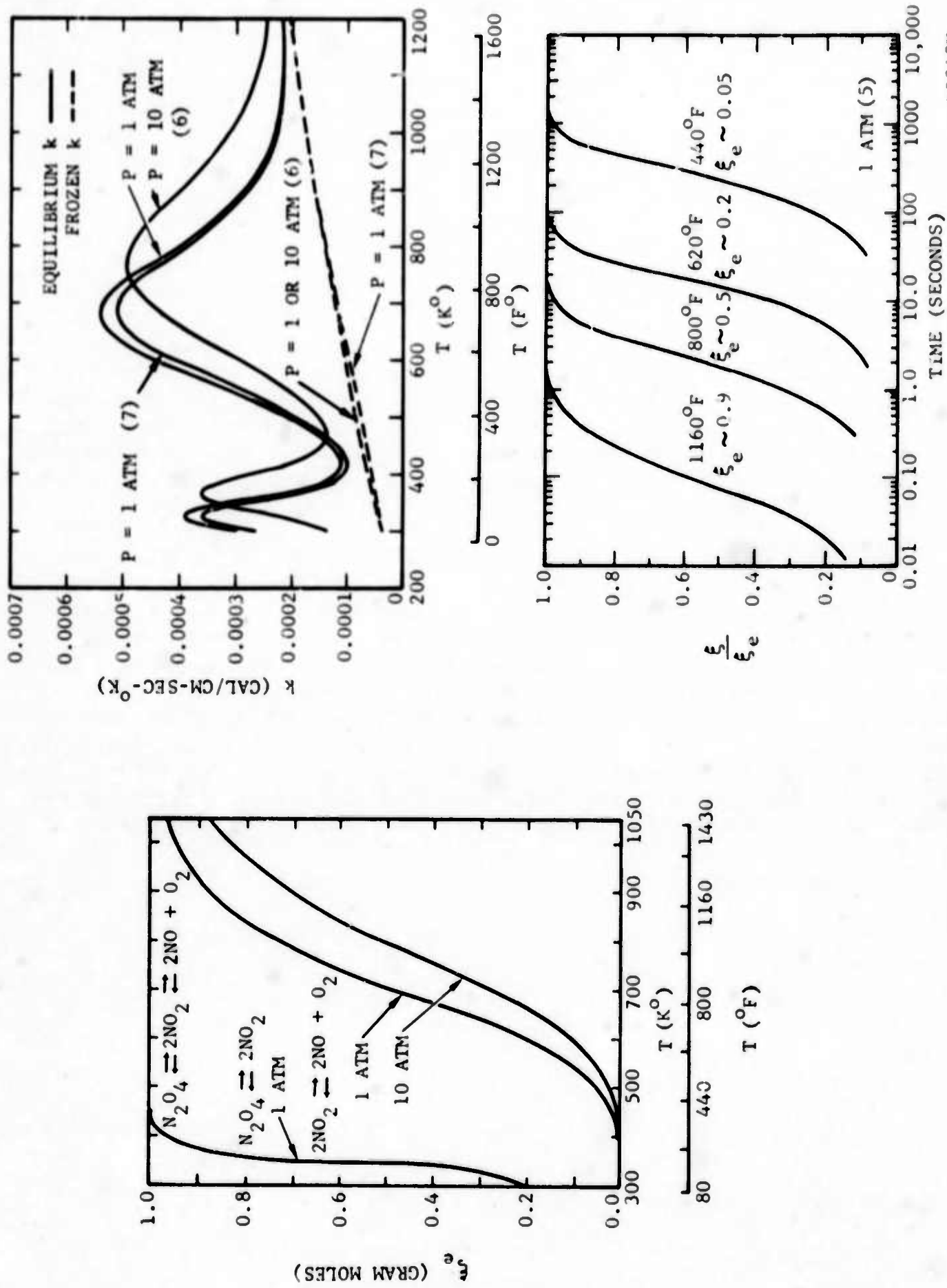
FIGURE 2. SELECTED THERMODYNAMIC, TRANSPORT, AND KINETIC PROPERTIES OF THE
N_2O_4-NO_2-NO-O_2 SYSTEM

SECTION III

EXPERIMENTAL EQUIPMENT AND CALIBRATION DATA

3.1 THE THERMODYNAMIC AND TRANSPORT PROPERTIES OF THE DISSOCIATING NO_2 SYSTEM

The thermodynamic and transport properties of both the frozen and equilibrium reacting N_2O_4-NO_2 system used in this investigation are those calculated by Svehla and Brokaw (References 6 and 8). The properties were tabulated for temperatures from 300 to 1280°K in 20°K increments and for pressures from 0.01 to 100 atmospheres. In the pressure range of 1 to 11 atm, all of the properties were tabulated at increments of 1 atm. These results are in good agreement with those obtained by Fan and Mason (Reference 7) for the same system at 1 atm total pressure. In formulating the Damkohler number (second type) it is necessary to have values for the binary ordinary molecular diffusion coefficients. These are obtained from Brokaw and Svehla (Reference 8) and Bodman (Reference 9).

Values of ξ_e, the equilibrium degree of advancement (related to the fraction dissociated), for both the N_2O_4 and NO_2 decompositions are shown in Figure 2. Also in this figure, the equilibrium and frozen thermal conductivities are shown for the two dissociating systems as a function of temperature for 1 and 10 atm total pressure.

3.2 FLOW SYSTEM - PIPING AND GASKETS

A schematic layout of the recirculating test loop is shown in Figure 3. All metallic parts were constructed of 316 stainless steel. The key overall dimensions of the loop, including the nominal pipe sizes are shown in Figure 4. All main piping connections were made with flanges and "Flexitallic" gaskets (layered chevron construction of blue asbestos and stainless steel) rather than screwed connections. The number of flanged joints was kept to a minimum in order to reduce the leakage control problem. Pipe wall and flange thicknesses were selected according to standard ASME 300 psig design in order to account for the elevated temperatures needed at the maximum expected test pressure of 150 psig. Expansion joints were required at the several locations shown in Figure 3. The piping system was thoroughly cleaned before NO_2 was brought into contact with it.

As is shown in the top part of Figure 3, a plenum section (containing screens, straightening vanes, and a contoured contraction) preceded the three portions of the test section and was designed to properly prepare the flow for its passage into the test section.

FIGURE 3. RECIRCULATING FLOW SYSTEM

-12-

4" TO 6" TRANSITION

6.5'

2" TO 4" TRANSITION

ENTRANCE
PLENUM

6" TO 2"

2.5'

ENTRANCE
SECTION

2" ID

5.0'

TEST
SECTION

2" ID

5.0'

20.5'   PREHEAT SECTION   2" ID

EXIT
SECTION

2" ID

5.0'

6" TO 2"
TRANS

3" TO 2" TRANSITION

ORIFICE PLATE SECTION 3" ID

EXIT
PLENUM

2" TO 6"

2.0'

1.5'

7.5'

6" TO 4"
TRANSITION

BYPASS LEG 16'
4" ID

7.5'   2" TO 4"
TRANSITION

3.0'

HEAT EXCHANGER
2" ID PIPE
12" OD SHELL

4.0'

4" TO 3"
TRANSITION

BYPASS VALVE

TURBOBLOWER

B0951U

FIGURE 4.   OVERALL DIMENSIONS AND NOMINAL PIPE SIZES OF THE
RECIRCULATING FLOW SYSTEM

-13-

3.3 TURBOBLOWER WITH MECHANICAL SHAFT SEAL

The prime mover for the system is a 3 horsepower, 4 bearing, overhung turbo-blower* rated at 100 ICFM for 1 psi with gas of specific gravity equal to 1.588 at 800°F and 175 psia (an approximation to the upper operating limit anticipated with the NO_2 system at the blower). The blower has 4 inch flanged inlet and outlet connections and is also provided with a 1 inch bypass line valved so as to provide flow rate control down to very low flow rates. Primary control of the flow rate is accomplished with a "Varidrive" variable speed motor system directly coupled to the blower shaft.

The seal between the hot reacting gases in the blower shell (at pressures to 10 atm) and atmospheric air is accomplished with a mechanical seal (Sealol #605 double bellows seal) cooled externally with water and attached to the rotating shaft of the blower. The gas seal occurred at the inter-face between a polished graphite ring rotating against a polished Stellite surface fixed to the blower shell. Great difficulty was encountered in effecting an adequate seal until various design modifications were made to the seal housing, the mounting plates, the static gaskets, and the bellows supports. Also, it was found that the alignment in all directions of the seal and shaft relative to the blower shell was an extremely critical factor in achieving the seal. Now that the required modifications have been made, the blower is now capable of running for extended periods of time with its shell heated to a temperature as high as 725°F without any significant leakage at the seal. What small NO_2 leakage does occur at the seal is not a hazard as the gas readily dissolves in the seal cooling water flow and passes to the drain.

A view of the turboblower is shown in the foreground of Figure 5. This figure shows the system before addition of the heating elements, instru-mentation, cooling lines, guard heaters, etc. The lower portion of the test section and the exit plenum are visible in the background. A two level platform system was built in order to provide access to the various parts of the veritical sections. A view of the system after the insulation and cooling lines had been installed is shown in Figure 6.

3.4 HEATING AND ASSOCIATED CONTROLS

The heating is accomplished with ~ 30 kw of ac power supplied to nichrome wire embedded in semicylindrical annular elements cast from alumina. The heating elements are each 1 foot long, conformed closely to the outside dimensions of the pipe, and are capable of dissipating ~ 1 kw of electrical power. The general distribution around the piping system is shown in Figure 3. The five 1-foot long heating elements in the center test section are controlled by proportional-mode type controllers so as to produce a desired back wall temperature (kept constant along the test section length) (see Appendix I, Table IV). The other ten heating elements in the entrance

---

* Manufactured by the Spencer Turbine Co., New Haven, Connecticut
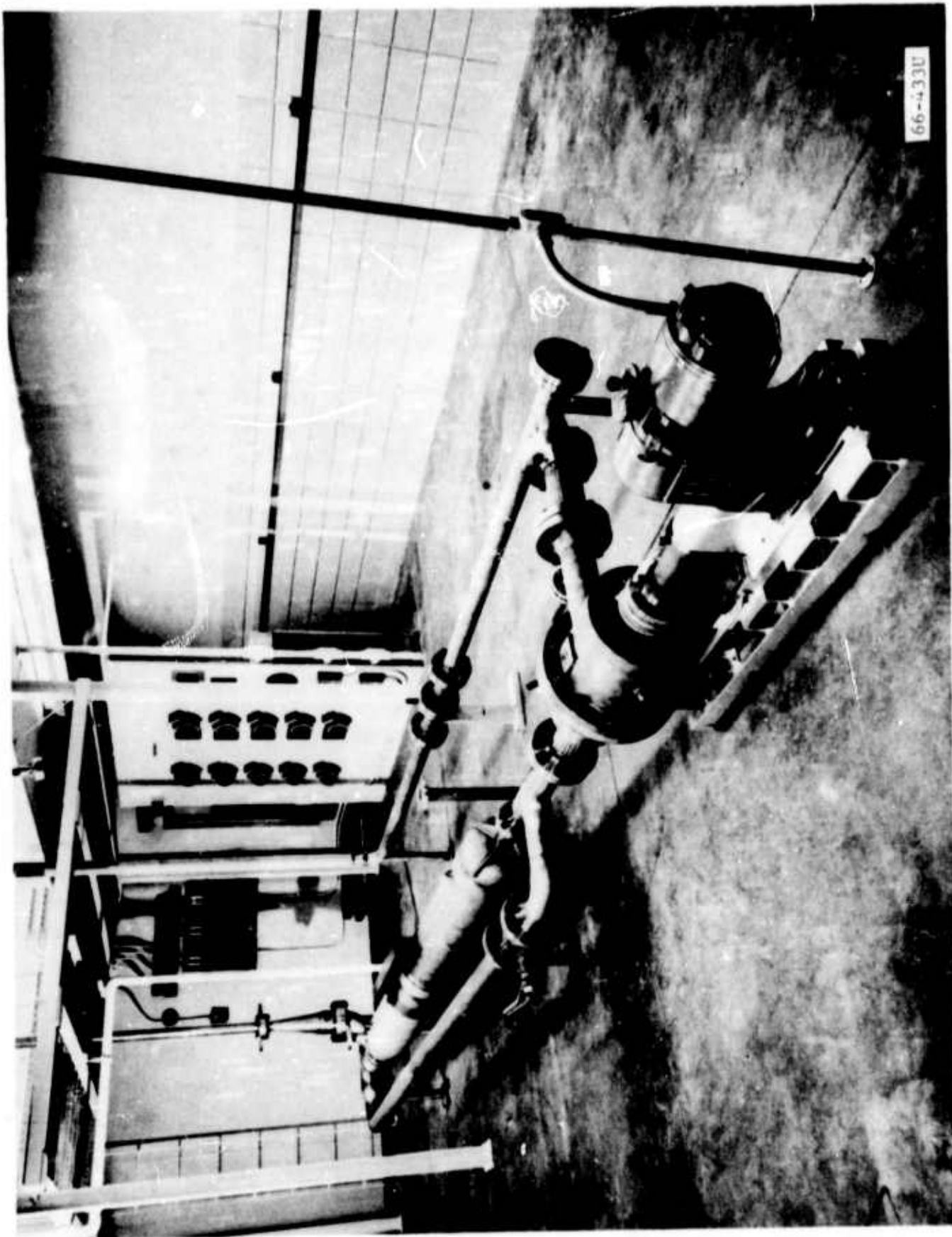
FIGURE 5. FIRST FLOOR VIEW OF THE RECIRCULATING FLOW SYSTEM SHORTLY AFTER INSTALLATION
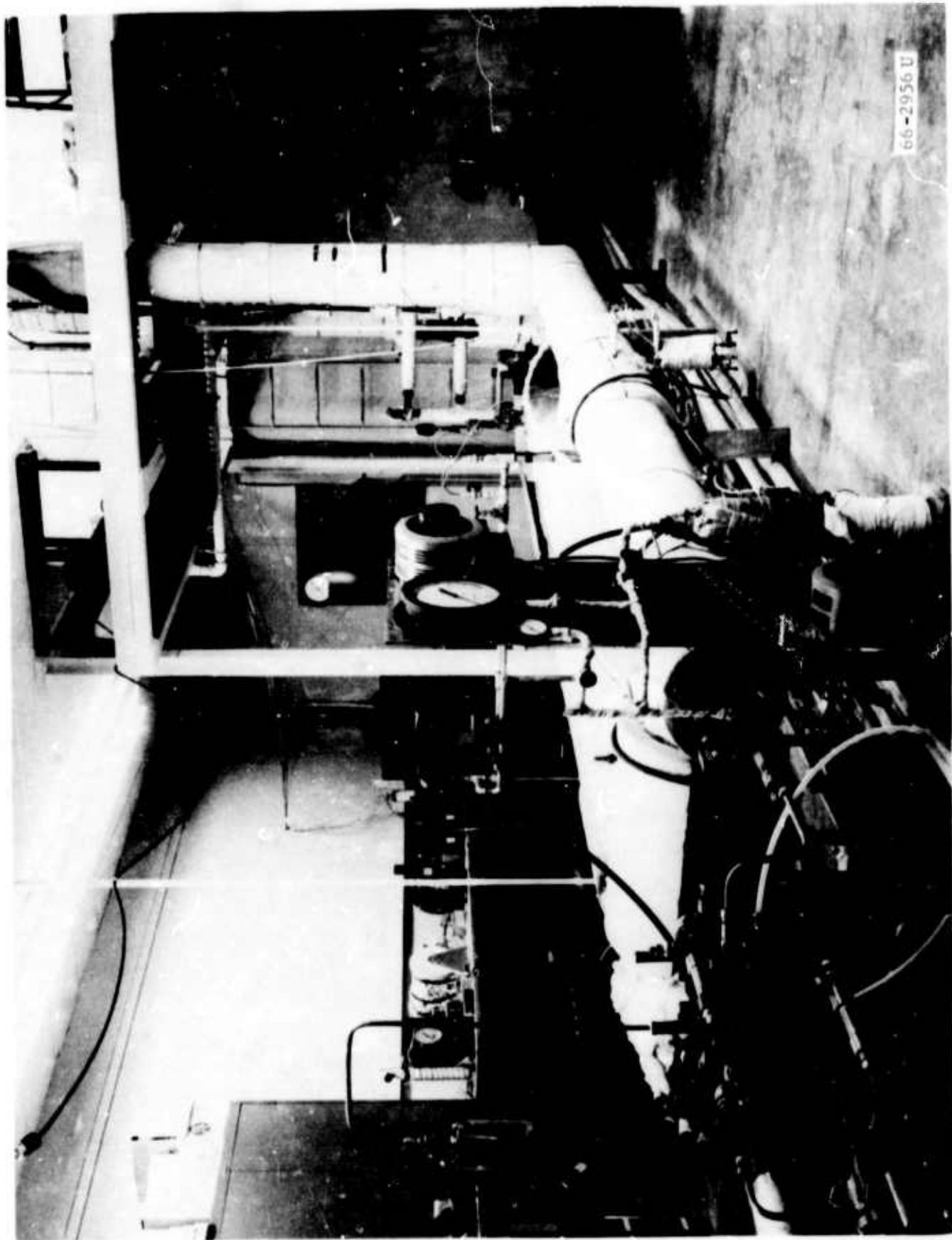
-15-

66-2956 U

FIGURE 6. FIRST FLOOR VIEW OF THE RECIRCULATING FLOW SYSTEM WITH INSULATION AND COOLING LINES IN PLACE

-16-

and exit sections are controlled manually with autotransformers. Both on/off controllers and a large autotransformer are used to control the preheater elements. The "fine" or trim heater located at the entrance to the top plenum is controlled by a Leeds & Northrup controller containing proportional, reset and rate modes of control. Control of the bulk gas temperature entering the top plenum is better than $\pm 1°F$. A portion of the electrical power control panel in the early stages of assembly of the system is shown in Figure 5.

Several of the cast alumina heating elements used on the test section (nominal 2 inch double extra heavy pipe honed out to 1.953 inches on the ID) are provided with holes to provide access for the probe holders and thermocouples spot welded to the back wall of the pipe. Numerous Chromel-Alumel thermocouples are located throughout the system to monitor the temperature variation with time at various critical locations.

3.5 NUCLEATE BOILING HEAT EXCHANGER

To cool the gas leaving the exit plenum down to a temperature compatible with the turboblower, a 2 inch tube in a 12 inch shell heat exchanger connected in parallel with a ball valve controlled 4 inch bypass line is installed upstream of the turboblower inlet. Boiling water, with the steam pressure controlled to 25 psig, has been found adequate for the various experiments so far completed. The liquid level in the shell is automatically controlled so as to maintain a level above the top of the center 2 inch pipe. The shell was designed so as to withstand pressures as high as 200 psig, thus permitting a much larger cooling capacity than has been found necessary.

All portions of the piping system are insulated with a 4 inch thickness of magnesia insulation. An approximately 2 inch thick blanket of magnesia insulation is wrapped around the turboblower shell as well.

3.6 PROBE HOLDERS AND ASSOCIATED SEALS

In Figure 7 the location of the heating elements, instrumentation probes, static pressure taps, and the trip plate are shown for the experiments discussed in Section 4. Also, a number of the important dimensions are shown in this figure.

Each of the probes used to obtain the radial profiles (TC, PT, and OP) is installed in a probe holder assembly (see Figure 8). The outer cylindrical housing of this assembly is sealed with a small "Flexitallic" gasket to the test section wall. A portion of the assembly consists of a barrel statically sealed to the probe with a compression fitting. The barrel is in turn sealed, with two Viton A o-rings in tandem, to the cylindrical housing. The o-rings provide a sliding seal. The cross section of the cylindrical housing is significantly reduced in the immediate vicinity of the test section wall. At that point a guard heater is installed to minimize the loss of heat from the test section wall by conduction to the ambient

-17-

$$D = 6"$$ $$L_5 = 24"$$
$$d = 1.952"$$ $$L_p = 1.3"$$
$$d_T = 1.5"$$ $$L_{sp} = 54"$$
$$L = 83"$$ $$L_6 = 12"$$
$$L_1 = 30"$$ $$L_7 = 6"$$
$$L_2 = 60"$$ $$L_H = 12"$$
$$L_3 = 60"$$ $$L_{TC} = 1.3"$$
$$L_4 = 60"$$

B0952U
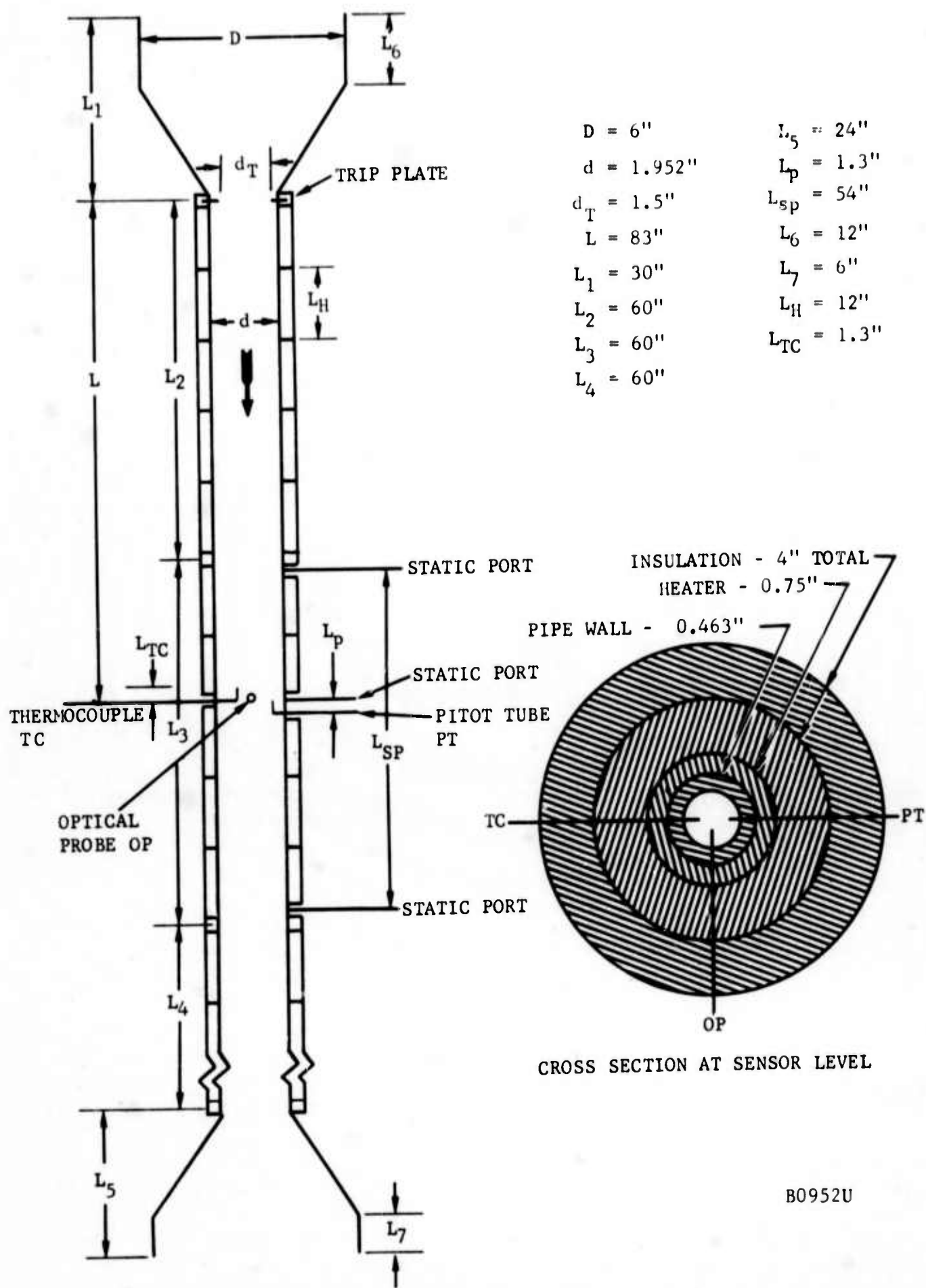
FIGURE 7. TEST SECTION DETAILS AND DIMENSIONS

-18-
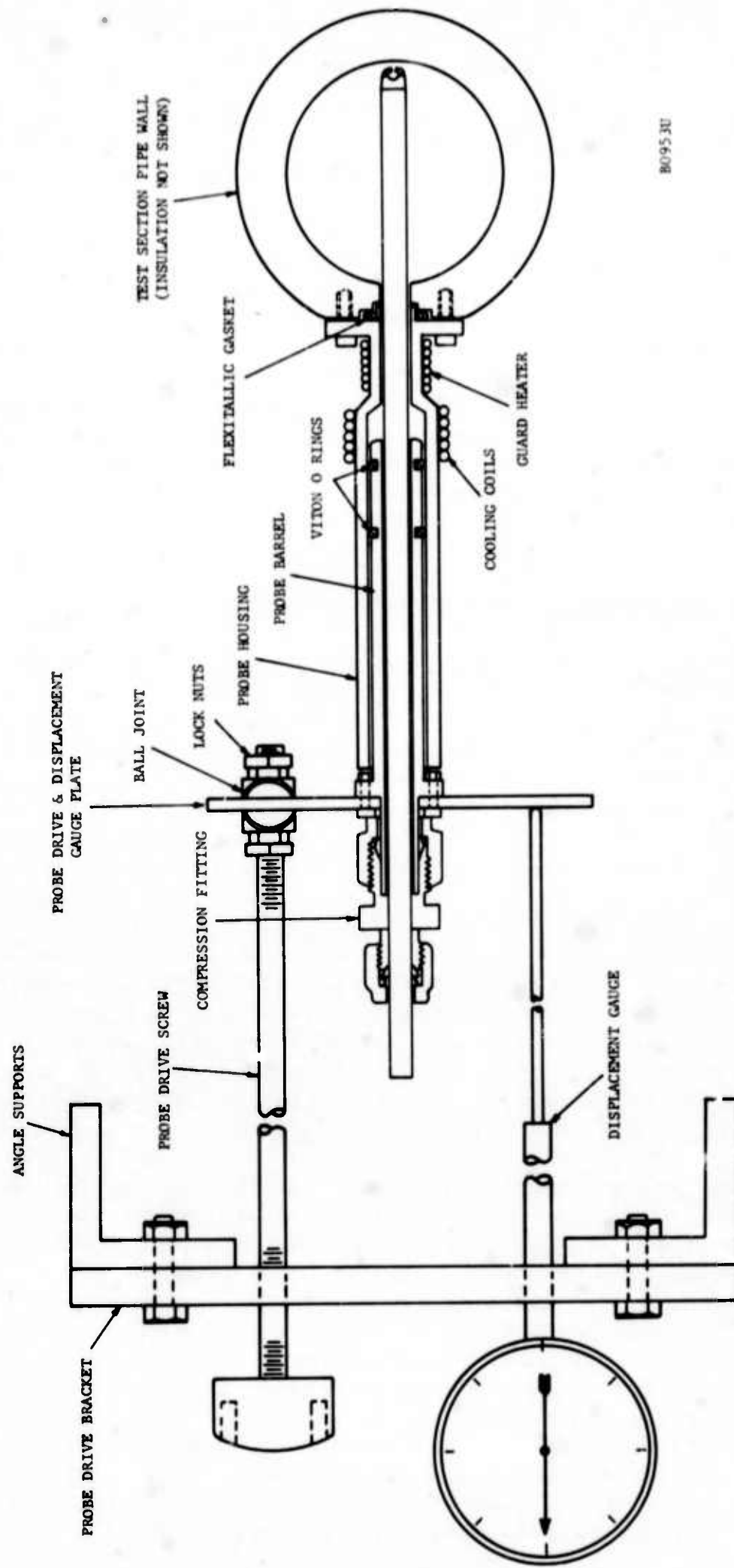
FIGURE 8. PROBE HOLDER ASSEMBLY (SHORT CONFIGURATION 9" PROBE; PROBE FULLY INSERTED)

ANGLE SUPPORTS

PROBE DRIVE BRACKET

PROBE DRIVE SCREW

COMPRESSION FITTING

PROBE DRIVE & DISPLACEMENT GAUGE PLATE

BALL JOINT

LOCK NUTS

PROBE HOUSING

PROBE BARREL

VITON O RINGS

COOLING COILS

GUARD HEATER

FLEXITALLIC GASKET

TEST SECTION PIPE WALL (INSULATION NOT SHOWN)

DISPLACEMENT GAUGE

B0953U

-19-

surroundings and to assist in maintaining a uniform temperature on the inside of the test section wall at the probe entry point. The temperature of the cylindrical housing near its flanged end at the test section wall is monitored with a thermocouple. The electrical power to the electrical resistance-type guard heater is manually adjusted so that this temperature is comparable to that measured at the outside wall of the test section. Farther back from the guard heater a small cooling coil is fitted to the outside of the cylindrical housing in order to maintain the temperature in the vicinity of the o-rings at a level which would ensure their proper functioning as seals ($< 400°F$). Each probe assembly is fitted with a calibrated drive system and displacement gauge sensitive to translations of 0.001 inch. The entire ensemble has made it possible to obtain reasonable radial profile data under quite hostile conditions.

3.7 INSTRUMENTATION

3.7.1 PRESSURE AND PRESSURE DIFFERENCE MEASUREMENTS

Since the vapor pressure of the N_2O_4-NO_2 system is such that at 10 atm total pressure the boiling point of liquid N_2O_4-$NO_$ is on the order of $80°C$, care must be taken to ensure that liquid droplets do not obstruct the pressure lines connected to the system. This has been accomplished by connecting each pressure line to a drip pot assembly (Reference 10) at a point close to the flow system itself and by guard heating to over $100°C$ the interconnecting pressure line between the system and the drip pot as well as the drip pot itself. The pressure line connecting the drip pot to the pressure sensor is, in each case, of considerable length. At the start of each experiment these lines are filled with dry N_2 to provide a buffer between the sensor and the drip pot. In no experiment has NO_2 vapor been detected at the sensor location. In some cases, erratic pressure difference measurements were thought to be caused by the hold-up of liquid N_2O_4-NO_2 in the pressure lines, possibly at some point between the drip pot and the sensor. When erratic results are being obtained, the simple expedient of purging with N_2 under pressure is used to clear the lines. This usually restores the system to its normal condition.

Total system pressure measurements are made with precision stainless steel bourdon tube gauges. All pressure difference measurements are made with the specially designed nulling-type micromanometer shown in Figure 9. Water is used as the displacement fluid. Displacements are measured to within 0.001 inch. Total displacements of up to 8 inches can be measured with this device. Both fine and coarse translations of the sloping glass capillary tube can be made. Accurate measurement of small pressure differences are required for the determination of mass flow rates with the aid of the orifice plate installed downstream of the blower outlet, for the determination of the static pressure drop down the test section (static pressure holes in the test section wall are 0.0135 inch in diameter), and for the determination of the local velocity in the test section with the aid of the total head tube and appropriately located static pressure tap (see Figure 7).
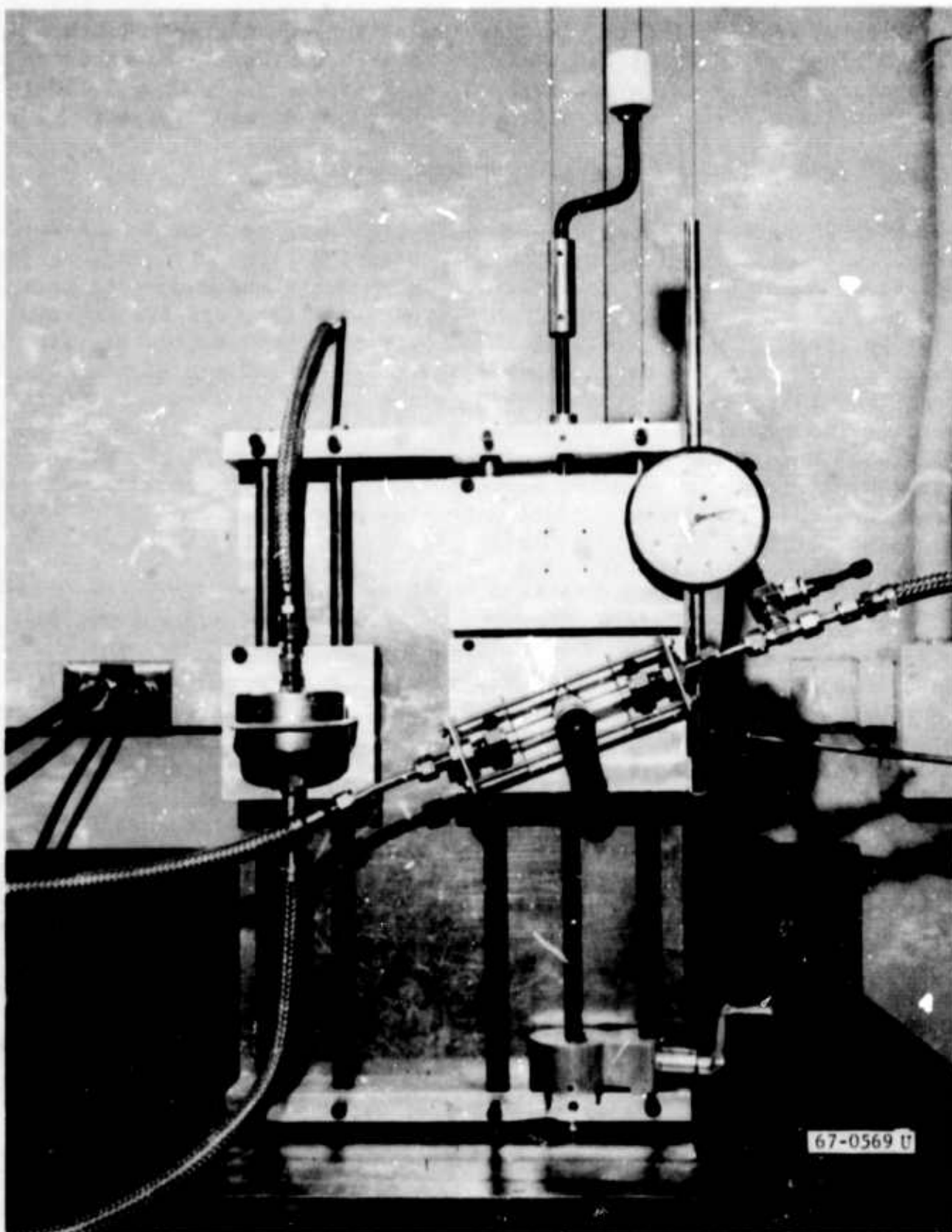
-20-

FIGURE 9.   PRECISION MICROMANOMETER FOR USE WITH HIGH PRESSURE
REACTING GASES

-21-

The orifice plate is of standard square edge design (orifice flange with orifice diameter of 2.15 inches — flange installed in a nominal 3 inch schedule 40 pipe). The sensing end of the total head tube is constructed of standard stainless steel hypodermic tubing (outside diameter $\simeq$ 0.050 inch or 0.065 inch, internal diameter $\simeq$ 0.034 inch or 0.040 inch, respectively).

3.7.2 MEAN TEMPERATURE AND HEAT FLUX MEASUREMENTS

The time-average radial temperature profiles are measured with a butt welded exposed junction of Chromel-Alumel thermocouple wire. The wires are sealed in a stainless steel support tube filled with magnesia and swaged to effect a pressure tight seal around each of the wires. The fast response thermocouple probe (see Paragraph 3.7.3) is also used for time-average profile measurements. It consists of an exposed junction of Platinum/Platinum-10 percent Rhodium. In both cases the junction is in the shape of a sphere several times larger than the supporting wire diameter. The sizes for the Chromel-Alumel couple are: sheath outside diameter = 0.062 inch, wire diameter = 0.011 inch and junction diameter = 0.020 inch. All temperatures are measured with a precision potentiometer (Leeds and Northrop Model K-3) (see Appendix I, Table V). The overall accuracy of the time-average temperature measurements is estimated to be within 0.1°F.

Wall heat fluxes are determined by measuring the electrical power dissipated in a 1 foot long heating element (consisting of two semicylindrical halves) located just upstream of the probe insertion position in the center test section (see Figure 7). Longitudinal losses in the test section wall are accounted for with the aid of axial back wall temperature measurements via spot-welded thermocouples (leads from the junction were "guard heated" by being aligned with and attached to the back wall for several inches away from the junction). Losses through the 4 inch thickness of magnesia insulation are accounted for by measuring the temperature at two different depths in the insulation. Inside wall temperatures at the steady state are determined by calculation knowing the net heat flux into the test section wall, the back wall temperature, the wall thickness, and the dependence on temperature of the thermal conductivity of the wall material. An indication of how the total power consumed by one heating element varies with time during the course of an experiment is shown in Figure 10. Note that approximately 4 hours are required for the heat flux to settle down to a reasonably steady value. Considering the uncertainty associated with the corrections, we estimate that the heat fluxes are known to within 10 percent (at best).

3.7.3 THE FAST RESPONSE THERMOCOUPLE PROBE AND ASSOCIATED ELECTRONICS

The sensor selected for use in measuring the fluctuating temperature and its dependence on frequency in the high temperature reacting NO_2 system is a fast response thermocouple based on the design of Sesonske and coworkers (References 11 and 12). The form being used in this investigation is shown in Figure 11. The junction size is expected to be small enough so that its frequency response should be good out to 10 kHz (Reference 11). The fluctuating dc signal from the thermocouple probe is amplified by a low noise

-22-
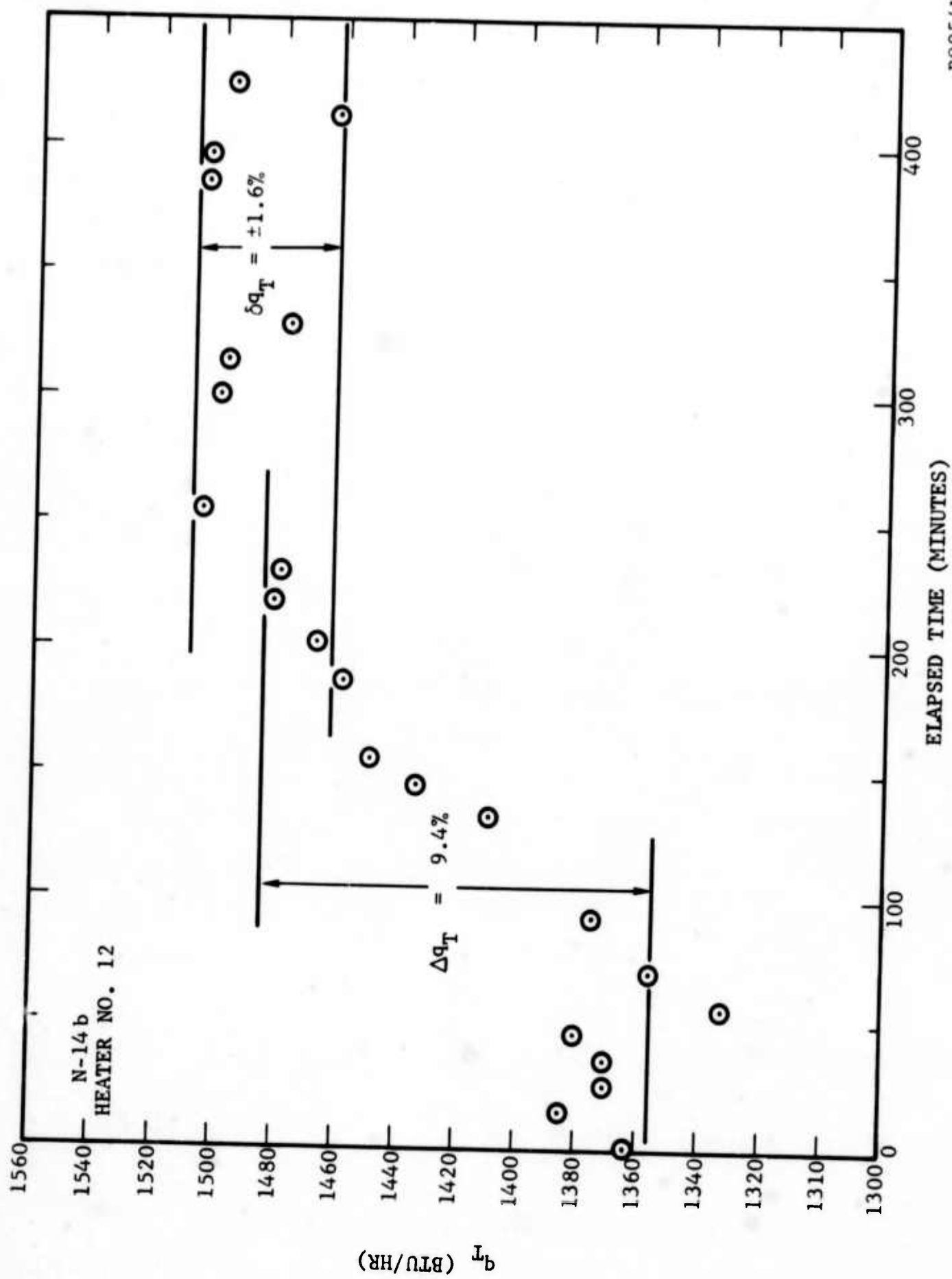
FIGURE 10. VARIATION WITH TIME OF THE TOTAL ELECTRICAL POWER REQUIRED BY ONE HEATING ELEMENT ON THE TEST SECTION (1 FOOT LENGTH)
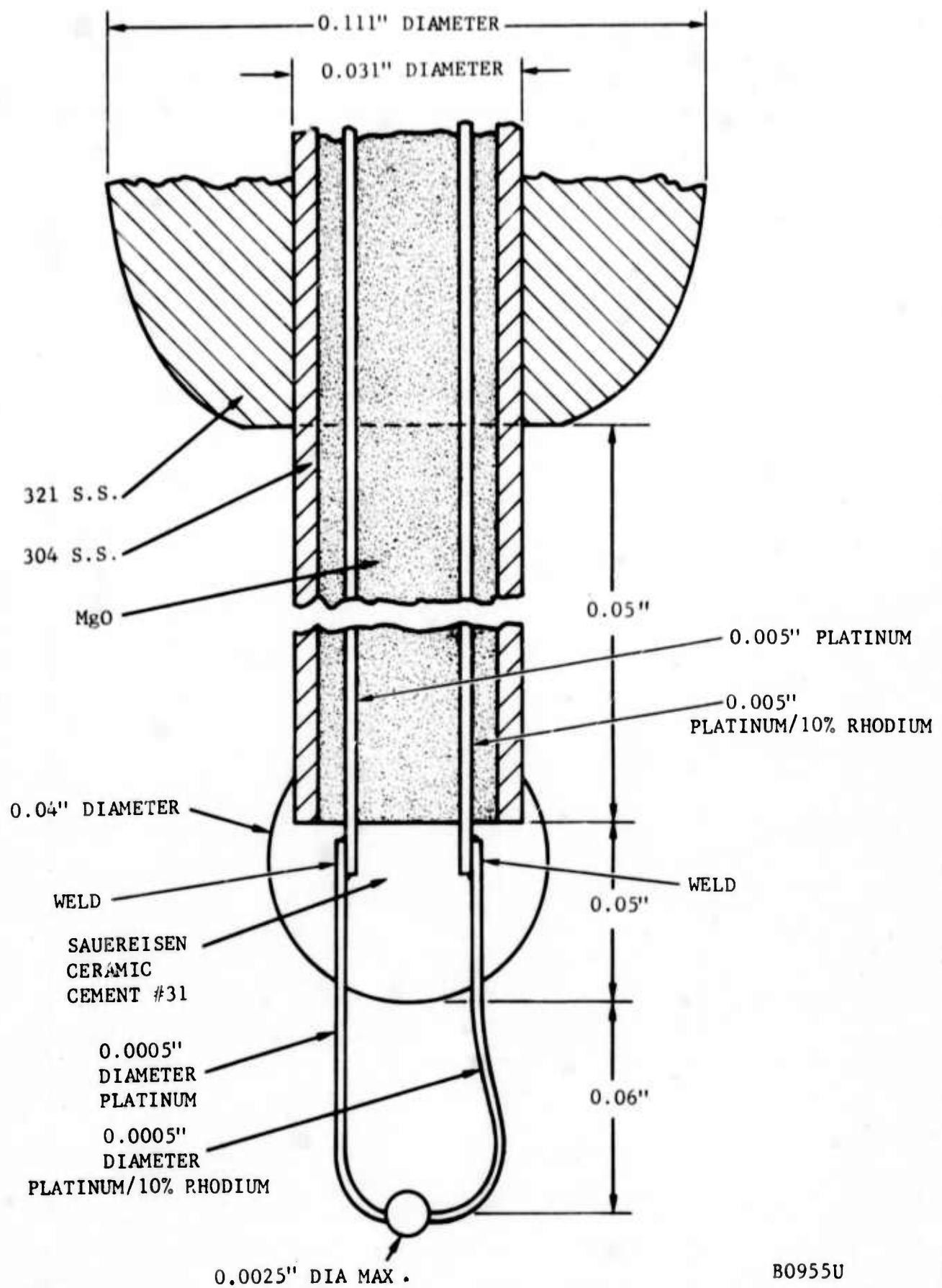
B0954U

-23-

FIGURE 11. SENSING END - FAST RESPONSE THERMOCOUPLE PROBE

-24-

amplifier modified so as to have a gain of 12,600:1 (References 13 and 14) see Appendix I, Table V). The output of the amplifier is independent of frequency in the range 10 Hz to 1 kHz. The narrow band noise was measured over this frequency range and was found to be on the order of 0.01 to 0.05 microvolt.. Input signal levels with the corrosion resistant Platinum/ Platinum-10 percent Rhodium thermocouple are on the order of 20 to >100 micro-volts. The data from the probe/amplifier system are processed according to the methods outlined by Rust (Reference 15). The electronic instruments used to carry out the data processing are shown in Figure 12 . The connections between the instruments is shown in Figure 13 . A bandwidth calibration for the wave analyzer used in obtaining the spectral information is shown in Figure 14 (Determined by the method of Reference 16). A true RMS meter is used to obtain the wide band, or total, rms fluctuating temperature.

3.7.4 THE OPTICAL PROBE SYSTEM FOR MEASUREMENT OF LOCAL NO_2 CONCENTRATIONS

Lambert-Beers absorption law,

$$\frac{I}{I_o} = \exp\left(- \epsilon_{NO_2} \ell \, c_{NO_2}\right) \qquad (3)$$

is the basis for the design of a light absorption system capable of measuring the local NO_2 concentration in the high temperature flow system in which the total gas pressure could reach values as high as 150 psig.*

An optical probe system used for making local transmittance measurements in dye and water flows at ~ 25°C and 1 atm has been described by Brodkey and coworkers (References 17 and 18). The system and probe design developed for use in this investigation are significantly different than that used by Brodkey and coworkers. It is a dual beam (sample and reference), chopped system with high signal-to-noise ratio characteristics and good stability.

The optical system used in this investigation is shown in Figures 15 and 16. Radiant energy emitted by the tungsten iodine light source (A) is divided into two separate channels, reference and sample, by the cubic beamsplitter (B). After traversing the two optical paths, the energy is brought to a common focus on the face of the photomultiplier tube (I). In order for the PMT to receive both reference and sample signals alternately, a reflective chopper is inserted in the system near the PMT. The chopper alternates passing the sample signal and reflecting the reference signal for equal amounts of time.

The sample channel which contains the optical test probe for the concentration measurements absorbs a significantly larger amount of radiation than the reference channel. Consequently, it requires a greater amount of input

_____

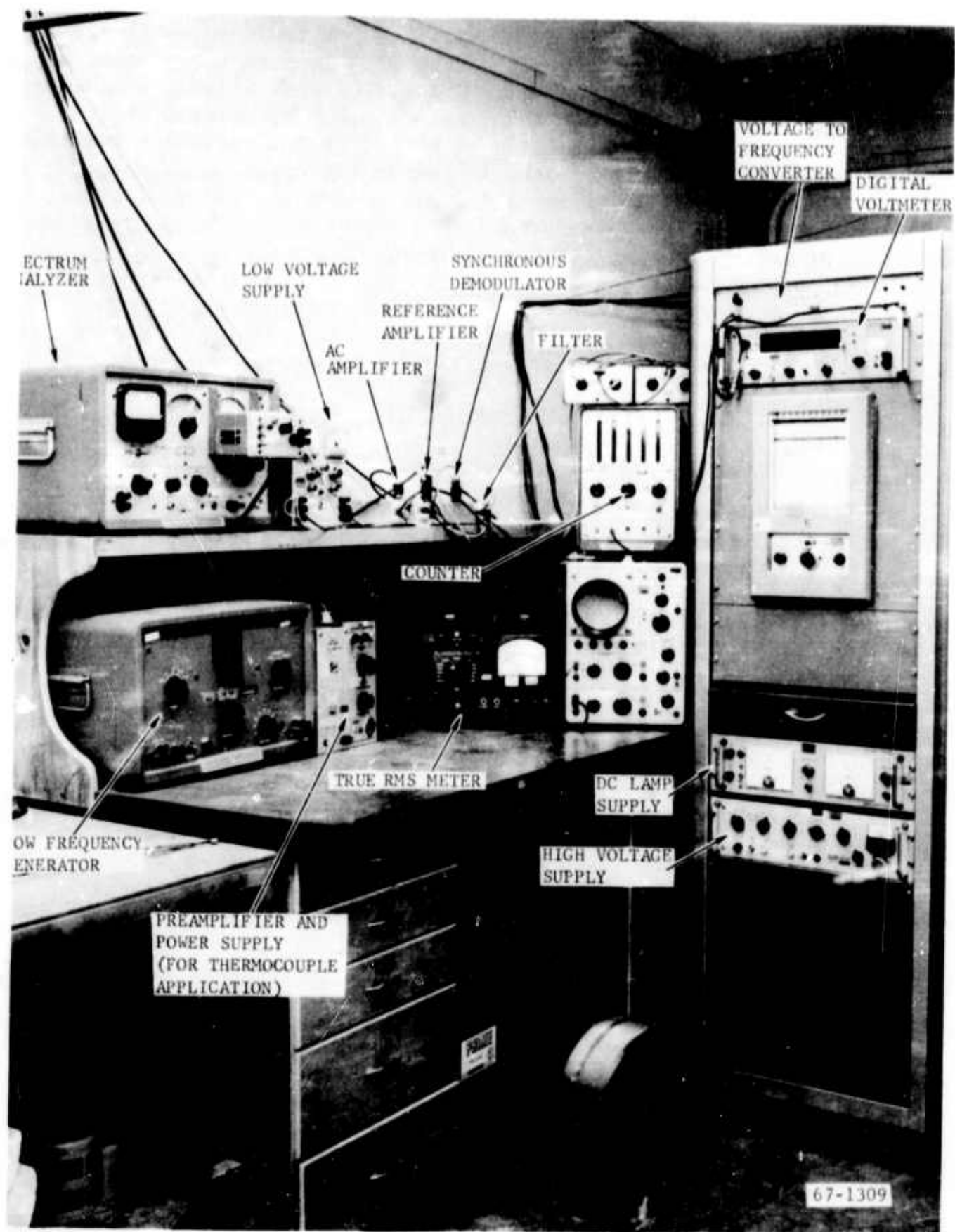*$\epsilon_{NO} = \epsilon_{O_2} \simeq 0$ for $3000 < \lambda < 5000$ angstroms.

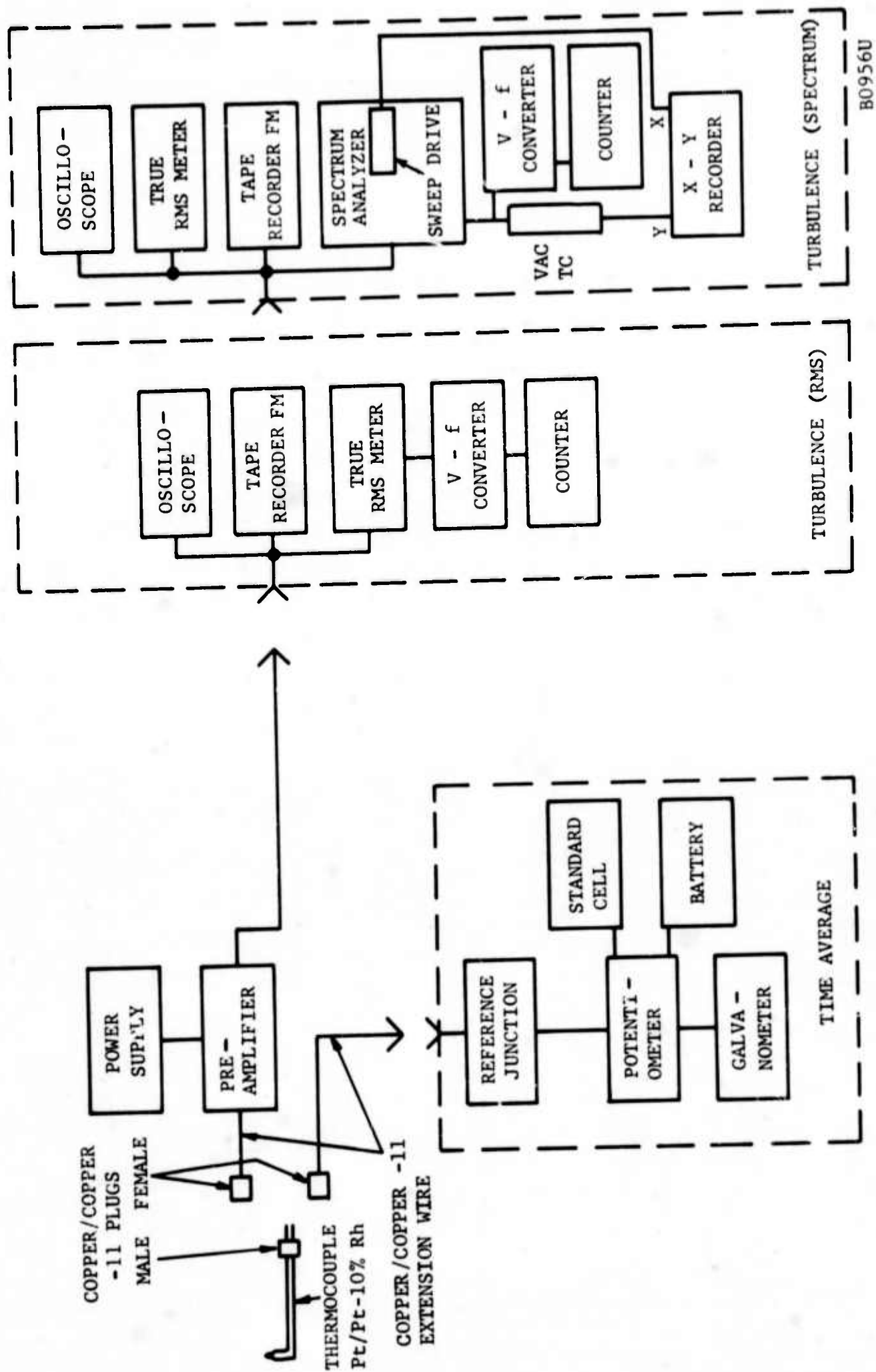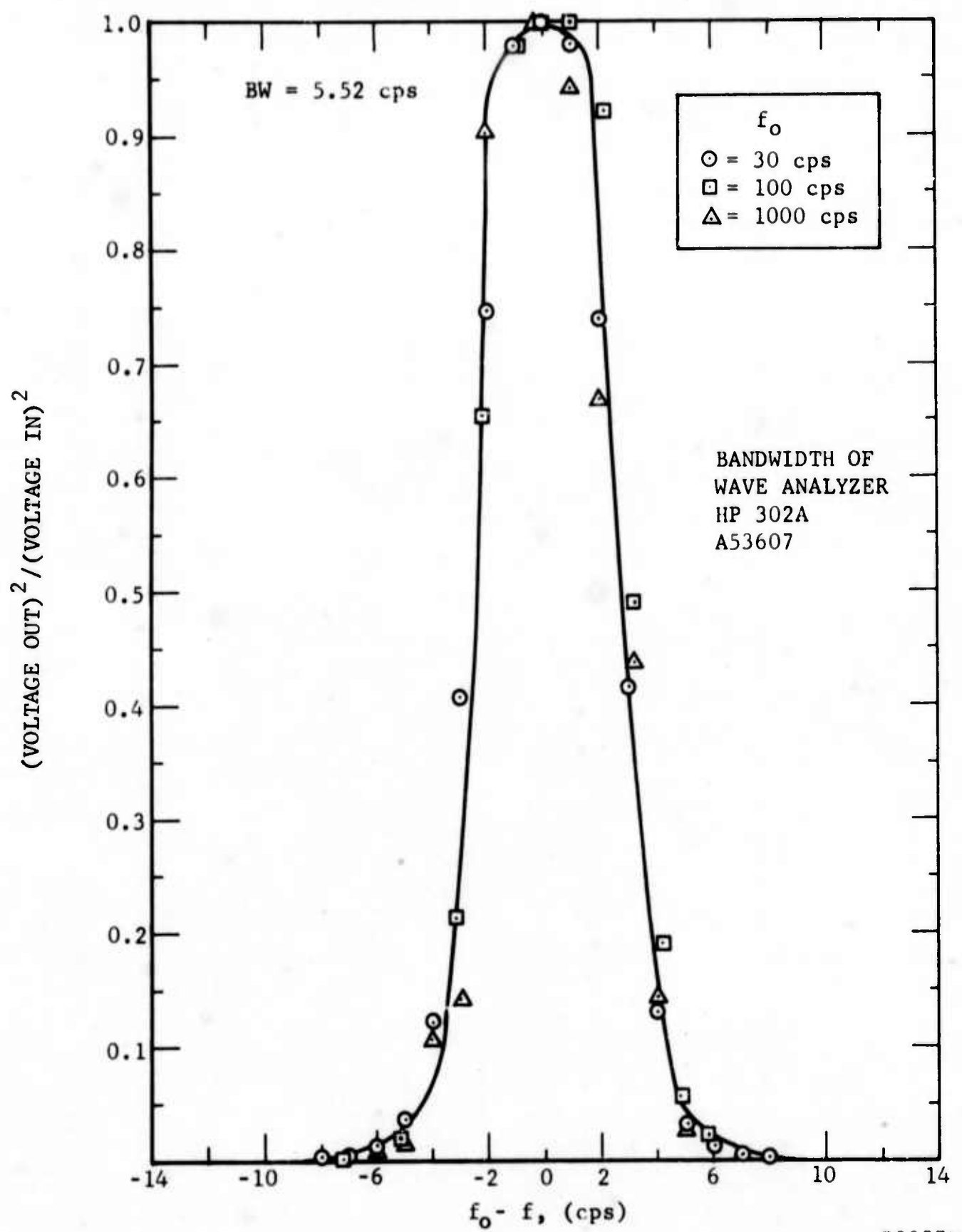FIGURE 12. INSTRUMENTATION FOR THE OPTICAL PROBE SYSTEM AND FOR THE FAST RESPONSE THERMOCOUPLE PROBE

FIGURE 13. SCHEMATIC DIAGRAM OF THE ELECTRONIC SYSTEMS USED FOR THE TIME AVERAGE AND FLUCTUATING TEMPERATURE MEASUREMENTS

-27-

FIGURE 14. BANDWIDTH CALIBRATION OF THE WAVE ANALYZER

radiation if a balance between the two channels is to be obtained at the PMT. The beamsplitter transmits more energy than it reflects; therefore, it is positioned so that the reference channel receives the reflected radiation and the sample channel receives the transmitted radiation.

The optical test probe consists of glass fiber bundles, plastic fibers, tapered light pipes, and plastic fiber bundles used as input and output optical leads. The overall configuration of the optical probe itself is shown in Figure 17. The probe tip region is shown in Figure 18. The gap between the optical fiber bundles is ~0.010 inch (the exact gap was different for each probe made). The optical fiber bundle diameter is 0.025 inch. The bundle pair is contained in a 0.25 inch OD 316 stainless steel tube ~12 inches long. The transition from the stiff fiber bundles containing the high temperature glass to the flexible fiber lines used to connect the probe to the optics is made with the plastic fibers and tapered light pipes in the rectangular housing shown in Figure 17. Ceramic cement is used to fix the gap width at the sensing end (Figure 18). It was found necessary to thermally condition the probe sensing end at high temperature to obtain stable performance characteristics. Measurements of the effect of thermal conditioning on the transmittance of light through the probe and a direct measurement of the probe tip gap width change with temperature are shown in Figures 19 and 20.

In addition to the apparatus discussed above, the sample channel also contains two lens assemblies, (J) and (N). Lens assembly (N) focuses the radiation from the source at the end of the input optical lead, and lens assembly (J) focuses the radiation emerging from the output fiber lead on the face of the PMT. The lens assemblies (J) and (N) have focal lengths of 2.3 inches and 1.3 inches, respectively.

The reference channel is similar to the sample channel, except for the addition of two iris diaphragms and the lack of an optical probe. The iris diaphragms are used to balance the two signals by controlling the amount of light passing through the reference channel.

To enhance the performance of the electronic system, an even level of illumination was maintained at the surface of the PMT by forming nearly identical images at the PMT face. Since the image of the sample channel was formed with a fiber bundle end as the object, a fiber bundle (E) has been used in the reference channel. The fiber bundle has the same effective 1/8 inch diameter as the input-output leads of the optical probe and has a length of 6 feet, approximately the same as the path length of the probe with leads (K) and (M) attached.

The lens assembly (C) focuses the energy of the source onto the end of the fiber bundle. The assembly consists of two single convex lenses with an effective focal length of 2.7 inches.

-29-

LIGHT SOURCE A

BEAMSPLITTER B

LENS ASSEMBLY N

INPUT FIBER LEAD M

SAMPLE PATH

LENS ASSEMBLY C

IRIS DIAPHRAGM D

REFERENCE PATH

REFERENCE FIBER BUNDLE E

LENS ASSEMBLY J

LED

CHOPPER MOTOR

OUTPUT FIBER LEAD K

SAMPLE PROBE

B0958U

IRIS DIAPHRAGM F

LENS ASSEMBLY G

PHOTO FET

CHOPPER MIRROR H

FILTER O

PHOTOMULTIPLIER TUBE I
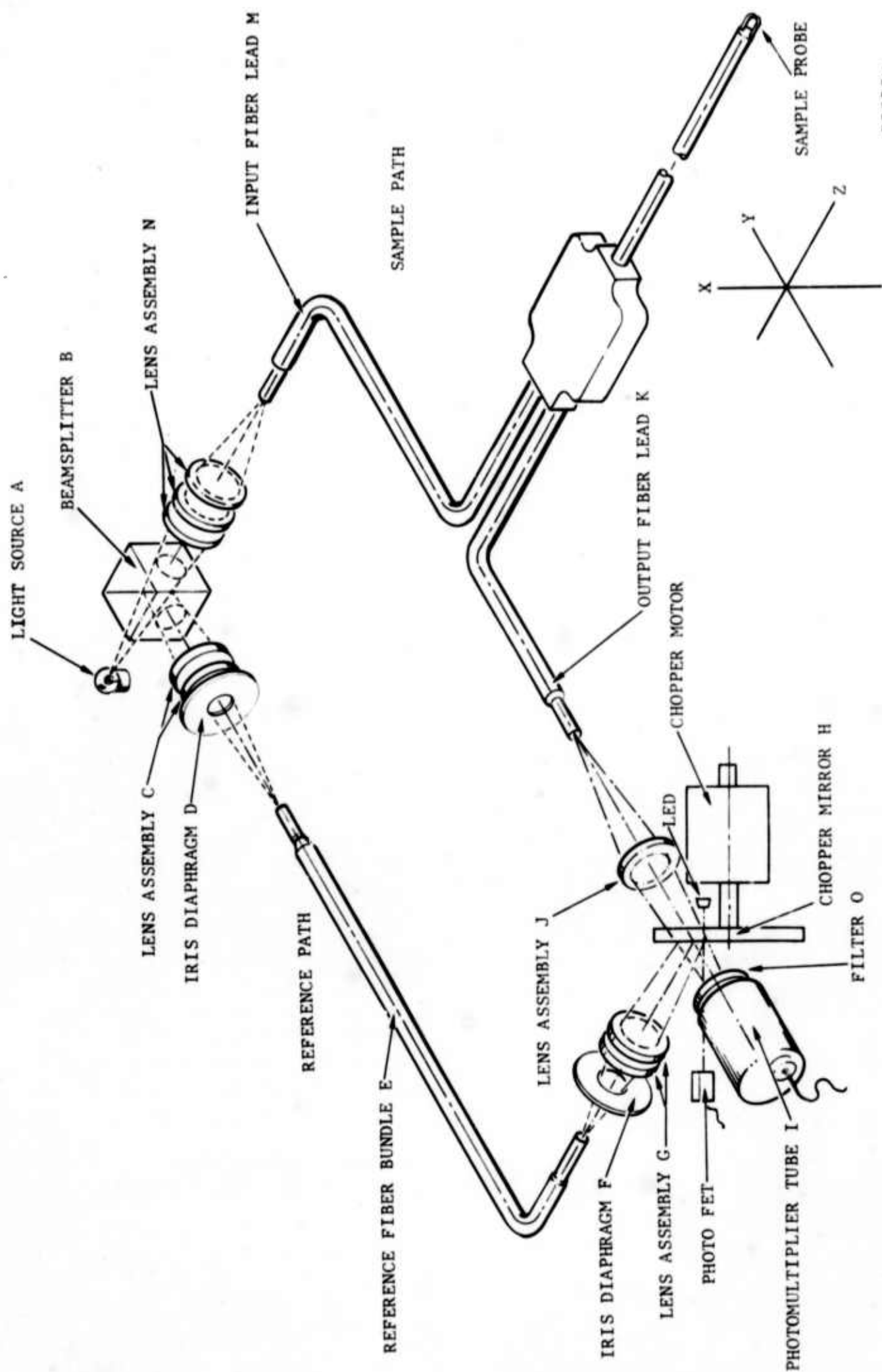
FIGURE 15. OPTICAL SYSTEM SCHEMATIC

-30-

FIGURE 16. OPTICAL SYSTEM SCHEMATIC

B0959U

-31-

68-0459U

FIGURE 17. OVERALL CONFIGURATION OF THE FIBER OPTICS PROBE
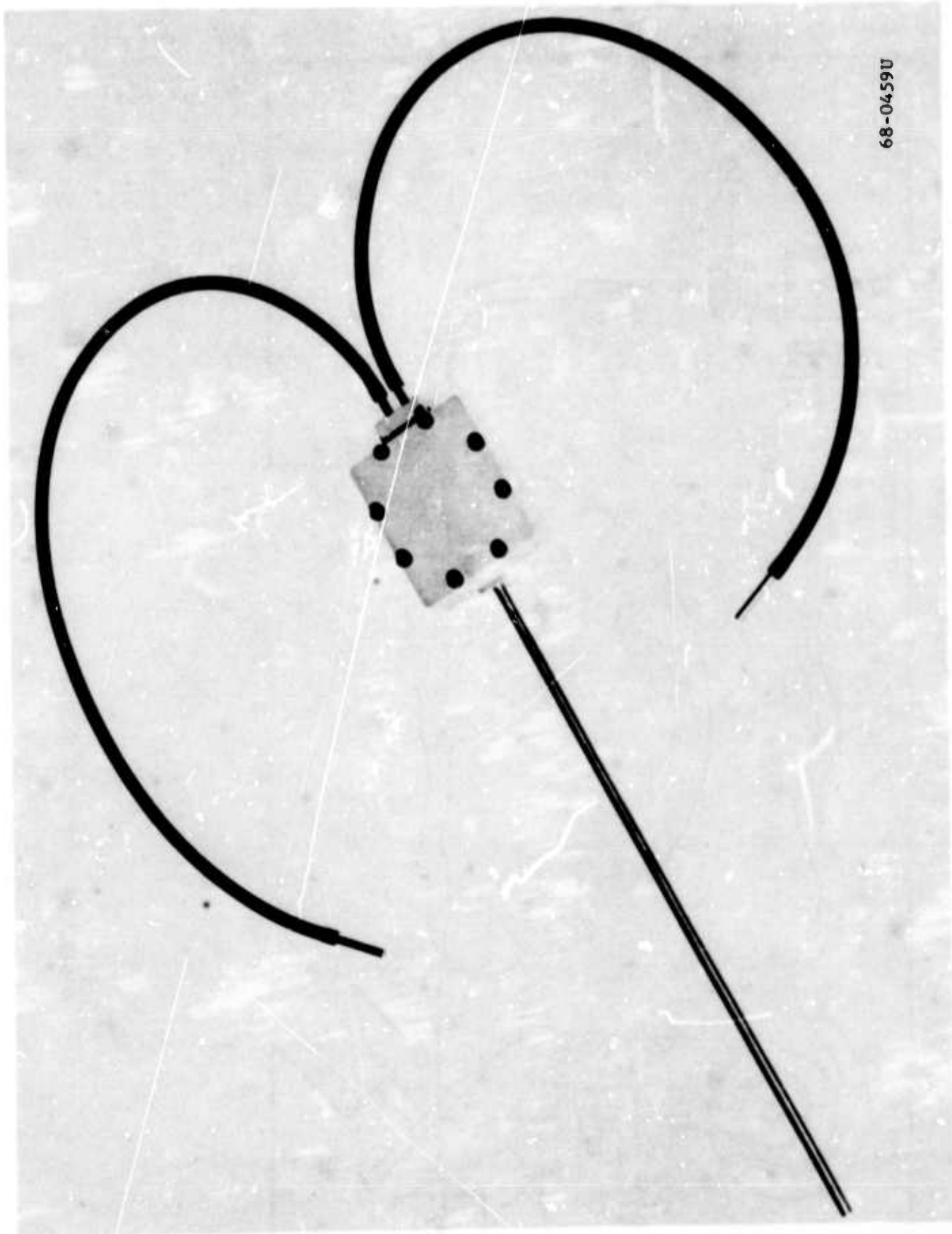(¼" IN OUTSIDE DIAMETER x ~ 12" LONG)

-32-
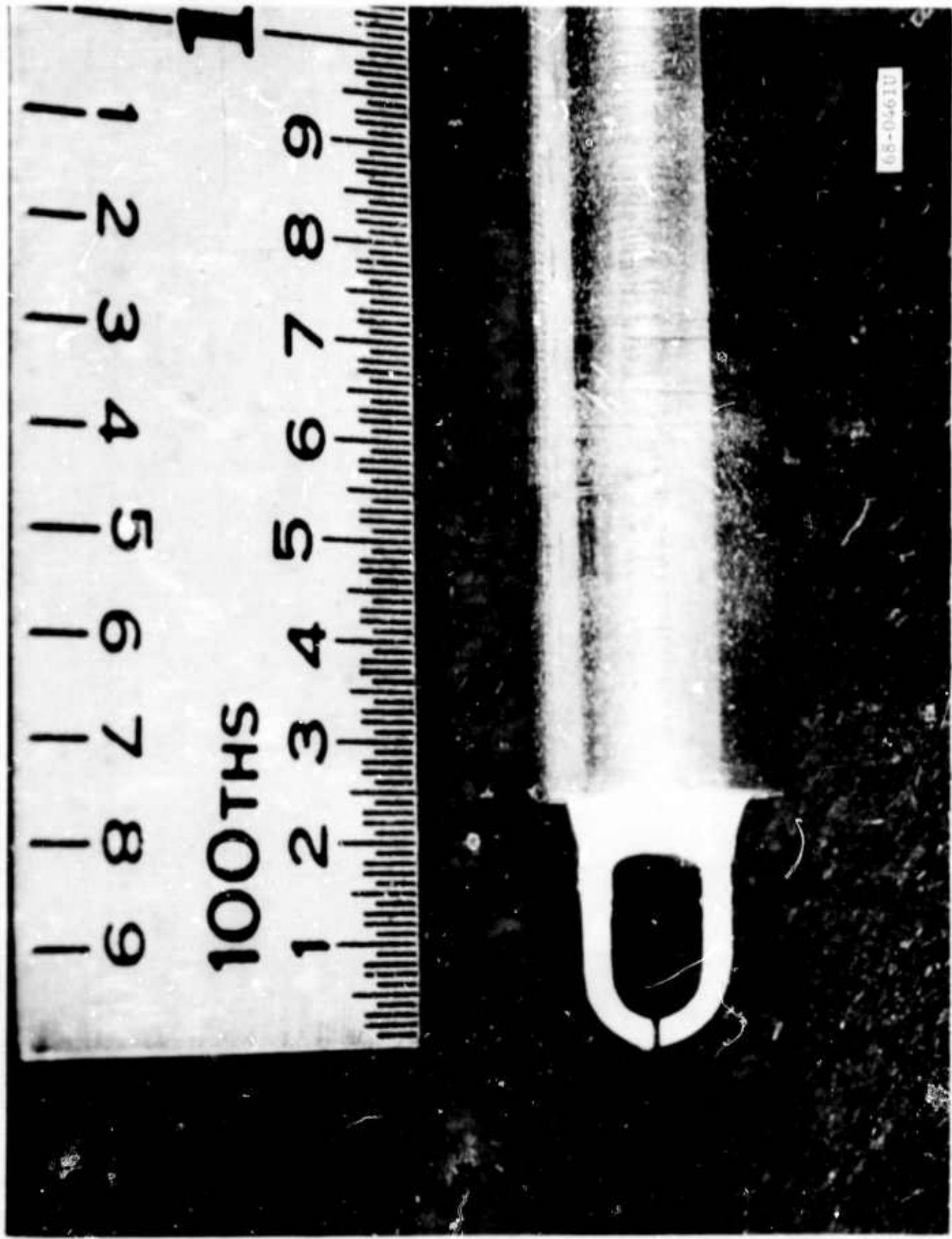
FIGURE 18. SENSING END OF THE FIBER OPTICS PROBE

-33-
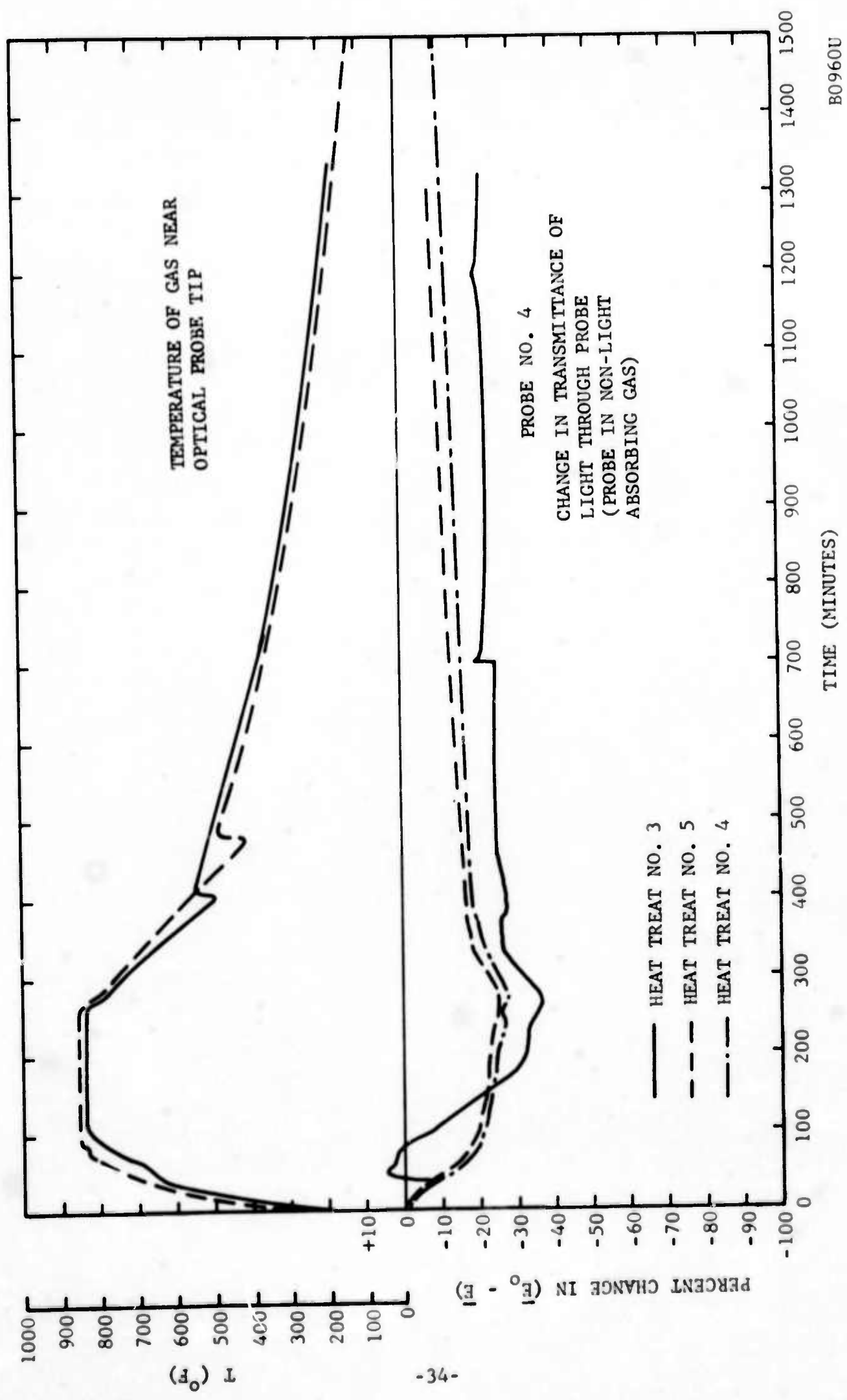
FIGURE 19. THERMAL CONDITIONING CHARACTERISTICS OF AN OPTICAL FIBER PROBE (AIR TESTS)

-34-
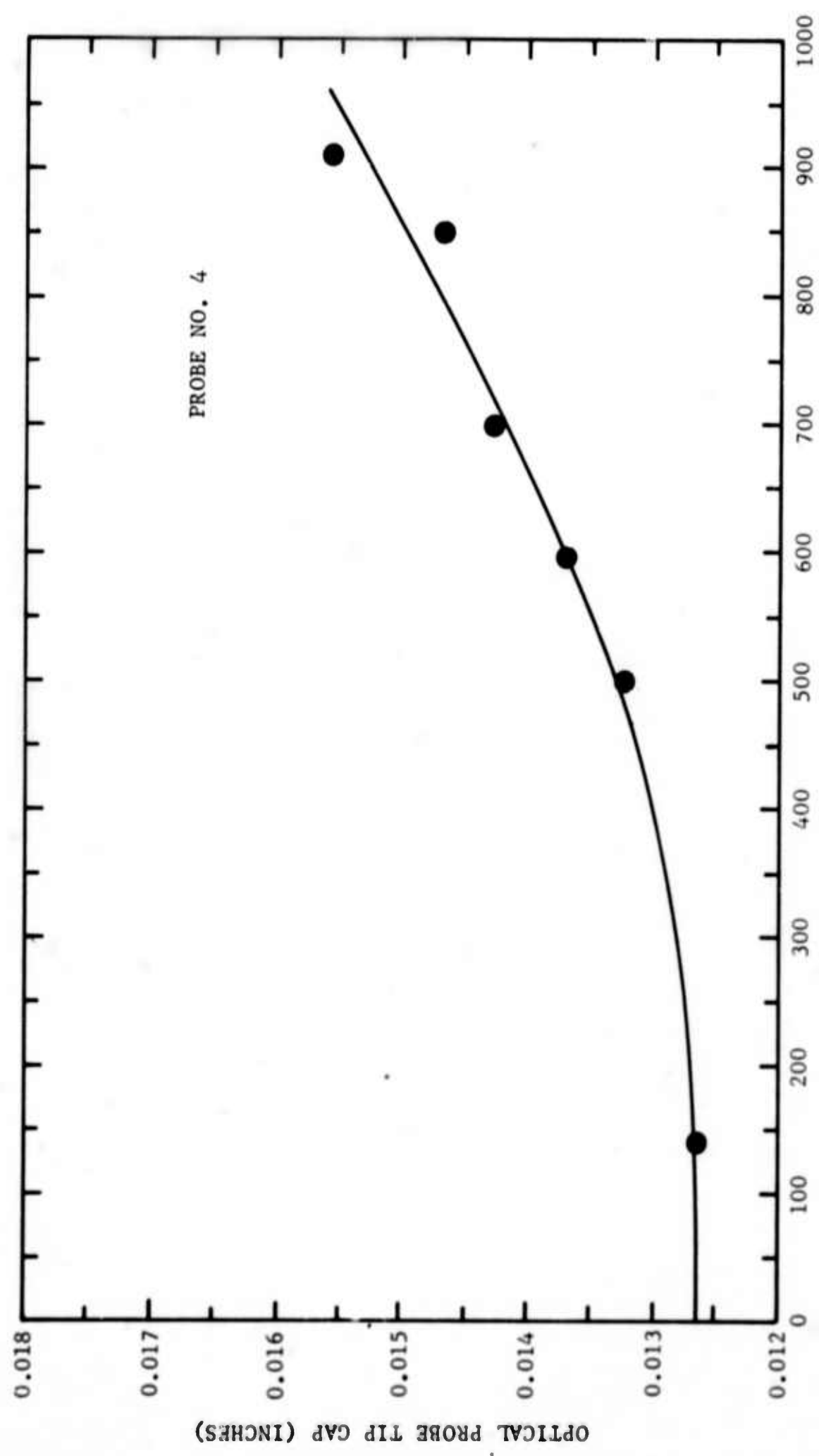
B0960U

FIGURE 20. CHANGE IN OPTICAL PROBE TIP GAP WIDTH WITH TEMPERATURE

B0961U

-35-

In addition to the two channels, a light emitting diode (LED) is used in combination with a field effect transistor and chopper for synchronous demodulation. An optical filter, located in front of the photomultiplier, eliminates extraneous LED radiation from reaching it. The filter also shapes the spectral composition of the light striking the photomultiplier tube.

The spectral characteristics of the photomultiplier tube and the filter are shown in Figure 21. The associated electronics layout is shown in Figure 22* (see Appendix I, Table VI). With the system so arranged the signal-to-noise ratio of the entire system was on the order of 250:1 which is quite adequate for measurement of both the time-average and fluctuating concentrations. The electronic instruments used with the optical probe are shown assembled in Figure 12.**

Measurements of the extinction coefficient $\epsilon_{NO_2}(\lambda, T)$ were made with a pair of 0.25 inch quartz rods in place of the optical fiber probe. The measurements were made with NO_2 contained in a static reactor consisting of a 1 foot long section of the same pipe material used in the test section. In Figure 24, the optical housing system is shown with the light-tight cover plates removed. Liquid N_2O_4-NO_2 was vaporized into the static reactor to the desired pressure. Temperature was controlled with resistance heaters around the outside of the reactor. The distance between the polished and optically flat ends of the quartz rods was measured to 0.001 inch with a precision displacement gauge. Measurements of transmittance with this system were commenced only after sufficient time had been allowed to elapse (Figure 2) so that chemical equilibrium would be expected to prevail throughout the gas in the static reactor. The 4360 angstrom results*** obtained for 2, 5, and 10 atm total pressure and temperatures to >900°K are shown in Figure 25 and Table I. The resulting extinction coefficient data are shown in Figure 26 compared to the scatter of the data of Schott and Davidson (References 19 and 20). The results are comparable.

---

*The filtered output of the synchronous demodulator is directly proportional to $\bar{E}_o$-$\bar{E}$, the time-average voltage difference corresponding to the reference and sample beams, respectively (see Figure 23).

**Neutral density filters were used in the transmittance calibration of the system.

***Obtained using a narrow band Bausch and Lomb interference filter.
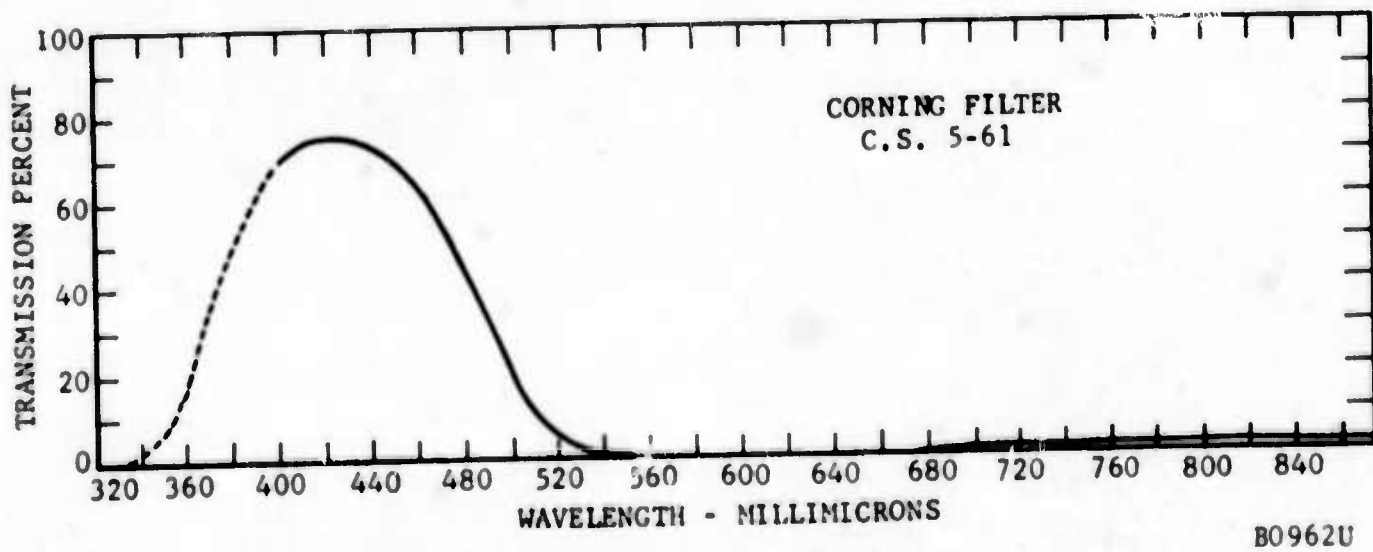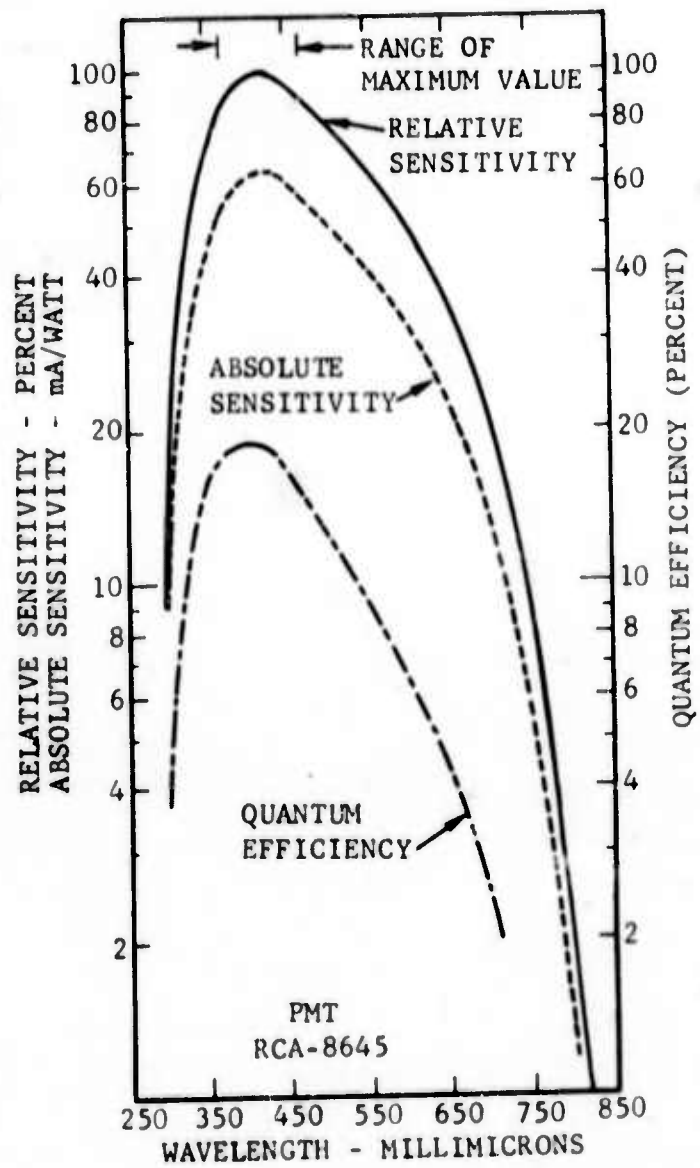
FIGURE 21. CHARACTERISTIC SPECTRAL CURVES OF THE PHOTOMULTIPLIER TUBE
AND THE FILTER

-37-
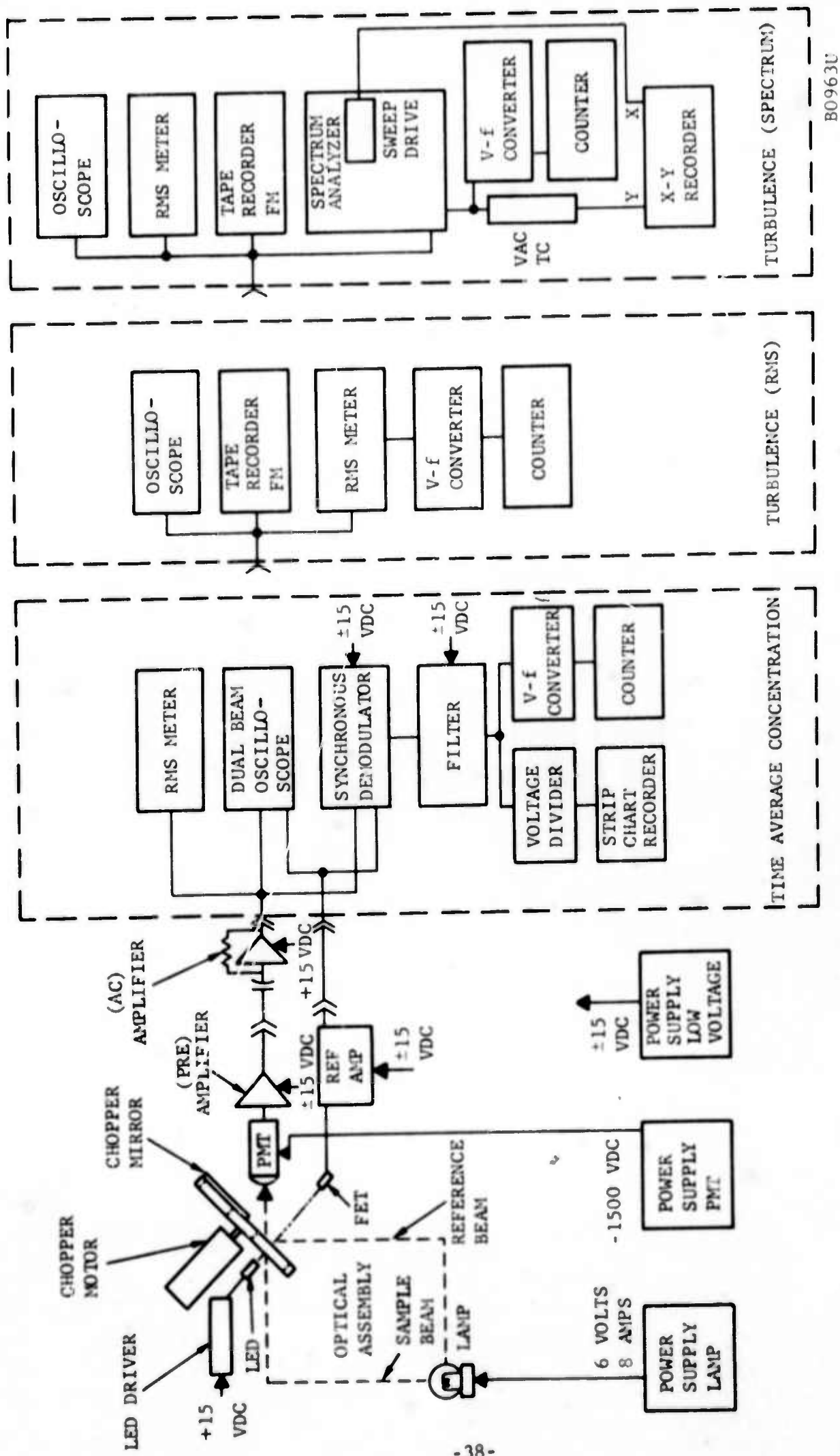
FIGURE 22. SCHEMATIC DIAGRAM OF ELECTRONIC SYSTEM USED FOR THE TIME AVERAGE AND FLUCTUATING CONCENTRATION MEASUREMENTS

-38-

E = E$_0$ CONDITION (BALANCE OF INTENSITIES -- SAMPLE
AND REFERENCE BEAMS)

UPPER BEAM
0.5 V/CM

AMPLIFIED PMT
OUTPUT $\propto (E_0 - E)$

LOWER BEAM
5 V/CM

AMPLIFIED FET
OUTPUT -
DEMODULATION
TRIGGER

TIME (MILLISECONDS)
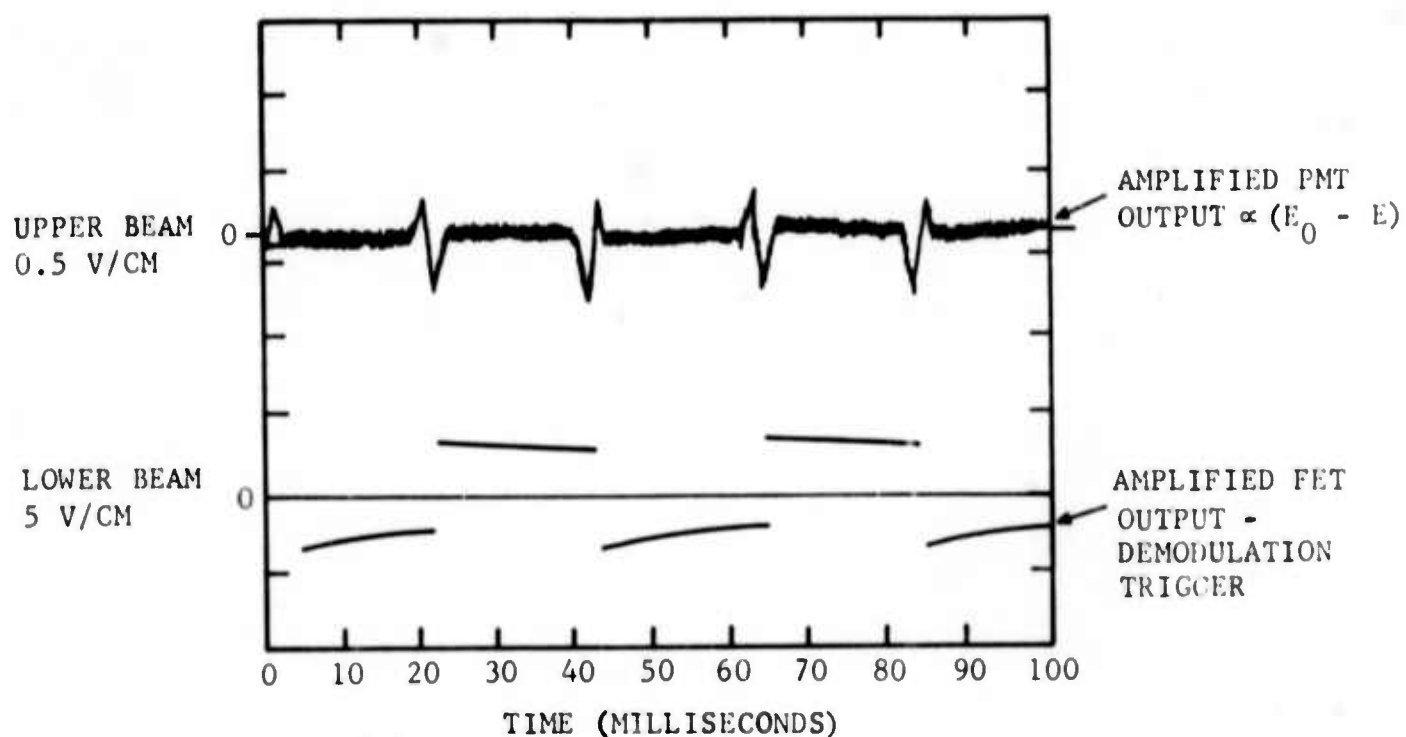
E = 0 CONDITION (SHUTTER BLOCKING SAMPLE BEAM:
$\overline{E}_0$ (FILTER OUTPUT) = -4.5V

UPPER BEAM
0.5 V/CM

AMPLIFIED PMT
OUTPUT $\propto (E_0 - E)$

LOWER BEAM
5 V/CM

AMPLIFIED FET
OUTPUT -
DEMODULATION
TRIGGER
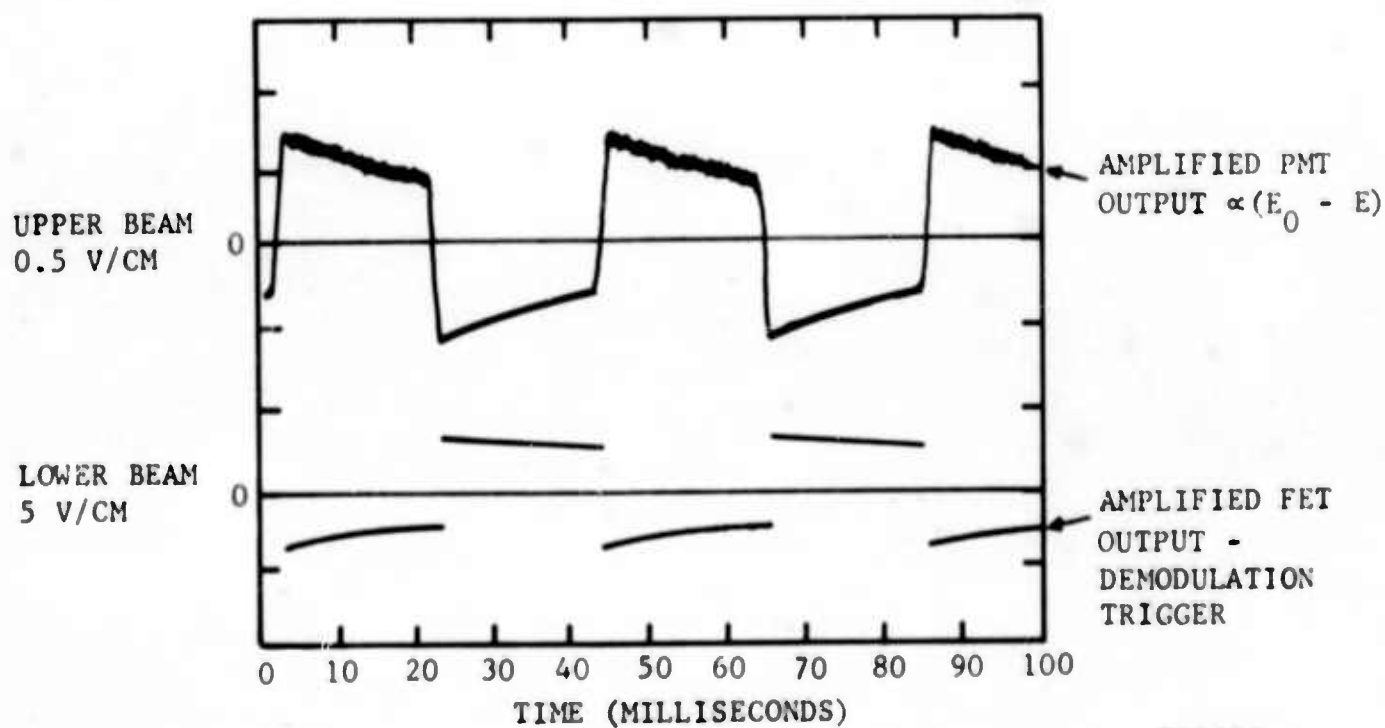
TIME (MILLISECONDS)

B0964U

FIGURE 23.   COMPARISON OF AMPLIFIED PMT AND FET OUTPUTS FOR THE CASE OF NO
ABSORPTION OF THE SAMPLE BEAM (E = E$_0$) AND MAXIMUM ABSORPTION OF
THE SAMPLE BEAM (E = 0) (U)
CHOPPING FREQUENCY = 23.3 Hz
PEAK WIDTH   21.5 MILLISECONDS

-39-
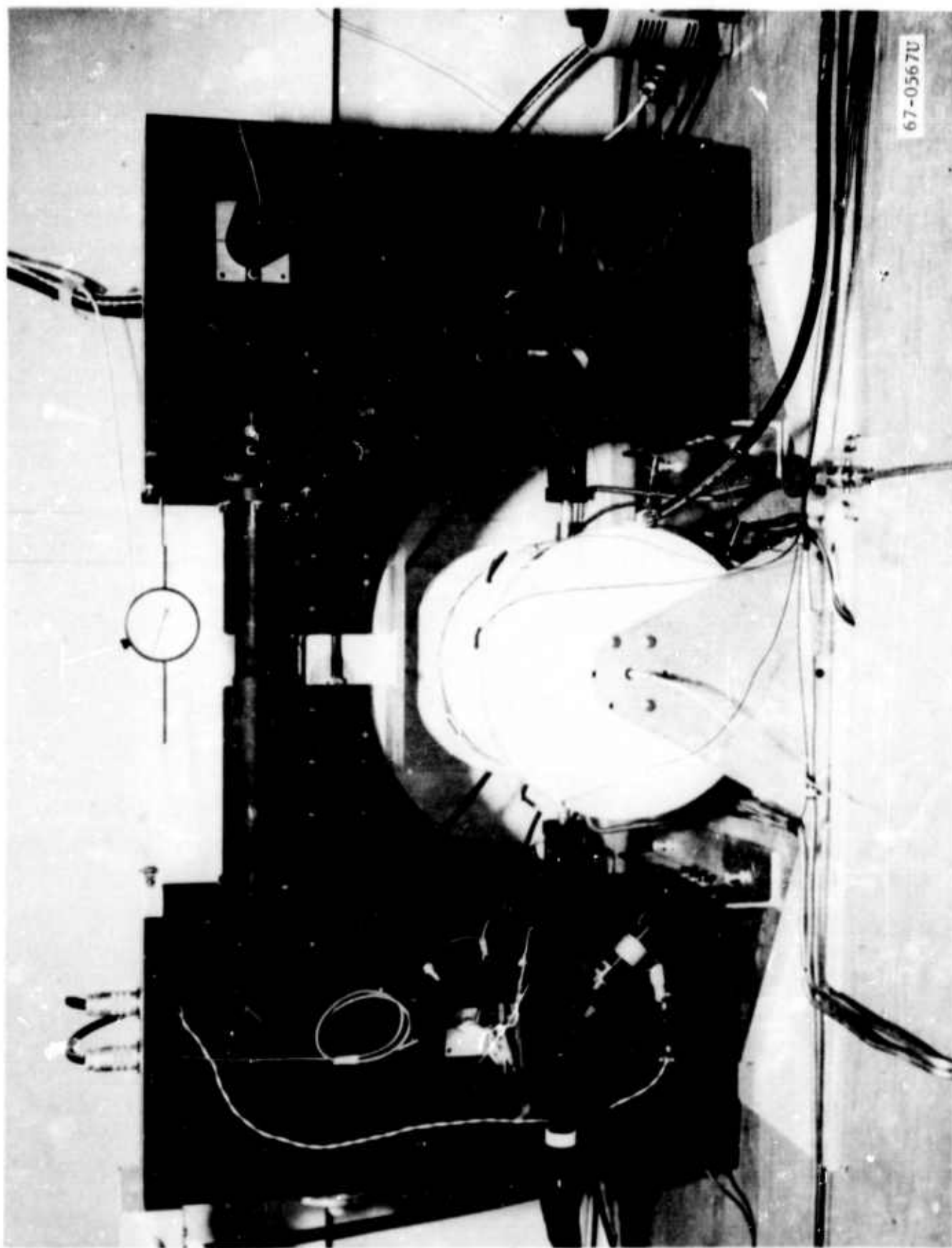
FIGURE 24. OPTICAL PROBE SYSTEM WITH QUARTZ RODS MOUNTED AT THE STATIC REACTOR (COVER PLATES REMOVED IN ORDER TO SHOW SYSTEM COMPONENTS)

67-0567U

-40-
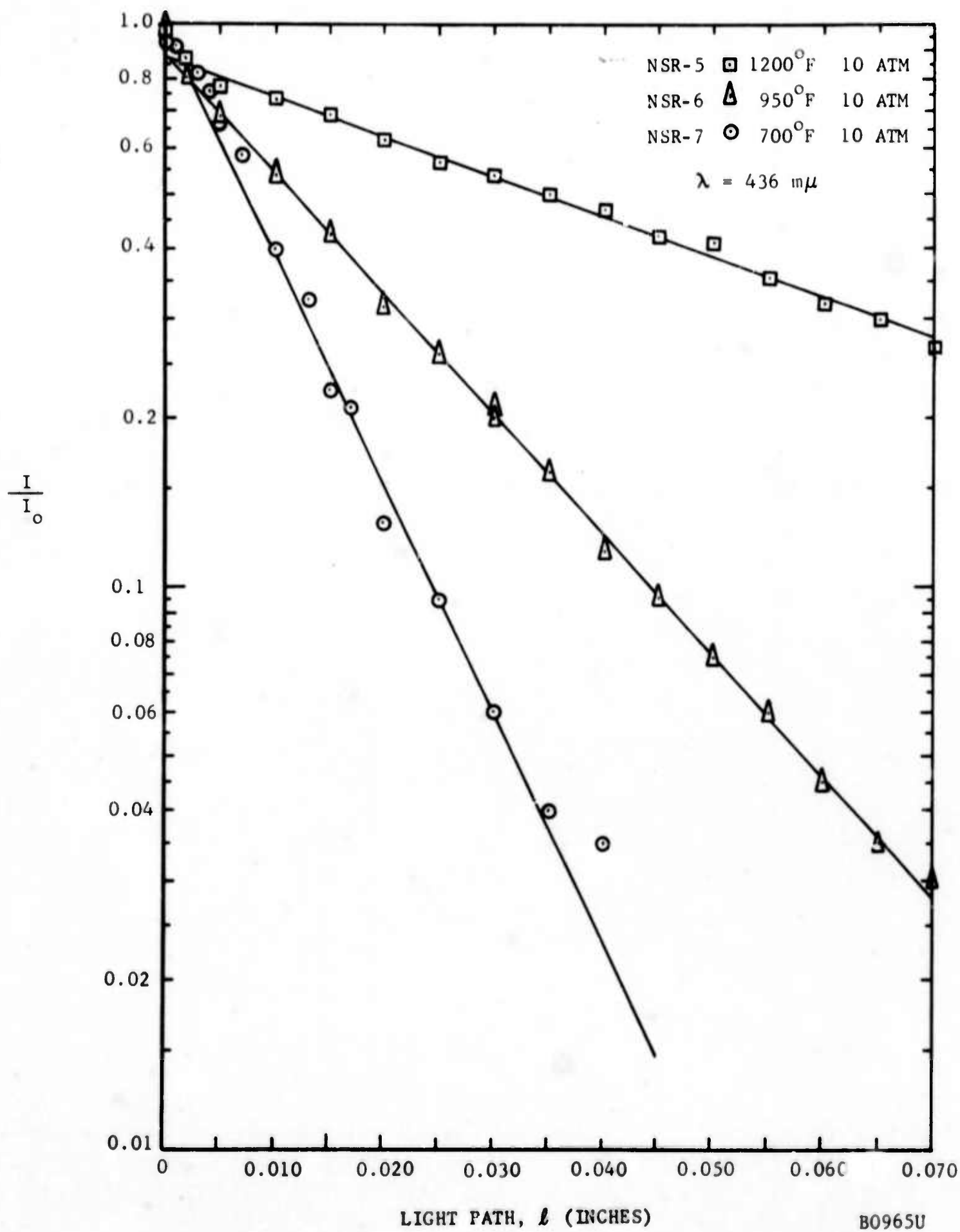
FIGURE 25. NO$_2$ TRANSMITTANCE DATA AS A FUNCTION OF THE LIGHT PATH LENGTH - MEASUREMENTS MADE UNDER EQUILIBRIUM CONDITIONS IN THE STATIC REACTOR

-41-

TABLE I. EXTINCTION COEFFICIENTS OF NO_2-EQUILIBRIUM CONDITIONS

Experiment Number NSR-	Reactor Temperature T ($^{\circ}$K)	Total Pressure P (atm)	Molar Concentration of NO_2 C_{NO_2} (moles/liter)	Extinction Coefficients[†] $\varepsilon^*_{NO_2}$ (liters/mole cm)	ε_{NO_2}	Deviation[‡] (percent)
8	644	2	0.024	123	127	-3.15
9	783	2	0.008	126	120	+5.00
10	922?	2	0.003	98	114	-14.0
2e	644	5	0.067	111	127	-12.6
3	783	5	0.027	135	120	+12.5
4	922	5	0.009	123	114	+7.89
7	644	10	0.144	111	127	-12.6
6	783	10	0.066	129	120	+7.50
5	922	10	0.024	114	114	0

Average % Deviation   8.36

[†] $\varepsilon^*_{NO_2}$ = Extinction coefficient measured at a wavelength of 4360 angstroms.

ε_{NO_2} = Value of extinction coefficient taken from curve drawn through the data given in Figure 2, p. 18, Ref. 19 (at a wavelength of 3660 angstroms).

[‡] Percent Deviation = $(\varepsilon^*_{NO_2} - \varepsilon_{NO_2})/\varepsilon_{NO_2}$ (100).

Average % Deviation = $\sum_n \left| (\varepsilon^*_{NO_2} - \varepsilon_{NO_2})(100) \right| / n \, \varepsilon_{NO_2}$.
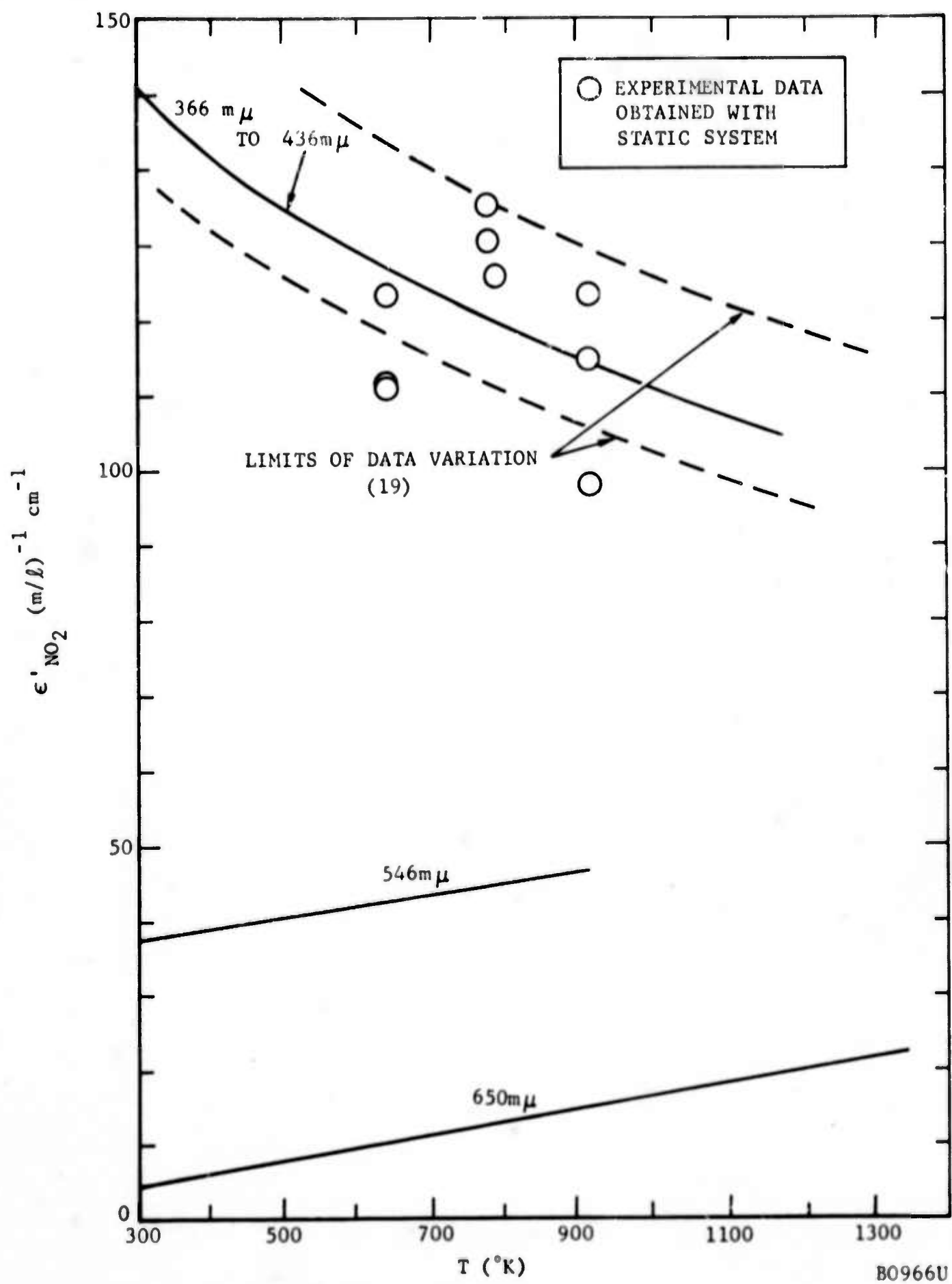
FIGURE 26. EXTINCTION COEFFICIENTS OF NO_2 - DATA FROM QUARTZ ROD SYSTEM

-43-

3.8 FLOW SYSTEM OPERATION

3.8.1 START-UP

A brief summary of the most important steps involved in the start-up of the flow system is as follows:

(1) Checkout of all instruments for proper functioning.

(2) Evacuation of the system (with a jet ejector) to a pressure of less than 0.1 atm.

(3) All electrical resistance heaters turned on (temperature of piping system in preheat sections kept <1400°F.)

(4) Guard heaters on probe holders turned on.

(5) Cooling water to cooling coils on probe holders turned on.

(6) Pressure lines between the flow system and the micromanometer and the Bourdon gauges filled with dry nitrogen to a pressure slightly exceeding the desired pressure for the experiment.

(7) Liquid N_2O_4-NO_2 vaporized into system at the rate of ~1 psi increase in total system pressure per minute.

(8) Cooling water to the mechanical seal housing of the turboblower turned on when total NO_2 gas pressure in the system reaches 5 psig.

(9) Turboblower turned on.

(10) Temperature controllers adjusted to give the desired temperatures in the bulk gas and at the back wall of the test section.

(11) Heat flux and wall temperatures monitored until a steady state is reached.

(12) Start experimental measurements.

From 4 to 6 hours were usually required for the completion of steps (2) through (11).

3.8.2 SHUT-DOWN

A brief summary of the most important steps involved in the shut-down of the flow system is as follows:

(1) All electrical power to the heaters shut off except for that to the probe holder guard heaters and to the drip pots.

(2) Vent hot gaseous NO_2 until total system pressure drops to 1 atm.

(3) Stop the turboblower.

(4) Drain the water from the mechanical seal housing; neutralize any residual acid with an aqueous sodium bicarbonate solution.

(5) Vent valve closed; system evacuated with the jet ejector (driven with water under pressure).

(6) Purging of the system continued for ~12 hours with room air entering the system through the micromanometer pressure lines; drip pot and probe holder guard heaters left on until the end of this purging.

Steps (1) through (5) usually take less than 1 hour to complete.

SECTION IV

DATA REDUCTION PROCEDURES AND EXPERIMENTAL RESULTS

4.1 DATA REDUCTION

All the equations required for reducing the data to forms considered in subsequent sections are given either in Appendix II or in the Nomenclature. In the discussion of the following sections, nonreacting air experiments are designated by a number with a suffix A-, while reacting NO_2 experiments are designated by a number with a suffix N-.

4.2 ERRORS AND CORRECTIONS

4.2.1 RADIATION CORRECTION TO GAS TEMPERATURE MEASUREMENTS

Estimates were made of the effect of radiation from the heated wall of the test section to the thermocouple junction (spherical in shape) of the temperature probes. For the case of an NO_2 experiment in which the measured temperatures were $T_W = 1190°F$ and $T_C = 930°F$, the true gas temperature at the centerline, taking into account the net radiant heat flux [in the manner described in Reference 21)] between the walls and the junction bead, was estimated to be ~9.3°F less than 930°F (or ~1 percent error). Since this represents less than a 4 percent error in ΔT, no attempt was made to correct the radial temperature profiles for radiation. For a smaller ΔT case with $T_W = 950°F$ and $T_C = 805°F$, the true gas temperature was estimated to be ~0.6°F less than that which would be actually measured. No attempt was made to correct for the specular absorption of the radiant energy as it passed through the NO_2 laden gas because such correction (Reference 9) was also thought to be significantly less than the error of the other measurements.

4.2.2 CHANGE IN OPTICAL PROBE GAP WIDTH WITH TEMPERATURE

Even after thermal conditioning, the gap width between the optically flat and polished ends of the glass fiber bundles would be expected to change with temperature due to the thermal expansion characteristics of the ceramic cement, glass, and outer stainless steel tube. An estimate was made of the net gap width change expected in heating the probe tip from 77°F to 852°F (bulk temperature for Experiment N-14b) taking into account the actual geometry of the sensing end ($\ell = 0.0095$ inch for Optical Probe No. 3 used in Experiment N-14b) and the known thermal expansion coefficients of the materials involved. The result showed that the gap width change over this temperature interval would be less than 10 percent of the initial gap width as measured under a microscope at ambient temperature. Such a change in ℓ would lead to a less than 10 percent change in the measured $\bar{C}_{NO_2}$ (i.e., the $\bar{C}_{NO_2}$ values obtained by using the ℓ based on an ambient temperature measurement should actually be decreased by up to 10 percent in order to take into account the actual gap width existing at the time when the transmittance measurements were made in the high temperature flow). Since direct

measurement of the gap width change with temperature was somewhat uncertain (gap width measured to within ±15 percent of its actual value), the gap width measured at ambient temperature was used in reducing the observed transmittance data to local time-average molar concentrations of NO_2.[*]

4.3 CONCENTRATION PROFILES - TIME-AVERAGE DATA[**]

As noted in Paragraph 3.7.4, the optical probe system was modified to accommodate 1/4-inch diameter quartz rods for use in measuring the extinction coefficients, $\epsilon_{NO_2}(\lambda, T)$, in the static reactor. This same assembly was used to make the measurement of $\bar{C}_{NO_2}(r)$ shown in Figure 27. The solid line drawn through the data points is shown in order to help define the trend of the data. For comparison, the dashed line shows how the equilibrium concentration profile would vary with radial position for the estimates of $\bar{T}(r)$ obtained from previous experiments characterized by similar operating conditions. The reference equilibrium concentrations shown at the center of the tube ($r/r_0 = 0$) indicate that the nonequilibrium concentration profile was the equivalent of ~6°F (in terms of equilibrium concentration differences) away from the equilibrium profile derived from the estimated temperature profile. Uncertainties in knowing the gap width, ℓ, at the pressures and temperatures of the experiments, problems with rod breakage caused by slight mesalignments (at high temperature conditions) between the probe holders on opposite sides of the test section, and difficulties in translating the entire optical assembly for each radial traverse strongly encouraged us to develop the fiber optics probe for use at temperatures to 1000°F (if necessary) and moderate pressures (< 11 atm).

The radial concentration profile data shown in Figure 28 were obtained with the fiber optics probe (ℓ = 0.0095 inch). The raw data were obtained two different ways (refer to Figure 22) - the values obtained from the electronic counter are expected to be more accurate. There is some uncertainty as to the exact radial position of the gap during this particular experiment. It is expected that the measured profile data should be shifted

---

[*] Direct measurements of the gap width were made with a traveling microscope (translational measurement accuracy of instrument = 0.0001 inch) sighted (through a quartz window) on the probe tip with the probe itself inserted into the test section at its usual location. The gap increased ~20 percent as the temperature of the gas flowing over the tip was increased from 77°F to 852°F (see Figure 20).

[**] In the se of the results presented in this and subsequent sections, radial profile measurements were made at essentially one longitudinal position. Profile measurements were made at an L/D of 43 from the trip plate at the beginning of the entrance section (d/D of 1.50 inch/1.95 inch)(see Figure 7). The flow was always directed vertically downward in the test section. In order to minimize the report length, most of the extensive profile measurements and property data used in the calculations was not tabulated.

-47-
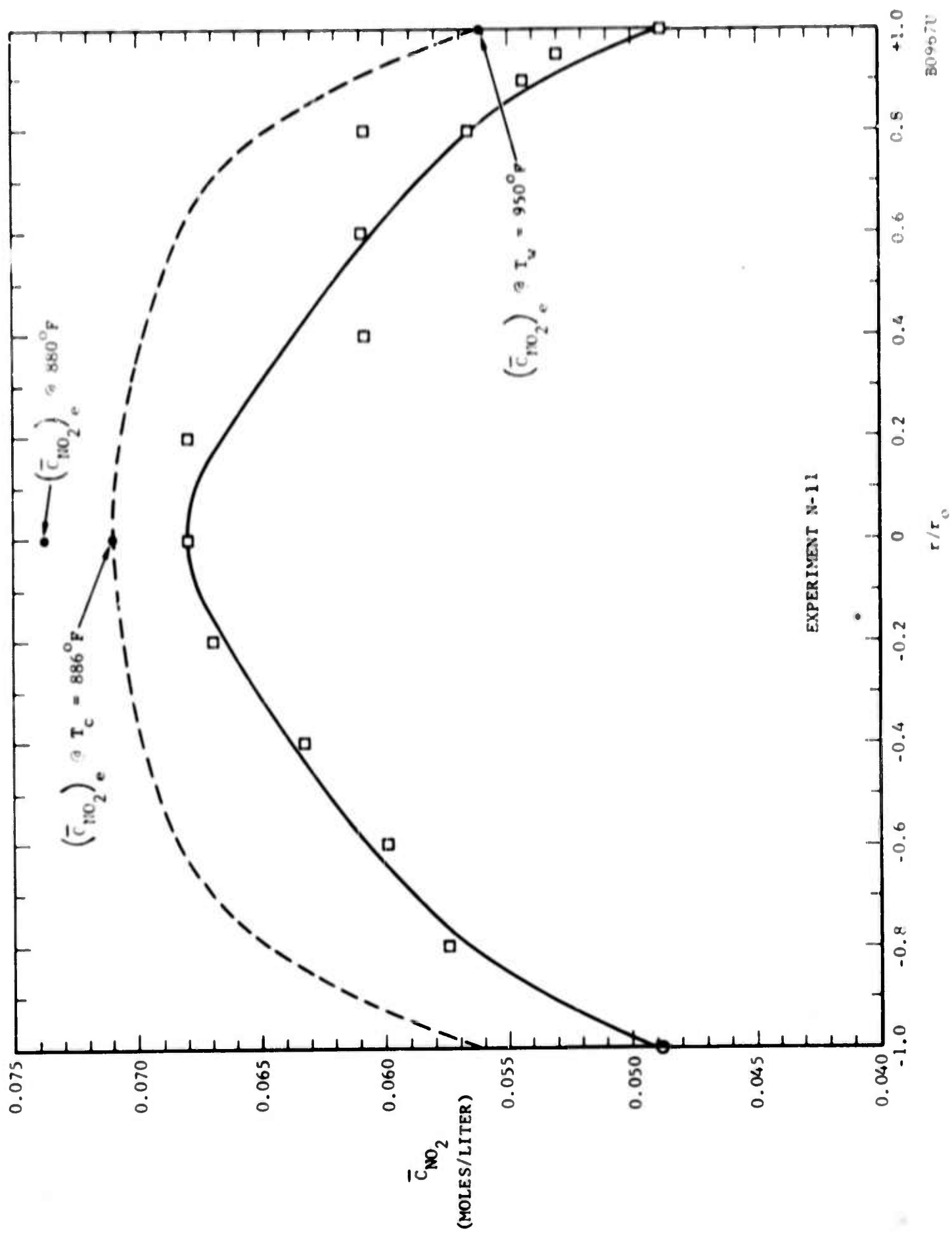
FIGURE 27. CONCENTRATION PROFILE OBTAINED FROM TRAVERSE OF QUARTZ RODS WITH FIXED GAP

EXPERIMENT N-11

-48-
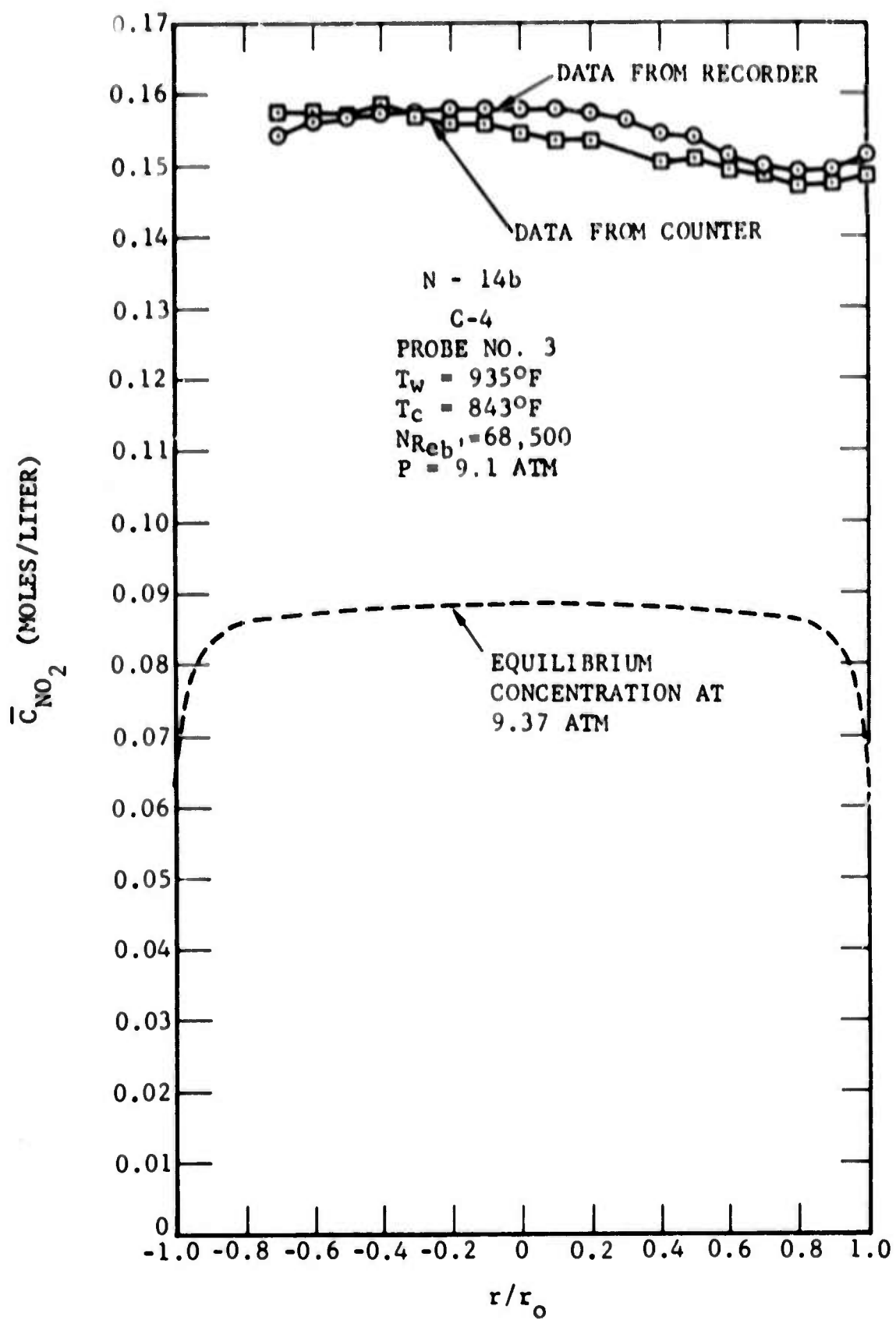
FIGURE 28. CONCENTRATION PROFILE OBTAINED FROM FIBER OPTICS PROBE

B0968U

-49-

to the right ~0.2 inch. In any event the results show that across the majority of the flow conduit, the gas is nearly twice as concentrated in NO_2 as would be predicted had equilibrium conditions prevailed (the dashed line is based on the measured temperature profile and the pressure which existed in the flow system at the time of the concentration profile measurement).

As indicated in Paragraph 4.2.2, approximate corrections for the change in gap width between the ends of the fiber bundles as the probe end was heated up to the test conditions for Experiment N-14b suggest that the actual non-equilibrium concentrations could be on the order of 20 percent less than the observed values shown in Figure 28.

These measurements demonstrate that the basic design of the optical probe is suitable for use in making time-average concentration measurements at the highest temperatures and concentrations which would be expected in this program. The performance of the probe has shown that a calibration of both gap width change and signal attenuation (caused by twisting of the fiber ends - especially important at the higher temperatures) should be made in heated air before and after each NO_2 experiment to ensure that the raw data can be corrected with confidence. These corrections are not nearly as important to the measurement of the fluctuating concentration data (see Paragraph 4.5) as they are for the determination of the absolute value of the concentration. An additional extinction coefficient calibration is now appropriate since we are using a relatively broad band filter with the optical probe instead of the narrow band interference filter which was used with the 1/4 inch in diameter quartz rod system.

4.4 TURBULENT TEMPERATURE RESULTS - NONREACTING AND NONEQUILIBRIUM REACTING SYSTEMS

Total rms temperature intensity data for the nonreacting air system (Experiment A-37) measured with the system described in Paragraph 3.7.3 is given in Figure 29. The usual minimum at the center of the pipe, the maximum values near the walls, and an intensity level on the order of 3 percent is consistent with the limited number of published results (References 11 and 22) for air under conditions of fully developed turbulent pipe flow with heat transfer.

The very surprising results obtained for the nonequilibrium reacting NO_2 system (key pertinent experimental conditions are given on the figures themselves) are shown in Figures 30 and 31. In the case of these experiments, the variation of intensity with radial position is the same as in the case of the nonreacting system results, but the presence of the non-equilibrium chemical reaction has caused a more than order of magnitude increase in the intensity level. A mixing model for the interpretation of these results has not yet been developed. The large change in level cannot be primarily due to the difference in thermal properties between the two systems, since the N_{Pr} and N_{Le} parameters are so similar. (Also, the difference in mass density between A-37 and N-15 is no more than ~ 3.) The values reported in Figures 29, 30, and 31 were obtained by either directly

-50-
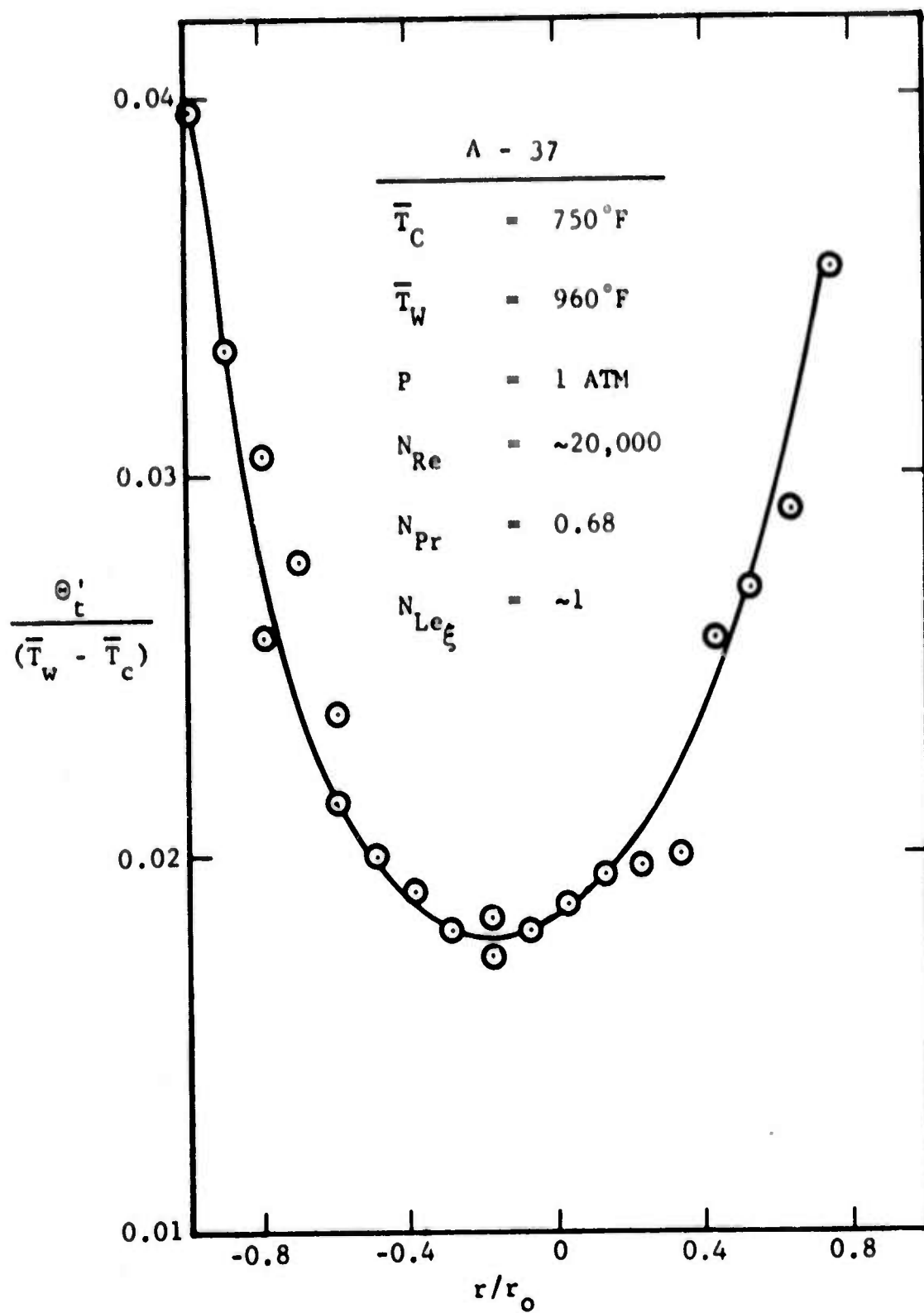
FIGURE 29. TOTAL RMS TEMPERATURE INTENSITIES AS A FUNCTION OF
RADIAL POSITION (EXPERIMENT A-37)
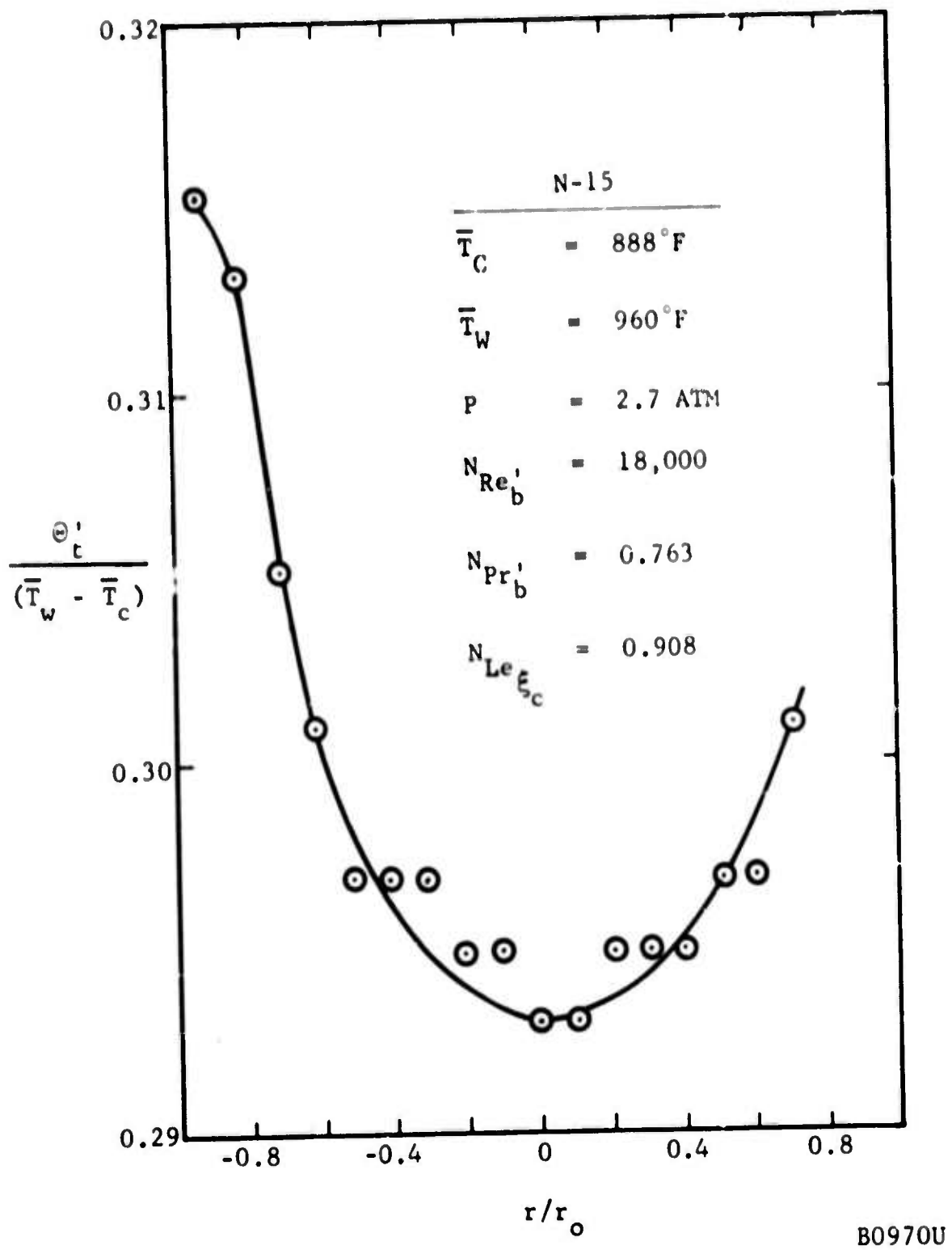
FIGURE 30. TOTAL RMS TEMPERATURE INTENSITIES AS A FUNCTION OF RADIAL POSITION (EXPERIMENT N-15)
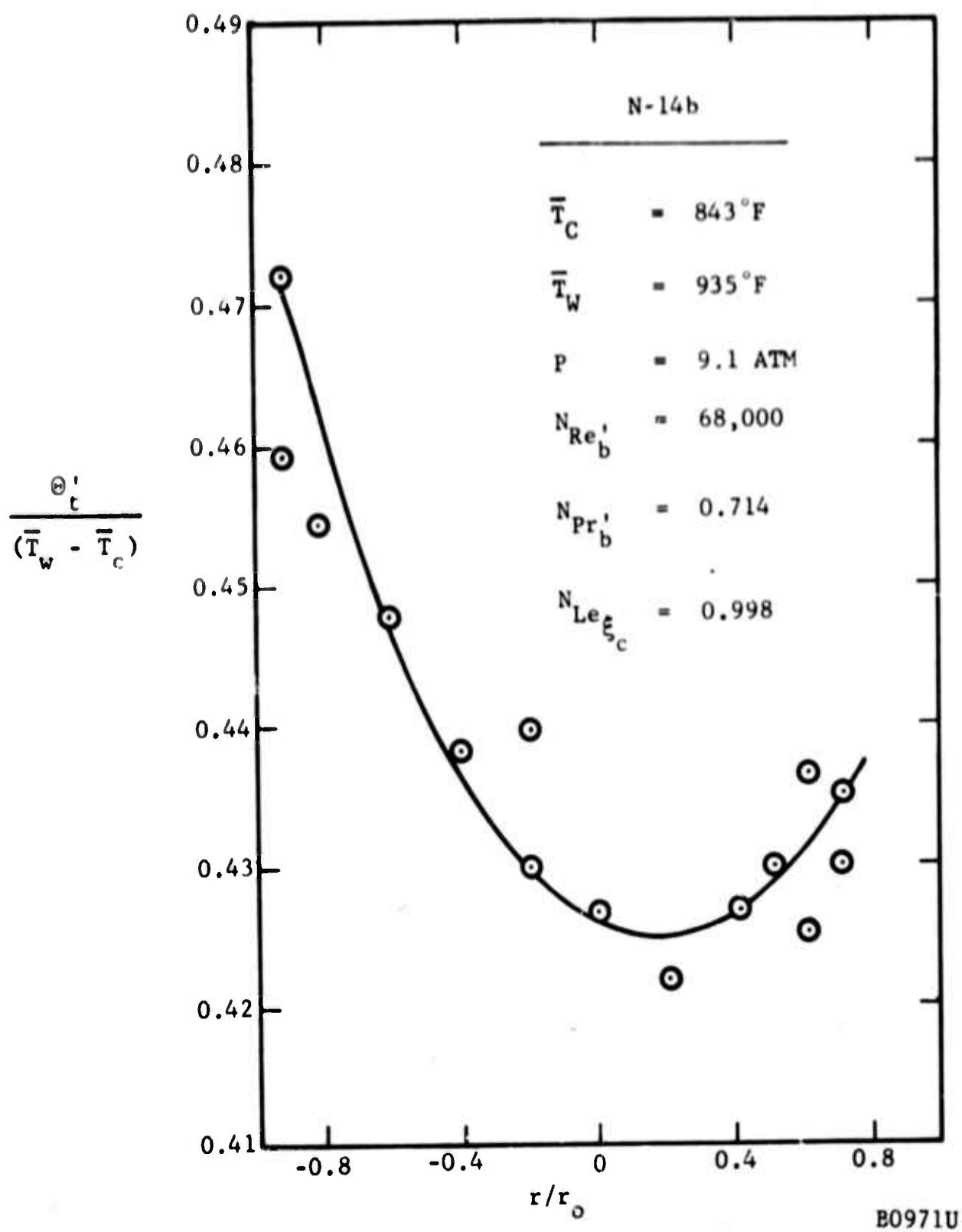
FIGURE 31. TOTAL RMS TEMPERATURE INTENSITIES AS A FUNCTION OF RADIAL POSITION (EXPERIMENT N-14b)

reading the dial of the true rms voltmeter or by recording the dc output of the rms voltmeter on a strip chart recorder and then estimating the mean of the rms output. More accurate time averaging (as indicated in Figure 13 - use of the voltage to frequency converter and counter in tandem) of the total rms output would be expected to yield more accurate profile results and will be used in future experiments.

The scalar mixing spectrum for temperature obtained with air at high temperature in the recirculating flow system is shown in Figure 32. The extended slope in the inertial subrange (the essentially straight line region) is probably due to the coexistence of both longitudinal and radial (or transverse) mixing at the sensor location. Longitudinal mixing effects would be expected to arise from the 1 foot long heaters situated along the test section, each pulsing on and off in a random fashion at a frequency between once per second to once per 5 minutes depending on the cooling and heating loads imposed on the system. Thus the energy contributed to the spectrum from longitudinal mixing effects will be characterized by low frequencies and will thus tend to extend the inertial subrange over a greater frequency range than the usual one to one and one half decades of frequency (or one dimensional wave number).* This extension probably accounts for the slope of the spectrum in the inertial subrange not equalling the expected -5/3 (Reference 23). For reference, the characteristic frequencies based on both the test section diameter (~ characteristic for transverse mixing), f_D, and the test section length, $f\ell_{TS}$, are given on Figure 32. The conditions of the experiment are also given there for reference purposes.

Temperature spectrum data for two different NO_2 experiments are given in Figures 33, 34, and 35. The presentation of the data is in a form quite similar to that used in Figure 32 except that the NO_2 data obtained at frequencies greater than f_D (or k_{1D}) which appear to lie in the inertial subrange exhibit, in each case, a slope very close to the characteristic -5/3. The data of Experiment N-15 are shown in the one-dimensional wave number form in Figure 34. The apparent diffusive cutoff at higher frequencies on the order of 10 kHz may be due more to a start in the fall-off in frequency response of the probe [estimated to be better than 10 kHz in Reference 11] than because of the start of a diffusive subrange. In Figure 35, the region exhibiting a -1 slope may be representative of a viscous-convective subrange. In this experiment (N-14b), there was very little turning on and off of the temperature controllers during the period of the turbulence measurements as compared with the other experiments (N-15 and A-37). This may help to explain why the N-14b spectrum results do not exhibit the extended inertial subrange to very low frequencies (the frequency response of the electronics instrumentation is good down to only 20 Hz). In any event, the spectra do not exhibit any unusual characteristics that cannot be ascribed to the nature of the experiment and/or equipment.

---

*Terms are defined in the Nomenclature; some pertinent relations are given in Appendix B.
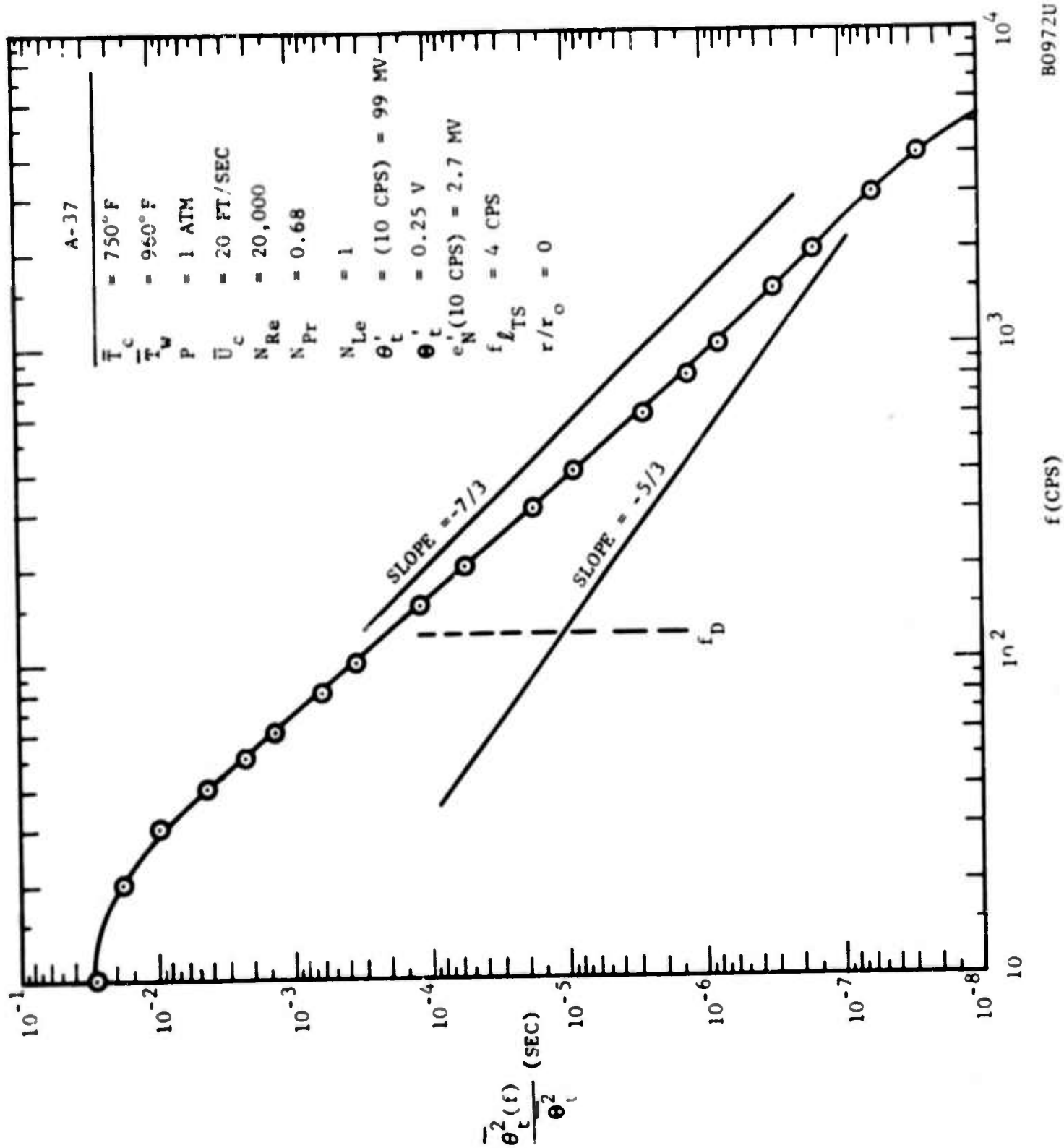
FIGURE 32. SCALAR MIXING SPECTRUM - TEMPERATURE (EXPERIMENT A-37)
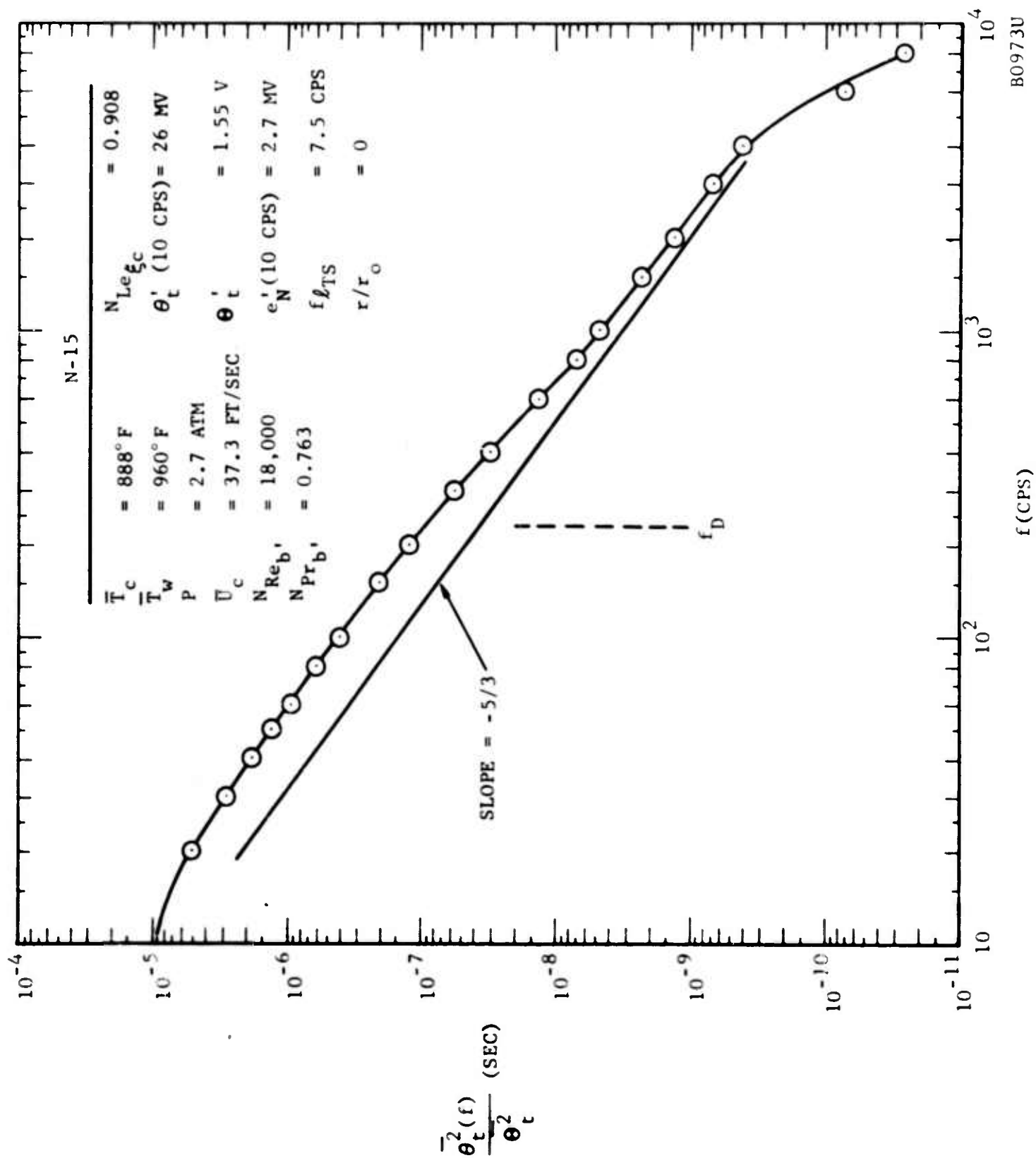
FIGURE 33. SCALAR MIXING SPECTRUM - TEMPERATURE (EXPERIMENT N-15)
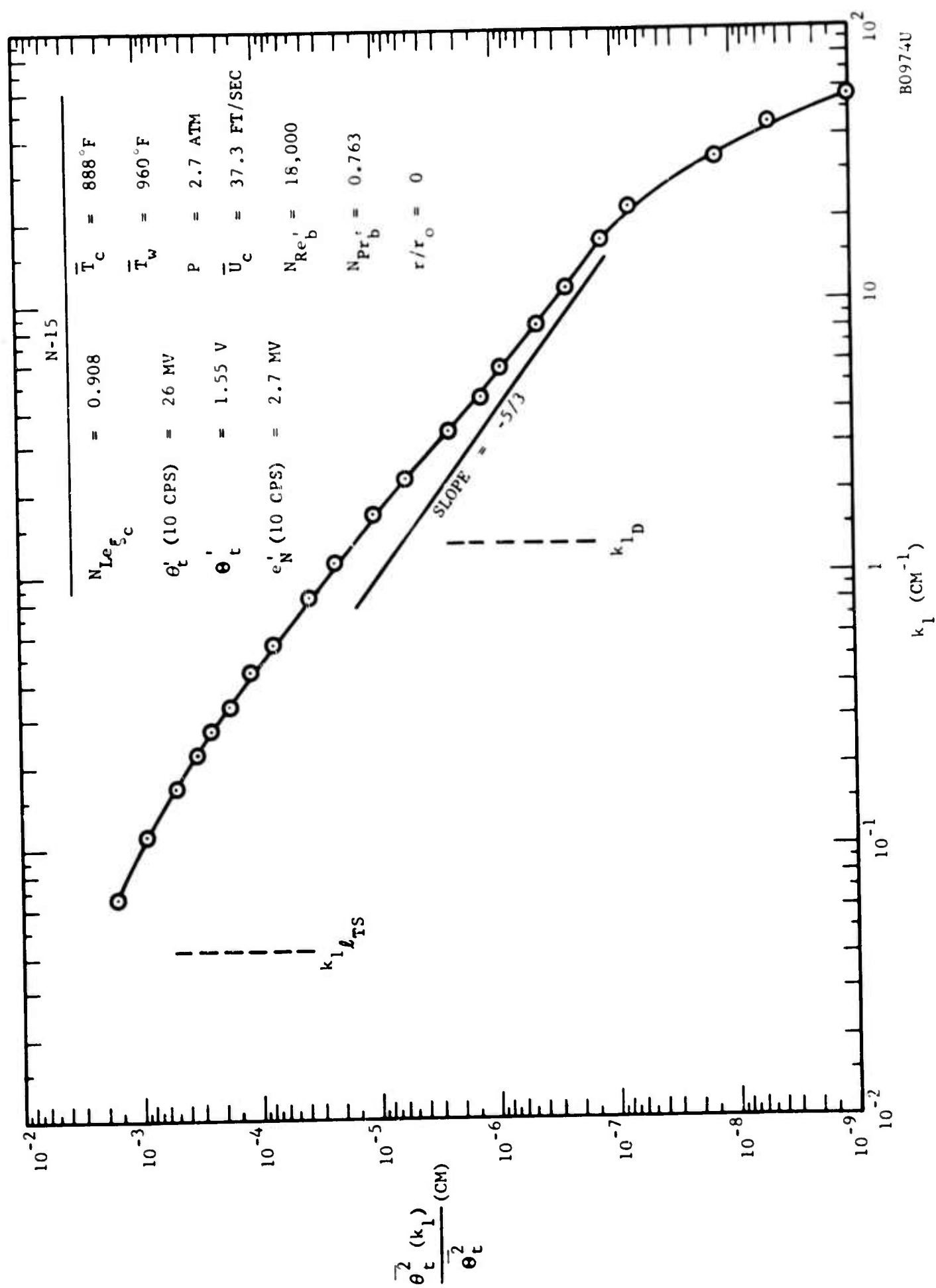
FIGURE 34. SCALAR MIXING SPECTRUM - TEMPERATURE (EXPERIMENT N-15)

-57-
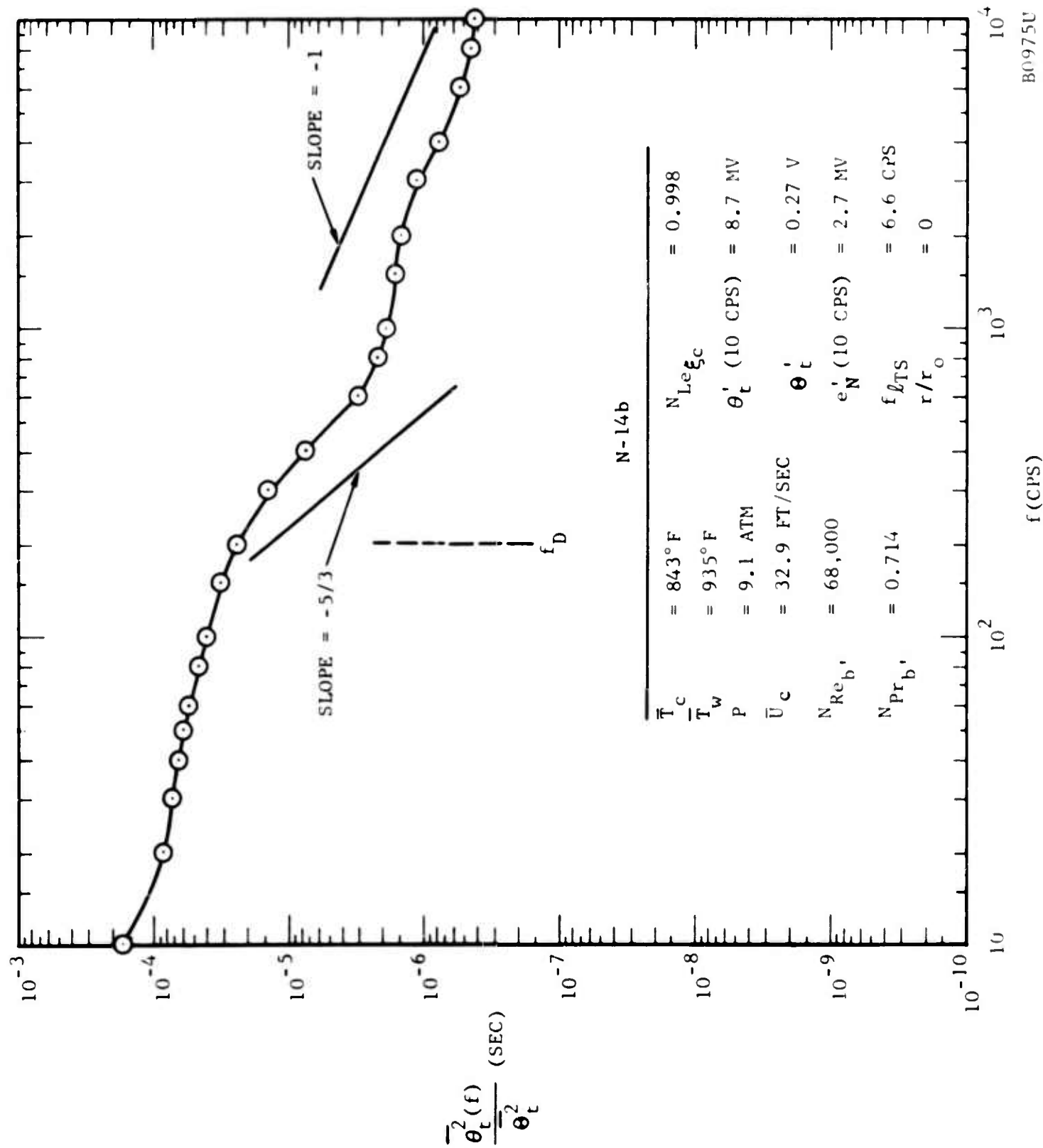
FIGURE 35. SCALAR MIXING SPECTRUM - TEMPERATURE (EXPERIMENT N-14b)

-58-

4.5 TURBULENT CONCENTRATION RESULTS

The total rms intensity data and the spectral data for the NO_2 experiment, N-14b, are tabulated in Tables II and III. The format of these tables has been arranged so that the steps employed in the reduction of the raw data to the results of interest are evident. The intensities have been calculated assuming that the equilibrium time-average concentration difference based on the measured temperature difference $(\bar{T}_w - \bar{T}_c)$ is a reasonable measure of the actual nonequilibrium time-average concentration difference $[(\bar{C}_{NO_2})_c - (\bar{C}_{NO_2})_w]$.*
The intensity results are shown in Figure 36. Consistent with the unusually large temperature intensity data given in Figures 30 and 31 for the NO_2 reacting system, the concentration intensity values are also large. The data in Figure 36 are plotted with a greatly expanded ordinate. Considering the accuracy of the measurement [limitations from boundary layer buildup on the ends of the fiber bundles - expected to be a small effect (Reference 18), slight change in flow conditions during the course of the experiment, etc.], the results given in Figure 36 should be interpreted as indicating that the intensity is essentially constant across the tubular test section (within ± 2 percent)

Lee (Reference 24) has made some interesting predictions, based on a statistical turbulence theory treatment, of how the turbulent concentration mixing spectra of an isotropic flow (one reactant; irreversible second order reaction) depends on the turbulence Peclet number, $N_{Pe}^{(t)}$, and the turbulence Damkohler number (of the second type), $N_{DaII}^{(t)}$. We have calculated these parameters for the conditions representative of Experiment N-14b and find for,

$$\theta_u' \sim 0.10 \ \bar{U}_c \quad [\text{From Reference 25, pp.521-522}]$$

with

$$\bar{U}_c \sim 40 \ \text{ft/sec}$$

$$\bar{D} \sim 0.2 \ \text{cm}^2/\text{sec}$$

$$k_{1_D} \sim 1.3 \ \text{cm}^{-1}$$

then

$$N_{Pe}^{(t)} \sim 490$$

_____

*A good measure of $(\bar{C}_{NO_2})_w$ was not experimentally obtained.

TABLE II. TOTAL RMS CONCENTRATION INTENSITIES AS A FUNCTION OF RADIAL POSITION

(Experiment N-14b)

r/r_o	$\left[(e'_{S+N})_{NO_2}\right]$ (millivolts)	$(e'_S)_{NO_2}$ (mv)	$\left[(e'_S)_{Air}-(e'_S)_{NO_2}\right]$ (mv)	$b^{-1}_{NO_2}$ $\left(\frac{moles}{liter}\right)$	$\bar{E}$ (volts)	$\Theta'_{C_{NO_2}} \times 10^3$ $\left(\frac{moles}{liter}\right)$	$\dfrac{\left[(\bar{c}_{NO_2})_{e_c}-(\bar{c}_{NO_2})_{e_w}\right]}{\Theta'_{C_{NO_2}}}$
+1.00	3.33	3.156	17.814	0.1493	1.190	11.62	0.471
+0.9	3.33	3.156	17.814	0.1469	1.182	11.51	0.466
+0.8	3.30	3.125	17.845	0.1466	1.180	11.52	0.466
+0.6	3.27	3.093	17.877	0.1465	1.162	11.72	0.475
+0.4	3.30	3.125	17.845	0.1465	1.151	11.81	0.478
+0.2	3.30	3.125	17.845	0.1464	1.127	12.05	0.488
0	3.33	3.156	17.814	0.1464	1.120	12.11	0.490
-0.2	3.33	3.156	17.814	0.1464	1.109	12.23	0.495
-0.4	3.33	3.156	17.814	0.1465	1.091	12.44	0.503
-0.6	3.33	3.156	17.814	0.1465	1.097	12.37	0.501

$(e'_N) = 1.06$ millivolts.

$(e'_{S+N})_{Air} = 21$ millivolts.

$(e'_S)_{Air} = 20.97$ millivolts.

$\bar{E}_o = 3.22$ volts

$G_2 = 5.5$

$G_1 = 28.6$

$\left(\bar{c}_{NO_2}\right)_{e_c} = 0.0884$ moles/liter.

$\left(\bar{c}_{NO_2}\right)_{e_w} = 0.0637$ moles/liter.

TABLE III. CONCENTRATION SPECTRUM (Experiment N-14b)

f	$(e'_{S+N})f_{Air}$	$(e'_{S+N})f_{NO_2}$	$(e'_N)f$	$(e'_S)f_{Air}$ $\times 10^2$	$(e'_S)f_{NO_2}$ $\times 10^2$	$\overline{\theta^2}_{C_{NO_2}}(f)$ $\times 10^8$	$\overline{\theta^2}_{C_{NO_2}}(f)/\overline{\theta^2}_{C_{NO_2}}$ $\times 10^6$
(cps)	(mv)	(mv)	(mv)	(mv)	(mv)	$[$(moles/liter)^2 sec$]$	(sec)
10	0.677	0.1580	0.0152	67.68	15.72	8.523	3.624
20	0.675	0.1575	0.0118	67.49	15.69	8.471	3.602
30	0.672	0.1570	0.0107	67.19	15.66	8.383	3.564
40	0.670	0.1565	0.0100	66.99	15.61	8.334	3.543
50	0.667	0.1560	0.0095	66.69	15.57	8.250	3.508
60	0.665	0.1555	0.0089	66.49	15.52	8.202	3.487
80	0.662	0.1550	0.0083	66.19	15.47	8.121	3.453
100	0.660	0.1545	0.0077	65.99	15.43	8.070	3.431
150	0.650	0.1530	0.0072	64.99	15.28	7.801	3.317
200	0.647	0.1510	0.0068	64.69	15.08	7.770	3.304
300	0.646	0.148	0.0067	64.59	14.78	7.833	3.330
400	0.643	0.145	0.0066	64.30	14.49	7.833	3.330
600	0.638	0.140	0.0065	63.80	13.98	7.836	3.332
800	0.629	0.135	0.0062	62.90	13.48	7.710	3.278
1,000	0.621	0.130	0.0060	62.10	12.99	7.614	3.237
1,500	0.592	0.120	0.0058	59.19	11.98	7.036	2.991
2,000	0.564	0.0960	0.0053	56.39	9.585	6.918	2.941
3,000	0.500	0.0857	0.0045	49.99	8.558	5.419	2.304
4,000	0.432	0.0753	0.0044	43.20	7.517	4.019	1.709
6,000	0.315	0.0612	0.0030	31.50	6.012	2.051	0.8720
8,000	0.245	0.0490	0.0025	24.49	4.894	1.213	0.5157
10,000	0.210	0.0375	0.0020	20.99	3.744	0.9395	0.3994

BW = 5.52 cps.

b_{NO_2} @ $r/r_o \approx -0.2$ (Profile C-4) = 6.83 liters/mole.

(ϵ = 283.04 liters/mole cm; ℓ = 0.02413 cm).

$\overline{E}$ = 1.109 volts = 1109 millivolts.

$\overline{\theta^2}_C$ (at $r/r_o \approx -0.2$) = 23.52 $\times 10^{-3}$ (moles/liter).
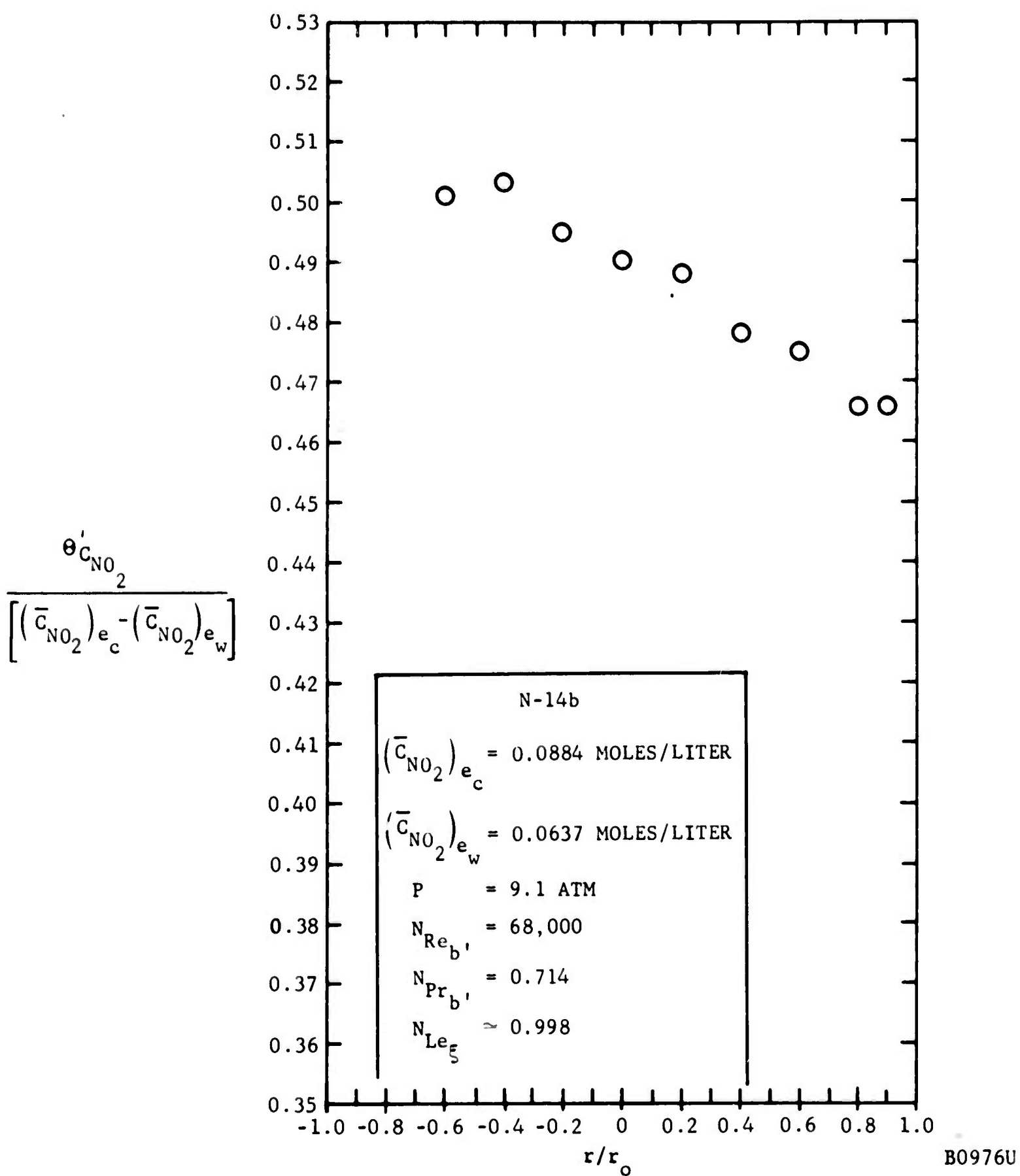
FIGURE 36. TOTAL RMS CONCENTRATION PROFILE AS A FUNCTION OF
RADIAL POSITION

and

$$N_{Da_{II_{NO_2}}}^{(t)} \simeq 8.9$$

so that the ratio $N_{Da_{II_{NO_2}}}^{(t)}/N_{Pe}^{(t)} \sim 0.02$ and thus, according to Lee's analysis, the NO_2 dissociation is a "slow" reaction. On the other hand, calculations show that the NO_2 recombination reaction (which is being used in the injection measurement) is "fast."

In Figure 37, the concentration spectrum for Experiment N-14b is shown for the frequency range 10 to 10^4 Hz (data were obtained out to 15 kHz). The solid line drawn through the data is shown in order to assist in discerning its variation with frequency. The results indicate that what might be considered an inertial subrange begins only at frequencies much greater than f_D. Most of the energy of the concentration spectrum is distributed uniformly across 2-1/2 decades of frequency with fall-off occurring only at comparatively high frequencies. Additional experiments should be carried out with probes with significantly different gap widths, ℓ, in order to determine if the shape of the concentration spectrum is more probe geometry-limited or phenomena-limited.
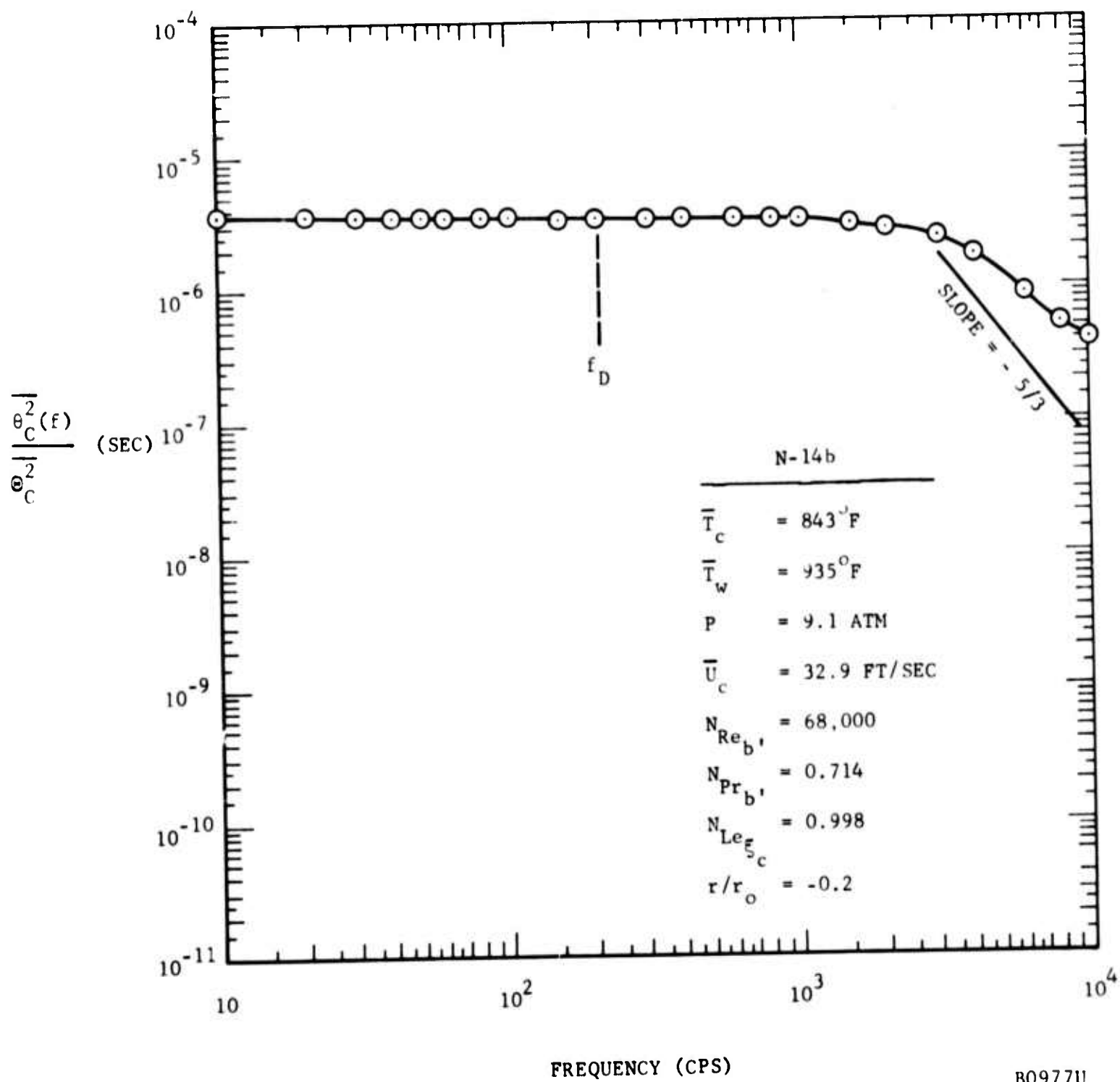
FIGURE 37. CONCENTRATION SPECTRUM
(EXPERIMENT N-14b)

SECTION 5

SUMMARY

The progress achieved in the first four and one-half months of the program was reviewed. The principal effort of this period has consisted of the design of experiments for demonstrating the effect of exothermic energy release on turbulent flow structure, the development of sensitive instrumentation for the accurate measurement of both time-average and fluctuating scalar quantities (temperature and concentration), the development of techniques for reducing the raw data derived from the sensors and their associated electronics to forms suitable for correlation and analysis, and the completion of several experiments under "self-mixing" conditions without injection.

Calculations of the effectiveness parameter for the NO_2 reacting system have shown that the recombining NO_2 system (to form N_2O_4) will exhibit a sufficiently large effectiveness parameter under laboratory conditions so that the turbulence in a grid or sphere wake would be significantly modified. The properties of the reacting NO_2 system were reviewed. Those conditions of temperature and pressure as well as test section - grid sizes required for the experiments were specified. Some pertinent characteristics of the recirculating flow system temperature measurement instrumentation were given.

An improved fiber optic probe was developed for use in the heated reacting gases (T to 800°K, P to 10 atm). Signal-to-noise ratios of >250:1 have now been obtained with this system. This performance should be more than adequate for both the time-average and the fluctuating measurements. Time-average and fluctuating concentration measurements were made in a 2-inch diameter test section with reacting NO_2 at 850°F and 9 atm. It was found necessary to thermally condition the probe in order to obtain a stable performance.

Several experiments were performed with both high temperature air and NO_2 in order to determine the operating characteristics of the fast response thermocouple probe system. Both total rms and spectral data were obtained. In the case of heated fully developed turbulent tube flow ("self-mixing" case), the temperature intensities were found to be, an order of magnitude higher (more endothermic reaction in the film near the heated wall, more exothermic reaction in the bulk flow reaction where the probe tips were situated) in the nonequilibrium reacting gas than in nonreacting air. The related spectral data exhibited the usual -5/3 slope in the inertial subrange. Both longitudinal and transverse mixing influenced the shape of the spectra at low wave numbers. The temperature intensities in the nonequilibrium reacting flow were about as large as the measured concentration intensities.

Now that the required instrumentation has been developed, the principal effort during the next quarter will be devoted to the installation and checkout of a sphere injection system as well as the acquisition of data for mixing in the near wake of the sphere (nonreacting and reacting systems). Further refinements in the probe tip designs and in data processing will be made.

TABLE IV

SPECIFICATIONS OF TEMPERATURE CONTROLLERS

<u>Temperature Controller - Indicator</u> (Test Section)

    Barber-Coleman Company

    Model 293C (Capacitrol)

    Power Requirements: 110-130 VAC, 50-60 Hz, ~20 watts

    Accuracy of Control: $\pm$ 1/2% of Control Set Point (Range 0 - 1600°F)

    Scale Divisions: 20°F

<u>Temperature Controller</u> (Preheat Section)

    Barber-Coleman Company

    Model 151P (Amplitrol)

    Power Requirements: 120 VAC, 60 Hz

    Accuracy of Dial Setting: 1% of scale range (Range = 100 - 1600°F)

    Sensitivity: 75 μvolts

    Scale Divisions: 20°F

<u>Temperature Controller - Recorder</u> (Gas Temperature Adjustment)

    Leeds & Northrup Company

    Series 60 Controller - Speedomax H Recorder - FDG1 Regulator

    Controller:

        Power Requirements: 120 VAC, 50-60 Hz, 30 VA

        Proportional, Rate and Reset Capabilities

    Recorder:

        Power Requirements: 120 VAC, 50-60 Hz, 30 VA

        Round Chart, 1 revolution in 24 hours, 0-1800°F using a

            Chromel Alumel Thermocouple

        Automatic reference junction compensation

        Accuracy: $\pm$ 0.3% of range   (Range = 0 - 1800°F)

        Dead Band: 0.2% of span

    Regulator:

        Fincor Model FDG-1

        Power Requirements: 200-240 VAC., 60 Hz Single phase 10 KVA

        Output Power: 198/216 VAC at 20 amps, 9 KVA

TABLE V

SPECIFICATIONS OF INSTRUMENTS USED FOR TIME AVERAGE TEMPERATURE MEASUREMENTS
AND AMPLIFICATION OF FLUCTUATING THERMOCOUPLE OUTPUT

Power Supply

Tektronix, Inc.

Model 125

Power Requirements: 105-125 VAC, 40-50 Hz, ~ 110 watts

Output Voltages: +135 V DC at 0-20 ma $\pm$ 3%

$\qquad$ - 90 V DC at 0-20 ma $\pm$ 3%

$\qquad$ -6 V DC at 0.7-4 amp $\pm$ 5%

Voltage Stability: $\pm$ 5 mV/hr at constant temperature

Preamplifier

Tektronix, Inc.

Model 122 (modified by conversion of first two stages to nuvistors)

Power Requirements: Supplied by Tektronix Model 125 Power Supply

Input Impedance: ~ 10 megohms

Output Impedance: 1000 ohms

Gain: 1,230 or 12,600

Noise Level: 0.054 to 0.021 μV from 200 Hz to 10 KHz with gain of 12,600

Frequency Response: -0.3 db from 10 Hz to 1 KHz

$\qquad$ -0.3 db to -0.9 db from 1 KHz to 17 KHz

Potentiometer

Leeds & Northrup Company

Model 7553-5

Type K-3

Measuring Ranges: 0 to 1.6110 volts (high range)

$\qquad$ 0 to 0.16110 volts (medium range)

$\qquad$ 0 to 0.016110 volts (low range)

Limits or Error: $\pm$ 0.1% of reading + 20 mV (high range)

$\qquad$ $\pm$ 0.15% of reading + 2 mV (medium range)

$\qquad$ $\pm$ 0.15% of reading + 0.5 mV (low range)

Standard Cell

    Eppley Laboratory, Inc.

    Catalog Number 100

    Internal Resistance: Less than 500 ohms

    Voltage: 1.01923 volts at 23°C

Galvanometer

    Leeds & Northrup Company

    Model 2430-C

    Sensitivity: 0.0033 μV/mm

    Internal Resistance: 24 ohms

    Period: 2.85 seconds

TABLE   VI

SPECIFICATIONS OF ELECTRONIC AND ELECTRICAL COMPONENTS OF
OPTICAL PROBE SYSTEM AND ASSOCIATED MEASUREMENT INSTRUMENTATION

Power Supply, Lamp

Hewlett-Packard Company - Harrison Division

MPB Series, Model 6282A

Power Requirements: 105-125 VAC, Single Phase 50-60 Hz, 3.5 A, 200 W

Output: 0-10 VDC at 0-10 A

Load Regulation - Constant Current: $<0.05\%$ + 1 mA for a zero to maximum
change in output voltage

Line Regulation - Constant Current: $<0.05\%$ + 1 mA for any line voltage
change within the rated input

Ripple and Noise - Constant Current: <5 mA rms

Temperature Coefficient - Constant Current: $<0.02\%$ + 5 mA/$^{\circ}$C

Stability - Constant Current: $<0.10\%$ + 25 mA total drift for 8 hours
after a 30-minute warm up

Lamp

General Electric

Catalog Number 1962

Design Volts: 8.5, 62 W, 80 CP

Construction: Quartz envelope

Rated Lifetime: 50 hours at 62 W, 80 CP
500 hours at 46 W, 45 CP
2500 hours at 30 W, 25 CP

Motor, Chopper

Globe Industries

Part Number: 31A512-2.56

Power Requirements: 115 VAC, single phase 60 Hz, 20 W

Speed: 1405 RPM synchronous

Torque: 1.0 inch-ounces

Motor Life: 500 hours

Photomultiplier Tube

Radio Corporation of America

Model RCA-8645

Power Requirements: Maximum Supply Voltage 1800

Average Anode Current 0.5 mA

Spectral Response: Covers the range from 2900 to 8000 angstroms

Maximum response occurs at about 4200 angstroms

Type S-20 Spectral Response Curve

Anode Dark Current: 6×10^{-10} Amperes

Integral Magnetic Shield and Voltage Divider Network

Output Impedance: 1 Megohm

Power Supply Photomultiplier Tube

John Fluke, Manufacturing Company, Inc.

Model 412B

Power Requirements: 115 VAC $\pm$ 10%, Single Phase 50-60 Hz, 300 VA

Output: 0 to $\pm$ 2100 VDC and 0 to 30 mA

Load Regulation: 0.001% to 5 mV for full load change

Line Regulation: 0.001% to 2 mV for 10% line change

Ripple and Noise: $<$ 500 μV rms, $<$ 1 mV peak to peak

Temperature Coefficient: $<$ 20 ppm/^{o}C from +10°C to +40°C

Stability: $\pm$ 0.005% per hour, $\pm$ 0.02% per day after warmup of 30 minutes

Calibration Accuracy: $\pm$ 0.25% to 100 mV with vernier at zero

Resetability: $\pm$ 0.05% to 50 mV

Power Supply, Low Voltage

Philbrick Researches, Inc.

Model PR-300

Power Requirements: 115 VAC $\pm$ 10%, Single Phase 50-400 Hz, 250 mA, $\sim$ 30 W

Output: $\pm$ 15 VDC, 0-300 mA

Load Regulation: $<$ 250 μvolts over 0-300 mV DC change

Line Regulation: $<$ 250 μvolts at 115 V $\pm$ 10%

Ripple and Noise: $<$ 250 μvolts peak to peak

Temperature Stability: 0.1% (15 mV) from -25°C to +85°C

Amplifier (gain = 1)

    Power Requirements: $\pm$ 15 VDC

    Input Impedance: ~ 100 Meg ohms

    Output Impedance: ~ 500 ohms

    Gain - Voltage: 1

    Gain-Current: 60 db

Amplifier, Operational (gain = 10)

    Power Requirements: $\pm$ 15 VDC

    Input Impedance: ~ 10,000 ohms

    Output Impedance: ~ 2,000 ohms

    Gain: 10

    Frequency Response: Flat to 40 KHz

Light Emitting Diode, Infrared (LED)

    General Electric

    LED-10

    Total Beam Output @ 100 mA dc = 0.1 mw

    Wavelength @ 100 mA dc = 0.9 microns

Field-Effect Transistor, P-Channel Diffused Silicon Photosensitive (FET)

    Siliconix, Inc.

    Type P-102

    Input Sensitivity @ λ = 0.9 microns $\approx$ 1.2 $\mu a/mw/cm^2$

    (Gate Current per unit radiant power density)

    Spectral Response (10% Points): 0.4 to 1.1 microns

    Output Amplified (gain: ~ 500 to 1000)

Reference Amplifier (Digital Switching Device)

    Power Requirements: $\pm$ 15 VDC

    Output Voltage: Square wave of peak amplitude ~ 5 V

Synchronous Demodulator

    Power Requirements: $\pm$ 15 VDC

    Input Impedance: ~ 130 K Ohms

    Output Impedance: ~ 200 Ohms

Filter

Power Requirements: $\pm$ 15 VAC

Input Impedance: $\sim$ 50 K ohms

Output Impedance: $\sim$ 200 ohms

Gain - Voltage: 10

Frequency Response: Filters ripple above 0.1 Hz

Voltage Divider

Electronic Instrument Company, Inc.

Model 1100 RTMA Resistance Boxes - 2 Utilized

Resistance Range: 15 ohms to 10 megohms

Accuracy: $\pm$ 10%

Power Dissipation: 1 watt at any setting

Input Resistance: 10,150 ohms $\pm$ 10%

Output Resistance: 150 ohms $\pm$ 10%

Recorder, Strip Chart

Leeds & Northrup Company

Speedomax H Continuously Adjustable AZAR

Power Requirements: 120 VAC, 60 Hz

Span: Calibrated steps of 2, 5, 10, 25, 50 or 100 mV

Uncalibrated - continuous dial adjusted attenuation

Span - Limits of Error: $\pm$ 0.3% of span for calibrated ranges

$\pm$ 0.5% of span for continuously adjusted

setting

Zero Adjustment: Suppression or elevation from 0 to 40 millivolts

+ or -

Dead Band: 0.1% of span

Chart Speed: 1 inch/minute

Converter, Voltage to Frequency

Vidar Corporation

Model 240-01

Power Requirements: 115 VAC $\pm$ 10%, Single Phase 50-60 Hz $\sim$ 8W

Range: $\pm$ 100 mV to $\pm$ 1000 V full scale in five steps

-73-

Polarity: Indicated by front panel lights

Accuracy: ± 0.05% of 1 volt range for all ranges

Linearity: Better than ± 0.025% of full scale from straight line

Drift: Less than ± 0.1% of full scale per week after one hour warmup

Temperature Coefficient: Less than ± 0.01% of full scale per $^{\circ}$C

Regulation - Line Voltage: Less than ± 0.02% of full scale for

± 10. change

Input Impedance: 100 k ohms ± 0.1% on 100 mV range

1 meg ohm ± 0.1% on all other ranges

Output Frequency: 100 KHz full scale

Output Voltage: ∿ 1.5 V peak to peak

Counter, Electronic

Hewlett Packard Company

Model 5245L

Power Requirements: 115 VAC ± 10%, Single Phase 50-60 Hz, 95W

Frequency Measurements: From 0 to 50 M Hz (dc input)

From 25 Hz to 50 M Hz (ac input)

Accuracy ± 1 count ± time base accuracy

Input: Maximum Sensitivity - 100 mV rms

Impedance - 1 megohm

Gate Time: 1 microsecond to 10 seconds in decade steps

Oscilloscope, Dual Beam

Tektronix, Inc.

Model 502

Power Requirements: 105 to 125 VAC, 50-60 Hz, ∿ 300 watts

Input Impedance: 1 megohm paralleled by 47 $\mu\mu$f

Vertical Deflection Factors: 200 μV/cm to 20 V/cm in sixteen calibrated

steps

Horizontal Sweep Rates: 1 μsec/cm to 5 sec/cm in twenty-one

calibrated steps

Voltmeter, Electronic, True Root Mean Square

Ballatine Laboratories, Inc.

Model 320

Power Supply: 105-125 VAC, Single Phase, 50-420 Hz, 65 W

-74-

Voltage Range: 100 μV to 320 V rms in 13 ranges, of 10 db steps

Frequency Range: 5 to 500,000 Hz

Input Impedance: 10 megohms

Accuracy: Sine Waves and non-sinusuoidal waves

        5% of meter reading from 5 to 15 Hz

        3% of meter reading from 15 to 150,000 Hz

        5% of meter reading from 150,000 to 500,000 Hz

Output Features: Main Amplifier Output: Maximum voltage gain
of 90 db $\pm$ 1 db balance to ground, decreasing
in 10 db steps to -30 db

        Monitor Output: maximum voltage gain of 84 db $\pm$ 1 db
single ended, in phase with the input, decreasing
in 10 db steps to -36 db

        Mean Square Output: negative dc output voltage of
0.2 V corresponding to full scale meter deflection

Oscilloscope

Tektronix, Inc.

Model 545 with 53/54 K plug-in Unit

Power Requirements: 105 to 125 VAC, 50-60 Hz, $\sim$ 545 watts

Input Impedance: 1 megohm, 20 $\mu\mu$f

Vertical Deflection Factors: 0.05 V/cm to 20 V/cm in nine calibrated
steps

Horizontal Sweep Rates: 0.1 μsec/cm to 5 sec/cm in twenty-four
calibrated steps

Tape Recorder, FM Record/Reproduce System

Consolidated Electrodynamics Corporation

Model VR-3300

Power Requirements: 115 VAC $\pm$ 10%, 48-65 Hz, single phase, 450 watts

Transport Data: Tape Speeds: 60, 30, 15, 7-1/2, 3-3/4, 1-7/8 ips

        Tape Speed Accuracy: $\pm$ 0.25%

        Flutter: Maximum cumulative flutter up to 300 cps -
0.3% peak-to-peak; up to 10 Kc - 0.55%
peak-to-peak at 60 ips

Record/Reproduce Data: Input Level: 1 volt rms to produce full scale
modulation

Input Sensitivity: 0.5 to 10 volts rms

Input Impedance: 10 K ohms minimum

AC and DC Linearity: $\pm$ 1.5% of full scale

Drift: Less than 2% of full scale in 8 hours

Frequency Response: 0-20 KHz $\pm$ 0.5 db at 60 ips

Signal to Noise Ratio: 43 db at 60 ips

Harmonic Distortion: 1.5% at 60 ips

Spectrum Analyzer:

Hewlett-Packard Company

Model 302A

Power Supply: 115 VAC $\pm$ 10%, Single Phase 50 to 1600 Hz, $\sim$ 3 W or 18
to 28 VDC

Voltage Range: 30 μV to 300 V in 15 ranges, steps of 10 db

Frequency Range: 20 to 50,000 Hz

Input Impedance: 100,000 ohms on 4 most sensitive ranges
1 megohm on remainder

Dial Accuracy: $\pm$ (1% + 5 Hz)

Voltage Accuracy: $\pm$ 5% of full scale value

Selectivity: $\pm$ 3-1/2 Hz bandwidth at least 3 db down

$\pm$ 25 Hz bandwidth at least 50 db down

$\pm$ 70 Hz bandwidth at least 80 db down

Output Features: Restored Frequency Output: Output voltage
proportional to meter reading. Output level
control provided. Maximum of 1 volt across
600 ohms at output terminals for full scale meter
deflection. Output impedance $\sim$ 600 ohms.

Oscillator Output: 1 volt across 600 ohms at
output terminal (mode selector in BFO). Output
level control. Output impedance $\sim$ 600 ohms.

Recorder Output: 1 ma dc into 1500 ohms or less
at full scale meter indication

Sweep Drive - Spectrum Analyzer

Hewlett-Packard Company

Model 297A

Power: 115 VAC ± 10%, Single Phase 50-60 Hz, 12 W

Sweep Range: 64 revolutions

Sweep Speed: 170 Hz/sec or 17 Hz/sec with 302A Wave Analyzer

Sweep Output: 0-15 VDC proportional to change in shaft position.
Full output may be obtained with either 2.1 revolutions
or with 50 revolutions of the output shaft.

Vacuum Thermocouple, Insulated

American Thermo-Electric Company

Catalog Number 22

Heater Resistance: 1100 ohms

Output: 5 mV/1.2 ma

Recorder, X-Y

F. L. Moseley Company

Model 2D

Power Requirements: 115 volts, Single Phase, 60 Hz, 185 VA

Recording Speed: 20 inches per second maximum pen speed each axis

DC Voltage Ranges: Sixteen calibrated ranges for each axis;
0.5 millivolts to 50 volts/inch

AC Voltage Range: Eight calibrated ranges for each axis;
0.1 to 20 volts/inch

Accuracy: Better than 0.2% of full scale, 0.1% resetability on DC ranges

AC Accuracy		Linearity
20 Hz to 20 KHz	0.5%	0.1%
20 KHz to 50 KHz	1.0%	0.3%
50 KHz to 100 KHz	2.0%	0.5%
100 KHz to 200 KHz	10.0%	1.0%

Input Resistance: 200,000 ohms/V up to 1 V/inch
2 megohms on all higher dc ranges and all ac ranges

APPENDIX II

EQUATIONS FOR DATA REDUCTION

<u>Momentum Transport</u> (time average understood):

$$m = 2\pi \int_0^{r_o} r\, U\, \rho\, dr \tag{B-1}$$

$$G = \frac{m}{\pi r_o^2} \tag{B-2}$$

$$m* = \frac{\pi d^2}{4} \left\{ \frac{C\, Y_1}{(1 - \beta^4)^{1/2}} \right\} \left[2\, g_c\, \rho_1\, (\Delta P)_{op} \right]^{1/2} \tag{B-3}*$$

$$U = \left[2\, g_c\, (\Delta P)_{pt} / \rho \right]^{1/2} \tag{B-4}*$$

$$(\Delta P)_{sp} = \left[h(\rho_M - \rho_g) - K_A\, \rho_A + K_B\, \rho_B \right] \frac{g}{g_c} \tag{B-5}*$$

$$\frac{(\Delta P)_F}{L} = \frac{(\Delta P)_{sp}}{L} + \frac{m^2}{g_c \left(\pi r_o^2 \right)} \left[\frac{1}{\rho_{b_1}} - \frac{1}{\rho_{b_2}} \right] + \frac{g}{g_c} \bar{\rho}_b \tag{B-6}$$

$$\rho_b = \frac{\int_0^{r_o} 2\pi \rho\, r\, dr}{\pi r_o^2} \tag{B-7}$$

$$\bar{\rho}_b = \frac{\int_1^2 \rho_b\, dz}{L} \tag{B-8}$$

$$(\Delta P)_{op \text{ or } pt} = \left[h\, (\rho_M - \rho_g) \right] \frac{g}{g_c} \tag{B-9}$$

---

*Note: $\Delta P \equiv P_1 - P_2$.

$$f = \frac{D}{4} \frac{g_c}{L} \left\{ \frac{(\Delta P)_F}{\left[\frac{1}{2} \bar{\rho}_b U^2\right]} \right\} \qquad (B\text{-}10)$$

$$\tau_w = \frac{D}{4 L}(\Delta P)_F \qquad (B\text{-}11)$$

<u>Concentration Calculations</u> (c_i = fluctuating concentration):

$$\frac{I}{I_o} = \exp\left(-\epsilon_i \, \ell \, C_j\right) \qquad C_i = \bar{C}_i + c_i \qquad I \equiv a \, E \qquad (B\text{-}12)$$

<u>Time-Average Concentration</u>:

For c_i small,

$$\bar{C}_i = -\frac{1}{b_i} \ln \frac{\bar{E}}{\bar{E}_o} \qquad (B\text{-}13)$$

For c_i large,

$$\bar{C}_i \simeq -\frac{1}{b_i} \ln \frac{\dfrac{\bar{E}}{\bar{E}_o}}{\left[1 + \dfrac{b_i^2}{2} \; \overline{c_i^2}\right]} \qquad (B\text{-}14)$$

<u>RMS Concentration at Frequency</u>, f ($e/\bar{E}$ small):

$$\theta'_{C_{NO_2}}(f) = \frac{\left[(e'_S)_{Air} - (e'_S)_{NO_2}\right]_f}{G_2 \, (b_{NO_2} \, \bar{E}/G_1)(BW)^{1/2}} \qquad (B\text{-}15)$$

$$(e'_S)_{f_{Air}} = \left[(e'_{S+N})^2_{Air} - (e'_N)^2\right]^{1/2}_f \qquad (B\text{-}16)$$

$$(e'_S)_{f_{NO_2}} = \left[(e'_{S+N})^2_{NO_2} - (e'_N)^2\right]^{1/2}_f \qquad (B\text{-}17)$$

G_1 = gain of preamp, ac amp, synchronous demodulator and filter

G_2 = Gain of preamp and ac amp = $f(\bar{E}_o)$

-79-

For $\bar{E}_0 = 3.216$ volts,

$$G_1 \simeq (5.2)(5.5) = 28.6$$
$$G_2 \simeq 5.5$$

<u>Total RMS Concentration</u> ($e/\bar{E}$ small):

$$\theta'_{C_{NO_2}} = \frac{\left[(e'_S)_{Air} - (e'_S)_{NO_2}\right]}{G_2 \, (b_{NO_2} \, \bar{E}/G_1)} \tag{B-18}$$

<u>Fluctuating Temperature</u>:

$$\theta'_t(f) = \frac{\left(\overline{e^2_{S+N}} - \overline{e^2_N}\right)_f^{1/2}}{CG(BW)^{1/2}} = \left[\overline{\theta^2_t(f)}\right]^{1/2} \tag{B-19}$$

$$\theta'_t = \frac{\left(\overline{e^2_{S+N}} - \overline{e^2_N}\right)^{1/2}}{CG} = \left[\overline{\theta^2_t}\right]^{1/2} \tag{B-20}$$

$G = 12,600$

$C = 5.34 \times 10^{-6}$ volts/$^\circ$F (Pt/Pt-10% Rh at $\sim 800^\circ$F)

$BW = 5.52$ Hz

$$k_1 = \frac{2\pi f}{U} \tag{B-21}$$

$$\overline{\theta^2_t(k_1)} = \frac{\bar{U}}{2\pi} \, \overline{\theta^2_t(f)} \tag{B-22}$$

$$k_{1_D} = \frac{2\pi}{D} \; ; \; k_{1_{l_{TS}}} = \frac{2\pi}{l_{TS}} \tag{B-23}$$

$$f_D = \frac{\bar{U}}{D} \; ; \; f_{l_{TS}} = \frac{\bar{U}}{l_{TS}} \tag{B-24}$$

-80-

REFERENCES

1. Eschenroeder, A. Q., "Intensification of Turbulence by Chemical Heat Release," Phys. of Fluids, Vol. 7 (1964), pp. 1735-1743.

2. Eschenroeder, A. Q., "Turbulence Spectra in a Reacting Gas," AIAA Journal, Vol. 3 (1965), pp. 1839-1846.

3. Vassilatos, G. and Toor, H. L., "Second-Order Chemical Reactions in a Nonhomogeneous Turbulent Fluid," AIChE Journal, Vol. 11 (1965), pp. 666-673.

4. Chu, B. and Kovasznay, L. S. G., "Nonlinear Interactions in a Viscous Heat-Conducting Compressible Gas," J. Fluid Mechanics, Vol. 3 (1958), pp. 494-514.

5. Richardson, John L., "Heat Transfer in an Equilibrium Chemically Reacting System," PhD Dissertation, Stanford, California: Department of Chemical Engineering, Stanford University (1964).

6. Svehla, Roger A. and Brokaw, Richard S., "Thermodynamic and Transport Properties for the $N_2O_4 \rightleftarrows 2\ NO_2 \rightleftarrows 2\ NO + O_2$ System," NASA TN D-3327, Washington, D.C.: NASA (March 1966).

7. Fan, S. S. T. and Mason, D. M., "Properties of the System $N_2O_4 \rightleftarrows 2\ NO_2 \rightleftarrows 2\ NO + O_2$," Journal of Chemical and Engineering Data, Vol. 7 (April 1962), pp. 183-186.

8. Brokaw, R. S. and Svehla, R., Private Communication (February 9, 1967).

9. Bodman, Sam W., "Heat Transfer Accompanied by a Nonequilibrium Reversible Chemical Reaction," ScD Thesis, Department of Chemical Engineering, Cambridge, Massachusetts: Massachusetts Institute of Technology (November 1964).

10. Presler, Alden F., "An Experimental Investigation of Heat Transfer to Turbulent Flow in Smooth Tubes for the Reacting N_2O_4-NO_2 System," NASA TN D-3230, Washington, D.C.: NASA (January 1966).

11. Rodriquez-Ramirez, Abraham, "Characteristics of Turbulent Temperature Fluctuations in Air," MS Thesis, Lafayette, Indiana: Department of Nuclear Engineering, Purdue University (June 1965).

12. Rust, J. H. and Sesonske, Alexander, "Turbulent Temperature Fluctuations in Mercury and Ethylene Glycol in Pipe Flow," International Journal of Heat and Mass Transfer, Vol. 9 (1966), pp. 215-227.

13. Brophy, James J., "Low Noise Modifications of the Tektronix Type 122 Preamplifier," Rev. of Sci. Instru., Vol. 26 (1955), p. 1076.

14. Eisenman, W. L., "Tektronix Type 122 Preamplifier Modification," *Applied Optics*, Vol. 4 (1965), p. 512.

15. Rust, James H., "Characteristics of Turbulent Temperature Fluctuations in Mercury and Ethylene Glycol," PhD Thesis, Lafayette, Indiana: Department of Nuclear Engineering, Purdue University (1965).

16. Gibson, Carl H., "Scalar Mixing in Turbulent Flow," PhD Dissertation, Stanford, California: Department of Chemical Engineering, Stanford University (1962), pp. 70-74.

17. Lee, Jon and Brodkey, Robert S., "Light Probe for the Measurement of Turbulent Concentration Fluctuations," *The Review of Scientific Instruments*, Vol. 34 (October 1963) pp. 1086-1090.

18. Nye, James O. and Brodkey, Robert S., "Light Probe for Measurement of Turbulent Concentration Fluctuations," *The Review of Scientific Instruments*, Vol. 38 (January 1967), pp. 26-28.

19. Schott, Garry L., "Chemical Studies in Shock Waves," PhD Thesis, Pasadena, California: California Institute of Technology (1956).

20. Schott, Garry L. and Davidson, Norman, "Shock Waves in Chemical Kinetics: The Decomposition of N_2O_5 at High Temperatures," JACS, Vol. 80 (1958), pp. 1841-1853.

21. McAdams, W. H., *Heat Transmission*, Third Edition, New York: McGraw-Hill Book Company, Inc. (1954), p.262.

22. Tanimoto, S. and Hanratty, T. J., "Fluid Temperature Fluctuations Accompanying Turbulent Heat Transfer in a Pipe," *Chem. Eng. Sci.*, Vol. 18 (1963), pp. 307-311.

23. Brodkey, Robert S., *The Phenomena of Fluid Motions*, Reading, Massachusetts: Addison-Wesley Publishing Company (1967), pp. 343-351.

24. Lee, Jon., "Isotropic Turbulent Mixing under a Second-order Chemical Reaction," *Physics of Fluids*, Vol. 9 (September 1966), pp. 1753-1763.

25. Hinze, J. O., *Turbulence - An Introduction to its Mechanism and Theory*, New York: McGraw-Hill Book Company, Inc. (1959).

26. Rosser, W. A. and Wise, H., "Thermal Decomposition of Nitrogen Dioxide," *J. Chem. Phys.*, Vol. 24 (1956), pp. 493-494.

27. Brown, F. and Mason, D.M., Personal Communication. Stanford, California; Stanford University, Department of Chemical Engineering (July 20, 1966).

28. Ashmore, P.G. and Burnett, M.G., "Concurrent Molecular and Free Radical Mechanisms in the Thermal Decomposition of Nitrogen Dioxide", _Faraday Society Transations_, Vol. 58 (1962), pp. 253-261.

29. Ashmore, P. G., Burnett, M. G., and Tyler, B.J. "Reaction of Nitric Oxide and Oxygen", _ibid._, Vol 58 (1962), pp. 685-691.

30. Brian, P. L. T., Reid, R. C., and Bodman, S. W., "Heat Transfer to Decomposing Nitrogen Dioxide in a Turbulent Boundary Layer". _A.I.Ch.E. Journal_, Vol. 11 (1965), pp. 809-814.

31. Prigogine, I. and Defay, R., _Chemical Thermodynamics_, London: Longmans Green (1954).

DOCUMENT CONTROL DATA - R&D

(Security classification of title, body of abstract and indexing annotation must be entered when the overall report is classified)

1 ORIGINATING ACTIVITY (Corporate author)	2a REPORT SECURITY CLASSIFICATION
Philco-Ford Corporation, Space and Re-entry Systems Division	Unclassified
	2b GROUP N/A

3 REPORT TITLE

Advanced Penetration Problems, Exothermic Additives for Wake Modification

4 DESCRIPTIVE NOTES (Type of report and inclusive dates)

Semiannual, 16 October 1967 through 15 April 1968

5 AUTHOR(S) (Last name, first name, initial)

Richardson, J. L. and Getz, R. J.

6 REPORT DATE	7a TOTAL NO OF PAGES	7b NO OF REFS
15 May 1968	94	31

8a CONTRACT OR GRANT NO	9a ORIGINATOR'S REPORT NUMBER(S)
F04701-68-C-0032	
b PROJECT NO	
ARPA Order 888	
c	9b OTHER REPORT NO(S) (Any other numbers that may be assigned this report)
d	SAMSO TR-68-362 Vol. III

10 AVAILABILITY/LIMITATION NOTICES

This document may be further distributed by any holder only with specific approval of SAMSO ▰▰▰▰▰▰▰▰▰▰▰▰▰▰▰▰▰▰▰▰▰.

11 SUPPLEMENTARY NOTES	12 SPONSORING MILITARY ACTIVITY
	SAMSO Norton Air Force Base California

13 ABSTRACT

The progress achieved in the first four and one-half months of the program was reviewed. The principal effort of this period has consisted of the design of experiments for demonstrating the effect of exothermic energy release on turbulent flow structure, the development of sensitive instrumentation for the accurate measurement of both time-average and fluctuating scalar quantities (temperature and concentration), the development of techniques for reducing the raw data derived from the sensors and their associated electronics to forms suitable for correlation and analysis, and the completion of several experiments in both nonreacting and nonequilibrium reacing gases. Calculations of the effectiveness parameter for the NO_2 reacting system have shown that the recombining NO_2 system (to form N_2O_4) will exhibit a sufficiently large effectiveness parameter under laboratory conditions so that the turbulence in a wake flow should be significantly modified. Appropriate experiments for demonstrating this effect were designed. An improved fiber optic probe was developed for use in the heated reacting gases (T to $800°K$, P to 10 atm). Several experiments were completed with both high temperature air and reacing NO_2. Both total rms and spectral data were obtained. In the case of heated fully developed turbulent tube flow, the temperature and concentration intensities were found to be an order of magnitude higher in the nonequilibrium reacting gas than in nonreacting air.

DD FORM 1 JAN 64 **1473**

14	LINK A		LINK B		LINK C	
KEY WORDS	ROLE	WT	ROLE	WT	ROLE	WT

INSTRUCTIONS

1. **ORIGINATING ACTIVITY:** Enter the name and address of the contractor, subcontractor, grantee, Department of Defense activity or other organization (*corporate author*) issuing the report.

2a. **REPORT SECURITY CLASSIFICATION:** Enter the overall security classification of the report. Indicate whether "Restricted Data" is included. Marking is to be in accordance with appropriate security regulations.

2b. **GROUP:** Automatic downgrading is specified in DoD Directive 5200.10 and Armed Forces Industrial Manual. Enter the group number. Also, when applicable, show that optional markings have been used for Group 3 and Group 4 as authorized.

3. **REPORT TITLE:** Enter the complete report title in all capital letters. Titles in all cases should be unclassified. If a meaningful title cannot be selected without classification, show title classification in all capitals in parenthesis immediately following the title.

4. **DESCRIPTIVE NOTES:** If appropriate, enter the type of report, e.g., interim, progress, summary, annual, or final. Give the inclusive dates when a specific reporting period is covered.

5. **AUTHOR(S):** Enter the name(s) of author(s) as shown on or in the report. Enter last name, first name, middle initial. If military, show rank and branch of service. The name of the principal author is an absolute minimum requirement.

6. **REPORT DATE:** Enter the date of the report as day, month, year; or month, year. If more than one date appears on the report, use date of publication.

7a. **TOTAL NUMBER OF PAGES:** The total page count should follow normal pagination procedures, i.e., enter the number of pages containing information.

7b. **NUMBER OF REFERENCES:** Enter the total number of references cited in the report.

8a. **CONTRACT OR GRANT NUMBER:** If appropriate, enter the applicable number of the contract or grant under which the report was written.

8b, 8c, & 8d. **PROJECT NUMBER:** Enter the appropriate military department identification, such as project number, subproject number, system numbers, task number, etc.

9a. **ORIGINATOR'S REPORT NUMBER(S):** Enter the official report number by which the document will be identified and controlled by the originating activity. This number must be unique to this report.

9b. **OTHER REPORT NUMBER(S):** If the report has been assigned any other report numbers (*either by the originator or by the sponsor*), also enter this number(s).

10. **AVAILABILITY/LIMITATION NOTICES:** Enter any limitations on further dissemination of the report, other than those imposed by security classification, using standard statements such as:

(1) "Qualified requesters may obtain copies of this report from DDC."

(2) "Foreign announcement and dissemination of this report by DDC is not authorized."

(3) "U. S. Government agencies may obtain copies of this report directly from DDC. Other qualified DDC users shall request through

_____ ."

(4) "U. S. military agencies may obtain copies of this report directly from DDC. Other qualified users shall request through

_____ ."

(5) "All distribution of this report is controlled. Qualified DDC users shall request through

_____ ."

If the report has been furnished to the Office of Technical Services, Department of Commerce, for sale to the public, indicate this fact and enter the price, if known.

11. **SUPPLEMENTARY NOTES:** Use for additional explanatory notes.

12. **SPONSORING MILITARY ACTIVITY:** Enter the name of the departmental project office or laboratory sponsoring (*paying for*) the research and development. Include address.

13. **ABSTRACT:** Enter an abstract giving a brief and factual summary of the document indicative of the report, even though it may also appear elsewhere in the body of the technical report. If additional space is required, a continuation sheet shall be attached.

It is highly desirable that the abstract of classified reports be unclassified. Each paragraph of the abstract shall end with an indication of the military security classification of the information in the paragraph, represented as (TS), (S), (C), or (U).

There is no limitation on the length of the abstract. However, the suggested length is from 150 to 225 words.

14. **KEY WORDS:** Key words are technically meaningful terms or short phrases that characterize a report and may be used as index entries for cataloging the report. Key words must be selected so that no security classification is required. Identifiers, such as equipment model designation, trade name, military project code name, geographic location, may be used as key words but will be followed by an indication of technical context. The assignment of links, rules, and weights is optional.

GPO 886-551